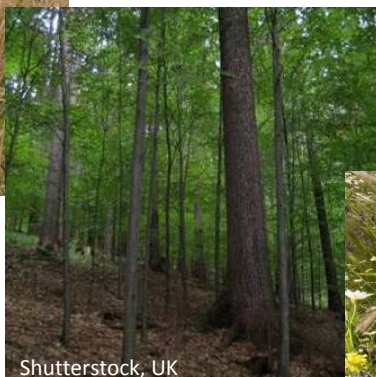# SCIENTIFIC BACKGROUND DOCUMENT B

Version November 2017

DEVELOPING AREAS OF RESEARCH OF RELEVANCE TO CHAPTER III (MAPPING CRITICAL LEVELS FOR VEGETATION) OF THE MODELLING AND MAPPING MANUAL OF THE LRTAP CONVENTION

F. Hayes, CEH Bangor

Shutterstock, UK

Shutterstock, UK

Chapter 3 of the Modelling and Mapping Manual of the LRTAP Convention describes the most up-to-date methodology and establishment of critical levels for adverse impacts of air pollutants (ozone, sulphur dioxide, nitrogen oxides and ammonia) on vegetation. The current version of Chapter 3 includes updates to critical levels for ozone agreed at the 30th ICP Vegetation Task Force Meeting, 14-17 February, 2017, Poznan, Poland. For ozone, further supporting information is provided in Scientific Background Document A (SBD-A) regarding the methodologies and critical levels described in Chapter 3.

Scientific Background Document B (SBD-B; this document) contains DO$_3$SE model parameterisations for additional species and information on developing areas of ozone research and the application of methodologies to further develop ozone critical levels in the future. Chapter 3 and both scientific background documents are available on the ICP Vegetation website at http://icpvegetation.ceh.ac.uk.

* International Cooperative Programme on Effects of Air Pollution on Natural Vegetation and Crops

Chapter 3 was prepared under the leadership of the ICP Vegetation and led by Gina Mills, Head of the ICP Vegetation Programme Coordination Centre (PCC), Centre for Ecology & Hydrology, Bangor, UK.

The editorial team for the revision of Chapter 3 and the production of SBD-A and B consisted of:

Gina Mills	UK	Lead (Head ICP Vegetation PCC)
Harry Harmens	UK	Editor (Chair ICP Vegetation)
Håkan Pleijel	Sweden	Chair Crops Working Group
Patrick Büker	UK	Chair Forest Trees Working Group
Ignacio González-Fernández	Spain	Chair (Semi-)natural Vegetation Working Group
Felicity Hayes	UK	(Semi-)natural Vegetation Working Group (PCC)

For Chapter 4 – 10 in SBD-B (this document), the authors are listed at the start of each Chapter. Additional editorial input to Chapter 3 in SBD-B regarding evergreen Mediterranean tree species was provided by Rocio Alonso (Spain).

Table of Contents

1   Introduction

This Scientific Background Document B (SBD-B) describes new and ongoing developments and research areas of relevance for the future development of Chapter III ('Mapping critical levels for vegetation') of the Modelling and Mapping Manual of the Convention on Long-range Transboundary Air Pollution (LRTAP), specifically regarding ozone (O_3) critical levels for vegetation. Chapter 3 of the manual was prepared under the leadership of the ICP Vegetation and was fully revised to include updates to critical levels for O_3 agreed at the 30th ICP Vegetation Task Force Meeting, 14-17 February, 2017, Poznan, Poland. The revised version of Chapter 3 was published in April 2017 on the ICP Vegetation website (http://icpvegetation.ceh.ac.uk). Some of the material included in SBD-B was included in the background document for the UNECE Ozone Critical Level Workshop, 7 – 8 November 2016, Madrid, Spain. However, the methodologies described in SBD-B were not considered robust enough yet or require further validation before they can be included in Chapter 3 of the Modelling and Mapping Manual. Included in SBD-B are also parameterisations of the DO_3SE model for additional crop species for which flux-effect relationships are currently not robust enough to derive flux-based critical levels at the European scale or for forest tree species for which the parameterisations of the DO_3SE model are for based on experiments with young trees to assess impacts.

SBD-B contains information on:

- DO_3SE model parameterisation for additional crop (Chapter 2) and forest tree species (Chapter 3);

- Handling soil moisture impacts on O_3 fluxes in the EMEP MSC-W model (Chapter 4);

- O_3 flux-effect relationships for the net annual increment of forest trees (Chapter 5);

- Improved methods for the assessment of crop and tree phenology: methods for determining the accumulation period for calculating stomatal O_3 fluxes and changes in a future climate (Chapter 6 - 8);

- Random effects method applied to O_3 flux-effect relationships (Chapter 9);

- Epidemiological analysis as a tool to evaluate O_3 impacts on vegetation at the landscape level (Chapter 10).

2   DO₃SE model parameterisations for additional crop species

2.1 Introduction

The 27th ICP Vegetation Task Force meeting (Paris, 2014) approved new O_3 stomatal flux parameterisations for grapevine, maize, soybean and sunflower. However, not enough effects data is available yet for these species to establish flux effect relationships.

Method of data selection

The initial, underpinning literature search to identify the relevant peer-reviewed information required to establish the species-specific parameterisation was carried according to the following criteria:

A. Experimental studies in field plots; if none found, then search for glasshouse and controlled environment growth chamber studies;

B. Experiments conducted in Europe; if none found, then also consider studies conducted in the USA proving that the climate was similar to that found in Europe (e.g. no studies performed under sub-tropical climate);

C. Reporting of g_{sto} and information about measuring device used, leaf area reference (total vs. projected) and conditions under which g_{sto} was measured;

D. Study published after 2005, if species was already searched for in last preliminary parameterisation study carried out in 2006.

Derivation of g_{max}

The values for g_{max} were extracted from figures or tables in the peer-reviewed literature. Only those studies were included that clearly stated the type of instrument used, the gas for which g_{sto} was measured (H_2O, CO_2 or O_3), the reference area (projected or measured), the name of the cultivar (European were preferred over North American cultivars; no tropical cultivars were used), the age of the plant or leaf used for g_{sto} measurements, the timing of the measurements and the climatic conditions during the measuring campaign (field experiments were preferred over glasshouse or chamber experiments). Data points referring to the total leaf area were recalculated to represent the projected leaf area as reference.

Only those reported g_{sto} values were deemed to represent g_{max} that were measured under non-limiting environmental conditions as clearly stated in the methods section of the respective paper. If g_{max} was reported for water vapour (g_{max} mmol H_2O m^{-2} PLA s^{-1}), which was the case in the majority of papers, it was converted to g_{max} for O_3 (g_{max} mmol O_3 m^{-2} PLA s^{-1}) using the conversion factor of 0.663 (Grünhage et al., 2012) to account for the difference in the molecular diffusivity of water vapour to that of O_3.

2.2 Parameterisation of the O3 stomatal flux model (DO3SE) for grapevine, maize, soybean and sunflower

Parameterisation of the O_3 stomatal flux model for additional crops species is provided in **Table 2.1**

Grapevine (Vitis vinifera)

The parameterisation of the flux model for grapevine provided in **Table 2.1** is considered robust. This is due to the use of both published data and g_{sto} measurement datasets that have been kindly donated by a number of scientists who have worked with this species in the past (**Table 2.2**). The median g_{max} value for grapevine is 229 mmol O_3 m^{-2} PLA s^{-1}, with a standard deviation of 72 mmol O_3 m^{-2} PLA s^{-1} (**Table 2.1; Figure 2.1**). When separating

red (n = 17; filled symbols in Figure 2.1) from white (n = 6, empty symbols in Figure 2.1) grapevine varieties, the median g_{max} value and standard deviation were 229 and 72 mmol O_3 m^{-2} PLA s^{-1} respectively for red varieties (i.e. identical to entire dataset) and 205 and 77 mmol O_3 m^{-2} PLA s^{-1} respectively for white varieties. In Table 2.1, the parameterisation provided is an average of all data available for red and white varieties of grape.

Table 2.1 *Parameterisation of the DO$_3$SE model for grapevine, maize, soybean, sunflower.*

Parameter	Units	Crop species parameterisation – POD$_6$SPEC			
Species	Common name	**Grapevine**	**Maize**	**Soybean**	**Sunflower**
	Latin name	***Vitis vinifera***	***Zea mays***	***Glycine max***	***Helianthus annuus***
g_{max}*	mmol O$_3$ m^{-2} PLA s^{-1}	229 (72) (DP: 23; S: 14)	323 (28) (DP: 6; S: 6)	706 (291) (DP: 8; S: 8)	386 (139) (DP: 15; S: 13)
f_{min}	fraction	0.01	0.05	0.06	0.05
light_a	-	0.0076	0.0048	0.0035	0.002
T_{min}	°C	9	2	17	2
T_{opt}	°C	30	25	28	25
T_{max}	°C	43	48	38	48
VPD_{max}	kPa	1.6	0	2.5	1.2
VPD_{min}	kPa	6.2	5.0	5.3	4.0
ΣVPD_{crit}	kPa	-	-	-	-
PAW_t^i	%	-	-	-	-
SWC_{max}^i	% volume	-	-	-	-
SWC_{min}^i	% volume	-	-	-	-
SWP_{max}	MPa	-0.35	-0.12	-1.5	-0.25
SWP_{min}	MPa	-1.2	-0.8	-4.0	-1.65
f_{O3}	POD$_0$ mmol O$_3$ m^{-2} PLA s^{-1} (wheat)	-	-	-	-
f_{O3}	AOT0, ppmh (potato)	-	-	-	-
f_{O3}	exponent	-	-	-	
A_{start}_ETS	°C day	105	130	160	150
A_{end}_ETS	°C day	270	250	270	250
Leaf dimension	cm	15	10	10	25
Canopy height	m	1.7	2.0	0.65	2.0
f_{phen_a}	fraction	0.2	0.1	0.4	0.6
f_{phen_b}	fraction	(1.0)	(1.0)	(1.0)	(1.0)
f_{phen_c}	fraction	1.0	1.0	1.0	1.0
f_{phen_d}	fraction	(1.0)	(1.0)	(1.0)	(1.0)
f_{phen_e}	fraction	0.2	1	0.4	0.4
$f_{phen\_1\_FD}$	no of days	60	15	50	34
$f_{phen\_2\_FD}$	no of days	(200)	(200)	(200)	(200)
$f_{phen\_3\_FD}$	no of days	(200)	(200)	(200)	(200)
$f_{phen\_4\_FD}$	no of days	45	45	45	34

The values in brackets represent "dummy" values required for DO$_3$SE modelling purposes. "-" = parameterisation not required for this species.

* Mean value (and standard deviation) of several data points (DP) and studies (S).

Table 2.2   *References for the parameterisation of the DO$_3$SE model for grapevine.*

Parameter	References for grapevine
g$_{max}$ [value – mmol O$_3$ m^{-2} PLA s^{-1}]	Correia et al., 1995 [305]; Jacobs et al., 1996 [231]; Massman et al., 1994 [348]; Medrano et al., 2003 [308, 225]; Naor and Wample, 1995 [229]; Patakas et al., 2003 [146, 149, 139]; Petit et al., 2008 [179]; Schultz, 2003a [248]; Schultz, 2003b [148, 166]; Tramontini et al., 2013 [225, 106]; Vitali et al., 2013 [232, 212]; Winkel and Rambal, 1990 [292, 371, 239]; Winkel and Rambal, 1993 [295, 213]; Zsófi et al., 2009 [325]
f$_{min}$	Jacobs et al., 1996
light_a	Jacobs et al., 1996; Lu et al., 2003; Massman et al., 1994; Schultz, 2003a; Winkel and Rambal, 1990; Winkel and Rambal, 1993
T$_{min}$, T$_{opt}$, T$_{max}$	Correia et al., 1995; Flexas et al., 1999; Jacobs et al., 1996; Massman et al., 1994; Schultz, 2003a; Schultz, 2003b
VPD$_{min}$, VPD$_{max}$	Correia et al., 1995; During, 1987; Jacobs et al., 1996; Massman et al., 1994; Medrano et al., 2003; Schultz, 2003a, Vitali et al., 2013
SWP$_{min}$, SWP$_{max}$	Correia et al., 1995; Quick et al., 1992; Winkel and Rambal, 1993
A$_{start}$_ETS, A$_{end}$_ETS	Jones et al., 2005
Leaf dimension, canopy height	Massman et al., 1994
f$_{phen}$ parameters	Correia et al., 1995; Winkel and Rambal, 1993
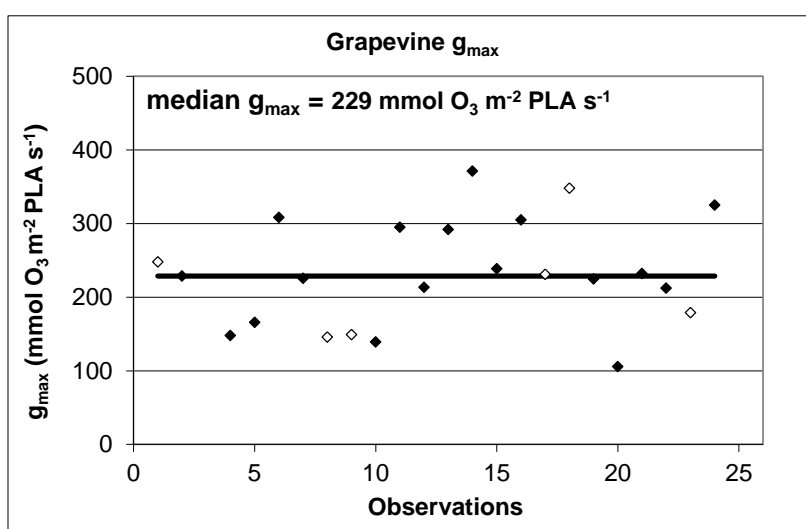
Figure 2.1   *g$_{max}$ derivation for grapevine. Filled symbols refer to red cultivars, empty symbols refer to white cultivars. The black line represents the median value for the combined paramaterisation for both red and white cultivars.*

Maize (Zea mays)

Using data from six studies (**Table 2.3**), the median g$_{max}$ value is 323 mmol O$_3$ m^{-2} PLA s^{-1}, with a standard deviation of 28 mmol O$_3$ m^{-2} PLA s^{-1} (**Table 2.1; Figure 2.2**). No recent data have been found to parameterise the phenological relationship so here we use the default parameterisation provided by Simpson et al. (2003). The f$_{light}$ parameterisation is based on seven studies, whereas f$_{temp}$, f$_{VPD}$ and f$_{SW}$ are parameterised each based only on one or two

studies (**Table 2.3**). This lack of corroboration by different datasets reduces the certainty of the O_3 stomatal flux model for maize.

Table 2.3 *References for the parameterisation of the DO_3SE model for maize.*

Parameter	References for maize
g_{max} [value – mmol O_3 m^{-2} PLA s^{-1}]	Körner et al., 1979 [343]; Ozier-Lafontaine et al., 1998 [326]; Sinclair et al., 1975 [386]; Stigter and Lammers, 1974 [321]; Tardieu et al., 1991 [312]; Vitale et al., 2007 [312]
f_{min}	Bethenod and Tardieu, 1990; Sanguineti et al., 1999
light_a	Bethenod and Tardieu, 1990; Guilioni et al., 2000; Machado and Lagôa, 1994; Olioso et al., 1995; Ozier-Lafontaine et al., 1998; Rochette et al., 1991; Turner and Begg, 1973; Vitale et al., 2007
T_{min}, T_{opt}, T_{max}	Rodriguez and Davies, 1982; Turner and Begg, 1973
VPD_{min}, VPD_{max}	Olioso et al., 1995
SWP_{min}, SWP_{max}	Davies et al., 1994; Tardieu et al., 1992
A_{start_ETS}, A_{end_ETS}	FAO, AGL (2002); http://www.fao.org
Leaf dimension, canopy height	FAO, AGL (2002); http://www.fao.org; Simpson et al., 2003
f_{phen} parameters	Simpson et al., 2003
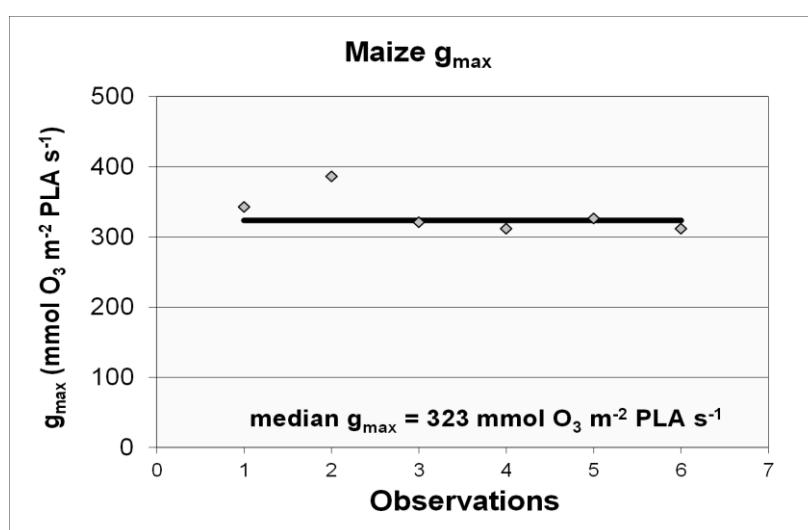
Figure 2.2 *g_{max} derivation for maize. The black line represents the median value.*

Soybean (Glycine max)

Most published studies for soybean have been conducted outside Europe, most commonly in North America (e.g. from the SoyFACE experiment in Illinois). Only two field studies from Europe (Bou Jaudé et al., 2008; Taconet et al., 1995) were deemed suitable for the derivation of g_{max}. Hence, the g_{max} parameterisation for soybean is based on two European and six North American datasets (**Table 2.4**). A median g_{max} of 706 mmol O_3 m^{-2} PLA s^{-1} and a fairly large standard deviation of 291 mmol O_3 m^{-2} PLA s^{-1} were derived, based on eight data points (**Table 2.1, Figure 2.3**).

Data for the parameterisation of environmental functions was patchy, but various peer-reviewed studies - together with an Italian primary dataset (Rana, pers. comm.) – enabled the derivation of a parameterisation for f_{light}, f_{temp}, f_{VPD} and f_{fhen}.

Table 2.4   *References for the parameterisation of the DO_3SE model for soybean.*

Parameter	References for soybean
g_{max} [value – mmol O_3 m^{-2} PLA s^{-1}]	Bernacchi et al., 2006 [484]; Betzelberger et al., 2012 [716]; Bou Jaudé et al., 2008 [1064]; Gilbert et al., 2011 [1061]; Gillespie et al., 2012 [696]; Taconet et al., 1995 [381]; Ward and Bunce, 1986)[431]; Wilson and Bunce, 1997 [1041]
f_{min}	Rana, pers. comm.
light_a	Gillespie et al., 2012 ; Rana, pers. comm.
T_{min}, T_{opt}, T_{max}	Bernacchi et al., 2006; Bunce, 1998, Rana, pers. comm.
VPD_{min}, VPD_{max}	Gilbert et al., 2011; Gillespie et al., 2012, Rana, pers. comm.
SWP_{min}, SWP_{max}	Rana, pers. comm.
A_{start_ETS}, A_{end_ETS}	Bou Jaudé et al., 2008; Taconet et al., 1995
Leaf dimension, canopy height	Taconet et al., 1995
f_{phen} parameters	Bernacchi et al., 2006; Bou Jaudé et al., 2008; Gillespie et al., 2012
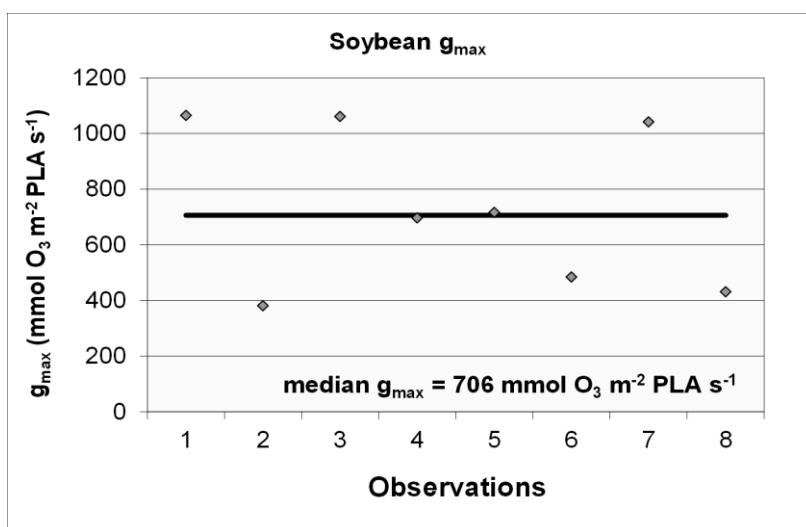
Figure 2.3   *g_{max} derivation for soybean. The black line represents the median value.*

Sunflower (Helianthus annuus)

The O_3 stomatal flux model that was established for sunflower is reasonably robust with the exception of f_{temp}, which could not be parameterised yet due to a lack of data on the relationship between g_{sto} and either air or leaf temperature. To overcome this problem, the f_{temp} parameterisation for maize is provided as a substitute.

A median g_{max} of 386 mmol O_3 m^{-2} PLA s^{-1} and a standard deviation of 136 mmol O_3 m^{-2} PLA s^{-1} were derived (**Table 2.1, Figure 2.4**), based on 15 data points from 13 studies (**Table 2.5**). Considering the fairly large number of peer-reviewed studies that contribute to

the DO$_3$SE parameterisation for sunflower, this parameterisation is considered to be fairly robust.

Table 2.5 *References for the parameterisation of the DO$_3$SE model for sunflower.*

Parameter	References for sunflower
g$_{max}$ [value – mmol O$_3$ m^{-2} PLA s^{-1}]	Connor and Jones, 1985 [353]; Csajbók et al., 2008 [226]; Hirasawa et al., 1995 [514]; Körner et al., 1979 [419; 386; 386]; Quick et al., 1992 [381]; Rivelli et al., 2002 [586]; Schurr et al., 1992 [431]; Steduto et al., 2000 [732]; Turner et al., 1984 [351]; Turner et al., 1985 [404]; Wample and Thornton, 1984 [254]; Ward and Bunce, 1986 [424]; Wookey et al., 1991 [166]
f$_{min}$	Hirasawa et al., 1995
light_a	Fay and Knapp, 1996; Turner, 1970
T$_{min}$, T$_{opt}$, T$_{max}$	Maize parameterisation used as default
VPD$_{min}$, VPD$_{max}$	Teubner, 1985; Turner et al., 1984; Ward and Bunce, 1986
SWP$_{min}$, SWP$_{max}$	Fambrini et al., 1994; Gollan et al., 1986; Hirasawa et al., 1995; Quick et al., 1992; Sadras et al., 1993; Zhang and Davies, 1989
A$_{start}$_ETS, A$_{end}$_ETS	Putnam et al. (2017): Alternative Field Crops Manual http://www.hort.purdue.edu/newcrop/afcm/sunflower.html
Leaf dimension, canopy height	Putnam et al. (2017): Alternative Field Crops Manual http://www.hort.purdue.edu/newcrop/afcm/sunflower.html
f$_{phen}$ parameters	Angadi and Entz, 2002; Connor and Jones, 1985; Wookey et al., 1991
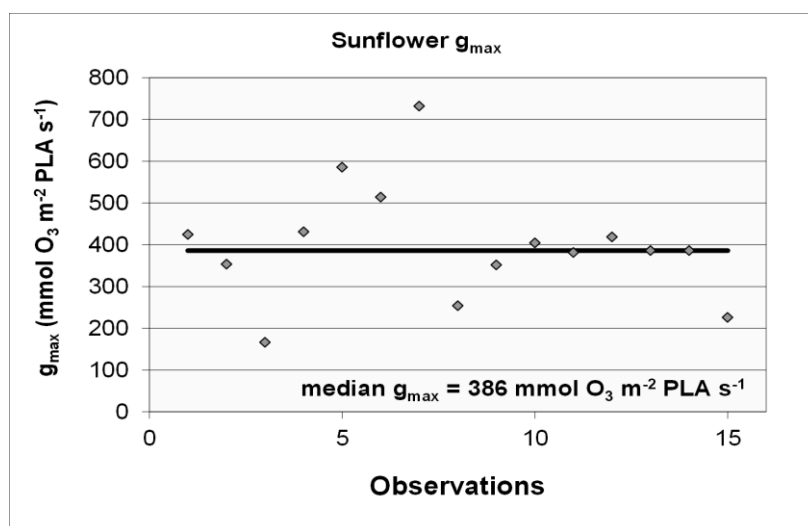
Figure 2.4 *g$_{max}$ derivation for sunflower. The black line represents the median value.*

2.3 Additional published parameterisations of DO$_3$SE for local-scale application in the Mediterranean: barley, bean and lettuce

The papers listed below have been published in the peer-reviewed literature and contain O$_3$ stomatal flux parameterisations. They have not been approved by the ICP Vegetation Task Force for use on a European scale, but are included here as a useful reference for those wishing to conduct a local-scale risk assessment in the Mediterranean region.

Barley (*Hordeum vulgare*)

Gerosa, G., Marzuoli, R., Cieslik, S., Ballarin-Denti, A., 2004. Stomatal ozone fluxes over a barley field in Italy. "Effective exposure" as a possible link between exposure-and flux-based approaches. Atmospheric Environment 38, 2421-2432.

Bean (*Phaseolus vulgaris*)

Gerosa, G., Marzuoli, R., Rossini, M., Panigada, C., Meroni, M., Colombo, R., Faoro, F., Iriti, M., 2009b. A flux-based assessment of the effects of ozone on foliar injury, photosynthesis, and yield of bean (cv. Borlotto Nano Lingua di Fuoco) in open-top chambers. Environmental Pollution 157, 1727-1736.

Lettuce (*Lactuca sativa* L.)

Goumenaki, E., González-Fernández, I., Papanikolaou, A., Papadopoulou, D., Askianakis, C., Kouvarakis, G., Barnes, J., 2007. Derivation of ozone flux-yield relationships for lettuce: A key horticultural crop. Environmental Pollution 146, 699-706.

Marzuoli, R., Finco, A., Chiesa, M., Gerosa, G., 2016. A dose-response relationship for marketable yield reduction of two lettuce (*Lactuca sativa* L.) cultivars exposed to tropospheric ozone in Southern Europe. Environmental Science and Pollution Research, 1-10.

For **lettuce**, the parameterisation provided by Goumenaki et al. (2007) can also be applied in the Atlantic region as represented by the UK. Both Goumenaki et al. (2007) and Marzuoli et al. (2016) reported significant flux-effect relationships for marketable lettuce yield. Marzuoli et al. (2016) obtained the best regression fit using an instantaneous flux threshold of 6 nmol O_3 m^{-2} s^{-1} (POD_6SPEC), i.e. the same threshold value as for wheat, potato and tomato. In contrast, Goumenaki et al. (2007) obtained the best regression fit using an instantaneous flux threshold of 0 or 1 nmol O_3 m^{-2} s^{-1}, with a significant flux-effect relationship being observed up to a threshold of 4 nmol O_3 m^{-2} s^{-1}. Further analysis of available data for lettuce is required to parameterise DO$_3$SE and develop a flux-effect relationship for application at the European scale, such that a critical level for marketable lettuce yield can be derived. Marzuoli et al. (2016) derived a critical level of 1 mmol O_3 m^{-2} (POD_6SPEC) for a 15% marketable yield loss in their study.

González-Fernández et al. (2016) studied the effects of O_3 on the marketable yield of the **leafy vegetables** spinach (*Spinacia oleracea* L.) and Swiss chard (*Beta vulgaris* L. *var. cycla*) under Mediterranean conditions. They concluded that leafy vegetables can be more sensitive to O_3 than other horticultural crops such as tomato. Hence, it is recommended to further analyse available data on O_3 flux-effect relationships to potentially establish flux-based critical levels for the marketable yield of leafy vegetables for application at the European scale (or at least for the Mediterranean region).

2.4 O$_3$-sensitivity of crops based on 7h mean O$_3$ data

A wide range in sensitivity to O_3 has been shown for different crops (Hayes and Mills, 2011). Earlier versions of Chapter 3 included the O_3 sensitivity index for crops published by Mills et al., 2007. This index has been updated here based on data published since 2007. The update uses published values for the most commonly reported concentration-based O_3 indices, the 7h or 8h mean. Hayes and Mills (2011) collated data from published papers where two or more O_3 treatments had been used. The exposure facilities used were mainly open-top chambers, although occasionally other methods were used, including glasshouses, controlled environment chambers, closed-top field chambers and field

fumigation. Only papers that included measurements relating to crop yield were included in the database. For the purposes of this study, only food crops were considered; information relating to crops such as cotton, tobacco and biofuels was not included. Searches in published papers for data on the yield in response to O_3 were also made for durum wheat, pumpkin, sunflower, rye, triticale, buckwheat, apples, millet, sorghum, carrot, lemon, cassava and chickpea. However, no suitable studies on the response of yield to O_3 were found for these crops.

For each crop, O_3 parameters were collated as given in the relevant paper. The vast majority of studies presented 7h mean data. For the very rare cases when this was not presented in the paper, the 7h mean was calculated using the exposure information available. For ease of analysis, 8h mean O_3 concentrations were considered to be the same as 7h mean concentrations as any differences were likely to be very small. Data from ICP Vegetation biomonitoring sites show that there is a close correlation between 7h mean and 12h mean O_3 data, with an r^2 of 0.98 with data from 2010, enabling publications with O_3 data only presented as 12h means to be used in the database.

For each individual study, data were compiled using the Fuhrer (1994) method: for each experiment, regression analysis of yield versus O_3 exposure (7h mean) was used to calculate the absolute yield at zero O_3 exposure. Where more than one variety was used, the absolute yield at zero O_3 exposure was calculated separately for each variety. The relative yield for each O_3 treatment used was then calculated for each observation of absolute yield. Therefore, a value of less than one indicates that there was a reduction in yield in that treatment. For each crop, relative yield was plotted against O_3 concentration (7 hour mean), using data from all relevant experiments, to determine a dose-response relationship. For all crops a linear dose-response relationship was assumed for comparison of O_3 sensitivity across crop species. The significance of the regression line of this dose-response relationship was determined using Minitab (version 16). Crops were grouped into sensitivity classes based on the slope of the regression, using the following classification (**Table 2.6**):

- Sensitive: slope <-0.004;

- Moderately sensitive: slope of -0.002 to -0.004;

- Moderately resistant: slope of -0.001 to -0.002;

- Resistant: slope >-0.001.

The most O_3-sensitive agricultural crop species include legumes such as peas and beans, soybean and the cereal wheat. Maize, rice and potato are moderately sensitive, whereas oat is moderately resistant (Table 2.6). The most O_3-sensitive horticultural crop species are onion and lettuce, whereas tomato is moderately sensitive. The most O_3-sensitive tree crop species are orange and plum. It should be considered in this comparison that the amount of information on O_3 sensitivity varies widely among species (see number of data points). Also, the O_3 sensitivity of some crops is based on information from old cultivars that may not represent cultivars currently grown in the field. Several studies have indicated that new, recently developed cultivars are more sensitive to O_3 than older cultivars (e.g. Biswas et al., 2006; Harmens et al., 2018; Osborne, 2016; Pleijel et al., 2006).

Table 2.6 *Sensitivity of crops to O_3 based on the slope of the regression where relative yield was plotted against the 7h mean O_3 concentration. Values in brackets represent classification based on a non-significant (p>0.05) regression (Hayes and Mills, 2011). Please see Hayes and Mills (2011) for figures and data sources for each crop.*

Crop	Ozone sensitivity	Number of data points	r^2	Significance of slope	Regression equation
Agricultural crops					
Peas and beans (including peanut)	Sensitive	60	0.48	<0.001	y = -0.0072x + 0.96
Sweet potato	(Sensitive)	6	0.50	0.118	y = -0.0074x + 1.00
Turnip	Sensitive	14	0.54	0.003	y = -0.0060x + 1.00
Soybean	Sensitive	50	0.66	<0.001	y = -0.0051x + 1.01
Wheat	Sensitive	93	0.59	<0.001	y = -0.0049x + 0.95
Alfalfa	Sensitive	23	0.50	<0.001	y = -0.0046x + 1.10
Sugar beet	Moderately sensitive	25	0.32	0.003	y = -0.0035x + 1.03
Oilseed rape	Moderately sensitive	29	0.26	0.004	y = -0.0031x + 0.94
Maize	Moderately sensitive	23	0.66	<0.001	y = -0.0031x + 1.03
Rice	Moderately sensitive	145	0.44	<0.001	y = -0.0028x + 0.99
Potato	Moderately sensitive	70	0.05	0.066	y = -0.0027x + 0.98
Barley	Moderately sensitive	59	0.08	0.038	y = -0.002x + 0.99
Oat	(Moderately Resistant)	6	0.03	ns	y = 0.001x + 1.00
Horticultural crops					
Onion	Sensitive	9	0.56	0.020	y = -0.0067x + 1.08
Lettuce	Sensitive	26	0.18	0.035	y = -0.0065x + 1.21
Watermelon	(Sensitive)	10	0.23	0.156	y = -0.0043x + 1.02
Tomato	Moderately sensitive	41	0.20	0.004	y = -0.0039x + 1.01
Field mustard	Moderately sensitive	5	0.94	0.006	y = -0.0035x + 0.99
Strawberry	(Resistant)	6	0.01	0.856	y = -0.0004x + 1.07
Broccoli	(Moderately Resistant)	12	0.00	0.857	y = 0.0018x + 1.00
Tree crops					
Orange	Sensitive	4	0.62	0.043	y = -0.0071x + 1.00
Plum	Sensitive	10	0.54	0.015	y = -0.0054x + 0.89
Olive	(Moderately sensitive)	4	0.62	0.212	y = -0.0038x + 1.00
Grape	(Moderately resistant)	4	0.79	0.113	y = -0.0015x + 1.00

2.5 References

Angadi, S.V., Entz, M.H., 2002. Water Relations of Standard Height and Dwarf Sunflower Cultivars. Crop Sci. 42, 152–159.

Bernacchi, C.J., Leakey, A.D.B., Heady, L.E., Morgan, P.B., Dohleman, F.G., Mcgrath, J.M., Gillespie, K.M., Wittig, V.E., Rogers, A., Long, S.P., Ort, D.R., 2006. Hourly and seasonal variation in photosynthesis and stomatal conductance of soybean grown at future CO 2 and ozone concentrations for 3 years under fully open-air field conditions. Plant Cell Environ. 29, 2077–2090.

Bethenod, O., Tardieu, F., 1990. Water Use Efficiency in Field-Grown Maize : Effects of Soil Structure, in: Baltscheffsky, M. (Ed.), Current Research in Photosynthesis. Springer Netherlands, pp. 3531–3534.

Betzelberger, A.M., Yendrek, C.R., Sun, J., Leisner, C.P., Nelson, R.L., Ort, D.R., Ainsworth, E.A., 2012. Ozone Exposure Response for U.S. Soybean Cultivars: Linear Reductions in Photosynthetic Potential, Biomass, and Yield. PLANT Physiol. 160, 1827–1839.

Biswas, D.K., Xu, H., Li, Y.G., Sun, J.Z., Wang, X.Z., Han, X.G., Jiang, G.M., 2008. Genotypic differences in leaf biochemical, physiological and growth responses to ozone in 20 winter wheat cultivars released over the past 60 years. Global Change Biology 14, 46–59.

Bou Jaudé, M., Katerji, N., Mastrorilli, M., Rana, G., 2008. Analysis of the effect of ozone on soybean in the Mediterranean region. I. The consequences on crop-water status. Eur. J. Agron. 28, 508–518.

Bunce, J.A., 1998. Effects of environment during growth on the sensitivity of leaf conductance to changes in humidity. Glob. Change Biol. 4, 269–274.

Connor, D.J., Jones, T.R., 1985. Response of sunflower to strategies of irrigation II. Morphological and physiological responses to water stress. Field Crops Res. 12, 91–103.

Correia, M.J., Pereira, J.S., Chaves, M.M., Rodrigues, M.L., Pacheco, C.A., 1995. ABA xylem concentrations determine maximum daily leaf conductance of field-grown Vitis vinifera L. plants. Plant Cell Environ. 18, 511–521.

Csajbók, J., Kutasy, E., Borbély-Hunyadi, É., Lesznyák, M., 2008. Effect of soil moisture on the photosynthetic activity and transpiration of plants. Cereal Res. Commun. 36, 603–606.

Davies, W.J., Tardieu, F., Trejo, C.L., 1994. How Do Chemical Signals Work in Plants that Grow in Drying Soil? Plant Physiol. 104, 309–314.

During, H., 1987. Stomatal responses to alterations of soil and air humidity in grapevines. Vitis - J. Grapevine Res. 26, 9–18.

Fambrini, M., Pugliesi, C., Vernieri, P., Pardossi, A., Baroncelli, S., 1994. Characterization of a wilty sunflower (*Helianthus annuus* L.) mutant II. Water relations, stomatal conductance, abscisic acid content in leaves and xylem sap of plants subjected to water deficiency. J. Exp. Bot. 45, 1809–1815.

Fay, P.A., Knapp, A.K., 1996. Photosynthetic and Stomatal Responses to Variable Light in a Cool-Season and a Warm-Season Prairie Forb. Int. J. Plant Sci. 157, 303–308.

Flexas, J., Escalona, J.M., Medrano, H., 1999. Water stress induces different levels of photosynthesis and electron transport rate regulation in grapevines. Plant Cell Environ. 22, 39–48.

Fuhrer, J., 1994. The critical level for ozone to protect agricultural crops – An assessment of data from European open-top chamber experiments. In: Fuhrer J. & Achermann, B., (Eds). Critical Levels for Ozone. UNECE Workshop Report, Schriftenreihe der FAC Berne-Liebefeld, pp. 42-57.

Gerosa, G., Marzuoli, R., Cieslik, S., Ballarin-Denti, A., 2004. Stomatal ozone fluxes over a barley field in Italy. "Effective exposure" as a possible link between exposure-and flux-based approaches. Atmospheric Environment 38, 2421-2432.

Gerosa, G., Marzuoli, R., Rossini, M., Panigada, C., Meroni, M., Colombo, R., Faoro, F., Iriti, M., 2009b. A flux-based assessment of the effects of ozone on foliar injury, photosynthesis, and yield of bean (cv. Borlotto Nano Lingua di Fuoco) in open-top chambers. Environmental Pollution 157, 1727-1736.

Gilbert, M.E., Holbrook, N.M., Zwieniecki, M.A., Sadok, W., Sinclair, T.R., 2011. Field confirmation of genetic variation in soybean transpiration response to vapor pressure deficit and photosynthetic compensation. Field Crops Res. 124, 85–92.

Gillespie, K.M., Xu, F., Richter, K.T., Mcgrath, J.M., Markelz, R.J.C., Ort, D.R., Leakey, A.D.B., Ainsworth, E.A., 2012. Greater antioxidant and respiratory metabolism in field-grown soybean exposed to elevated O3 under both ambient and elevated CO2: Antioxidant response to elevated O3 and CO2. Plant Cell Environ. 35, 169–184.

Gollan, T., Richards, R., Passioura, J., Rawson, H., Munns, R., Johnson, D., 1986. Soil Water Status Affects the Stomata1. Aust. J. Plant Physiol. 13, 459.

González-Fernández, I., Elvira, S., Calatayud, V., Calvo, E., Aparicio, P., Sánchez, M., Alonso, R., Bermejo Bermejo, V. (2016). Ozone effect on the physiology and Marketable biomass of leafy vegetables under Mediterranean conditions: spinach (*Spinacia oleracea* L.) and Swiss chard (*Beta vulgaris* L. *var. cycla*). Agriculture, Ecosystems and Environment 235, 215-228.

Goumenaki, E., González-Fernández, I., Papanikolaou, A., Papadopoulou, D., Askianakis, C., Kouvarakis, G., Barnes, J., 2007. Derivation of ozone flux-yield relationships for lettuce: A key horticultural crop. Environmental Pollution 146, 699-706.

Grünhage, L., Pleijel, H., Mills, G., Bender, J., Danielsson, H., Lehmann, Y., Castell, J.-F., Bethenod, O., 2012. Updated stomatal flux and flux-effect models for wheat for quantifying effects of ozone on grain yield, grain mass and protein yield. Environ. Pollut. 165, 147–157.

Guilioni, L., Cellier, P., Ruget, F., Nicoullaud, B., Bonhomme, R., 2000. A model to estimate the temperature of a maize apex from meteorological data. Agric. For. Meteorol. 100, 213–230.

Harmens, H., Hayes, F., Mills, G., Sharps, K., Osborne, S., Pleijel, H., 2018. Wheat yield responses to stomatal uptake of ozone: Peak vs rising background ozone conditions. Atmospheric Environment 173, 1-5.

Hayes and Mills, 2011. The range of sensitivity of crops to ozone. In: Mills, G., Harmens, H. (Eds.). Ozone pollution: A hidden threat to food security. Centre for Ecology & Hydrogogy, Bangor, UK. ISBN: 978-1-906698-27-0.

Hirasawa, T., Wakabayashi, K., Touya, S., Ishihara, K., 1995. Stomatal Responses to Water Deficits and Abscisic Acid in Leaves of Sunflower Plants (Helianthus annuus L.) Grown under Different Conditions. Plant Cell Physiol. 36, 955–964.

Jacobs, C.M.J., van den Hurk, B.M.M., de Bruin, H.A.R., 1996. Stomatal behaviour and photosynthetic rate of unstressed grapevines in semi-arid conditions. Agric. For. Meteorol. 80, 111–134.

Jones, G.V., Duchêne, E., Tomasi, D., Yuste, J., Braslavska, O., Schultz, H., Martinez, C., Boso, S., Langellier, F., Perruchot, C., Guimberteau, G., 2005. Changes in European winegrape phenology and relationships with climate. Presented at the XIV International GESCO Viticulture Congress, pp. pp. 54–61.

Körner, C., Scheel, J.A., Bauer, H., 1979. Maximum leaf diffusive conductance in vascular plants. Photosynthetica 13, 45–82.

Lu, P., Yunusa, I.A.M., Walker, R.R., Iler, W.J., 2003. Regulation of canopy conductance and transpiration and their modelling in irrigated grapevines. Funct. Plant Biol. 30, 689–698.

Machado, E.C., Lagôa, A.M.M.A., 1994. Trocas gasosas e condutância estomática em três espécies de gramíneas. Bragantia 53, 141–149.

Marzuoli, R., Finco, A., Chiesa, M., Gerosa, G., 2016. A dose-response relationship for marketable yield reduction of two lettuce (*Lactuca sativa* L.) cultivars exposed to tropospheric ozone in Southern Europe. Environmental Science and Pollution Research, 1-10.

Massman, W.J., Pederson, J., Delany, A., Grantz, D., den Hartog, G., Neumann, H.H., Oncley, S.P., Pearson, R., Shaw, R.H., 1994. An evaluation of the regional acid deposition model surface module for ozone uptake at three sites in the San Joaquin Valley of California. J. Geophys. Res. 99, 8281.

Medrano, H., lito, Escalona, J., M, Cifre, J., Bota, J., Flexas, J., 2003. A ten-year study on the physiology of two Spanish grapevine cultivars under field conditions: effects of water availability from leaf photosynthesis to grape yield and quality. Funct. Plant Biol. 30, 607–619.

Naor, A., Wample, R.L., 1995. A rapid field method for measuring net assimilation rate-stomatal conductance relationship: a feasibility test using grapevine leaves. Sci. Hortic. 60, 287–292.

Olioso, A., Bethenod, O., Rambal, S., Thamitchian, M., 1995. Comparison of empirical leaf photosynthesis and stomatal conductance models. Presented at the 10th International Photosynthesis Congress, p. 4pp.

Osborne, S.A., Mills, G., Hayes, F, Ainsworth, E.A., Büker, P., Emberson, L., 2016. Has the sensitivity of soybean cultivars to ozone pollution increased with time? An analysis of published dose-response data. Global Change Biology 22, 3097-3111.

Ozier-Lafontaine, H., Lafolie, F., Bruckler, L., Tournebize, R., Mollier, A., 1998. Modelling competition for water in intercrops: theory and comparison with field experiments. Plant Soil 204, 183–201.

Patakas, A., Kofidis, G., Bosabalidis, A.M., 2003. The relationships between CO2 transfer mesophyll resistance and photosynthetic efficiency in grapevine cultivars. Sci. Hortic. 97, 255–263.

Petit, A.N., Fontaine, F., Clément, C., Vaillant-Gaveau, N., 2008. Photosynthesis limitations of grapevine after treatment with the fungicide fludioxonil. J. Agric. Food Chem. 56, 6761–6767.

Pleijel, H., Eriksen, A.B., Danielsson, H., Bondesson, N., Sellden, G., 2006. Differential ozone sensitivity in an old and a modern Swedish wheat cultivar – grain yield and quality, leaf chlorophyll and stomatal conductance. Environmental and Experimental Botany 56, 63–71.

Quick, W.P., Chaves, M.M., Wendler, R., David, M., Rodrigues, M.L., Passaharinho, J.A., Pereira, J.S., Adcock, M.D., Leegood, R.C., Stitt, M., 1992. The effect of water stress on photosynthetic carbon metabolism in four species grown under field conditions. Plant Cell Environ. 15, 25–35.

Rivelli, A.R., Lovelli, S., Perniola, M., 2002. Effects of salinity on gas exchange, water relations and growth of sunflower (Helianthus annuus). Funct. Plant Biol. 29, 1405–1415.

Rochette, P., Pattey, E., Desjardins, R.L., Dwyer, L.M., Stewart, D.W., Dubé, P.A., 1991. Estimation of maize (Zea mays L.) canopy conductance by scaling up leaf stomatal conductance. Agric. For. Meteorol. 54, 241–261.

Rodriguez, J.L., Davies, W.J., 1982. The Effects of Temperature and ABA on Stomata of Zea mays L. J. Exp. Bot. 33, 977–987.

Sadras, V.O., Villalobos, F.J., Fereres, E., Wolfe, D.W., 1993. Leaf responses to soil water deficits: Comparative sensitivity of leaf expansion rate and leaf conductance in field-grown sunflower (Helianthus annuus L.). Plant Soil 153, 189–194.

Sanguineti, M.C., Tuberosa, R., Landi, P., Salvi, S., Maccaferri, M., Casarini, E., Conti, S., 1999. QTL analysis of drought-related traits and grain yield in relation to genetic variation for leaf abscisic acid concentration in field-grown maize. J. Exp. Bot. 50, 1289–1297.

Schultz, H.R., 2003a. Extension of a Farquhar model for limitations of leaf photosynthesis induced by light environment, phenology and leaf age in grapevines (Vitis vinifera L. cvv. White Riesling and Zinfandel). Funct. Plant Biol. 30, 673–687.

Schultz, H.R., 2003b. Differences in hydraulic architecture account for near-isohydric and anisohydric behaviour of two field-grown Vitis vinifera L. cultivars during drought. Plant Cell Environ. 26, 1393–1405.

Schurr, U., Gollan, T., Schulze, E.D., 1992. Stomatal response to drying soil in relation to changes in the xylem sap composition of Helianthus annuus. II. Stomatal sensitivity to abscisic acid imported from the xylem sap. Plant Cell Environ. 15, 561–567.

Simpson D., Fagerli H., Jonson J.E., Tsyro S., Wind, P., 2003. Transboundary Acidification, Eutrophication and Ground Level Ozone in Europe. Part I - Unified EMEP Model Description. Norwegian Meteorological Institute, Oslo, EMEP MSC-W Note 1/2003, http://www.emep.int/publ/common_publications.html, 104p.

Sinclair, T.R., Bingham, G.E., Lemon, E.R., Allen, L.H., 1975. Water Use Efficiency of Field-grown Maize during Moisture Stress. Plant Physiol. 56, 245–249.

Steduto, P., Albrizio, R., Giorio, P., Sorrentino, G., 2000. Gas-exchange response and stomatal and non-stomatal limitations to carbon assimilation of sunflower under salinity. Environ. Exp. Bot. 44, 243–255.

Stigter, C.J., Lammers, B., 1974. III. Results regarding the improved diffusion porometer in growth rooms and fields of Indian corn (Zea mays). In: Landbouwhogesch., M. (Ed.), Leaf Diffusion Resistance to Water Vapour and Its Direct Measurement . Mededelingen Landbouwhogeschool, Wageningen, pp. 1–76.

Taconet, O., Olioso, A., Ben Mehrez, M., Brisson, N., 1995. Seasonal estimation of evaporation and stomatal conductance over a soybean field using surface IR temperatures. Agric. For. Meteorol. 73, 321–337.

Tardieu, F., Katerji, N., Bethenod, O., Zhang, J., Davies, W.J., 1991. Maize stomatal conductance in the field: its relationship with soil and plant water potentials, mechanical constraints and ABA concentration in the xylem sap. Plant Cell Environ. 14, 121–126.

Tardieu, F., Zhang, J., Davies, W.J., 1992. What information is conveyed by an ABA signal from maize roots in drying field soil? Plant Cell Environ. 15, 185–191.

Teubner, F., 1985. Messung der Photosynthese und Transpiration an Weizen, Kartoffel und Sonnenblume. Diplomarbeit University Bayreuth, West Germany.

Tramontini, S., van Leeuwen, C., Domec, J.C., Destrac-Irvine, A., Basteau, C., Vitali, M., Mosbach-Schulz, O., Lovisolo, C., 2013. Impact of soil texture and water availability on the hydraulic control of plant and grape-berry development. Plant Soil 368, 215–230.

Turner, N.C., 1970. Response of Adaxial and Abaxial Stomata to Light. New Phytol. 69, 647–653.

Turner, N.C., Begg, J.E., 1973. Stomatal Behavior and Water Status of Maize, Sorghum, and Tobacco under Field Conditions. I. At High Soil Water Potential. Plant Physiol. 51, 31–36.

Turner, N.C., Schulze, E.D., Gollan, T., 1984. The Responses of Stomata and Leaf Gas Exchange to Vapour Pressure Deficits and Soil Water Content. I. Species Comparisons at High Soil Water Contents. Oecologia 63, 338–342.

Turner, N.C., Schulze, E.D., Gollan, T., 1985. The Responses of Stomata and Leaf Gas Exchange to Vapour Pressure Deficits and Soil Water Content. II. In the Mesophytic Herbaceous Species Helianthus annuus. Oecologia 65, 348–355.

Vitale, L., Di Tommasi, P., Arena, C., Fierro, A., Virzo De Santo, A., Magliulo, V., 2007. Effects of water stress on gas exchange of field grown Zea mays L. in Southern Italy: An analysis at canopy and leaf level. Acta Physiol. Plant. 29, 317–326.

Vitali, M., Chitarra, W., Galetto, L., Bosco, D., Marzachì, C., Gullino, M.L., Spanna, F., Lovisolo, C., 2013. Flavescence dorée phytoplasma deregulates stomatal control of photosynthesis in Vitis vinifera. Ann. Appl. Biol. 162, 335–346.

Wample, R.L., Thornton, R.K., 1984. Differences in the response of sunflower (Helianthus annuus) subjected to flooding and drought stress. Physiol. Plant. 61, 611–616.

Ward, D.A., Bunce, J.A., 1986. Responses of net photosynthesis and conductance to independent changes in the humidity environments of the upper and lower surfaces of leaves of sunflower and soybean. J. Exp. Bot. 37, 1842–1853.

Wilson, K.B., Bunce, J.A., 1997. Effects of carbon dioxide concentration on the interactive effects of temperature and water vapour on stomatal conductance in soybean. Plant Cell Environ. 20, 230–238.

Winkel, T., Rambal, S., 1990. Stomatal conductance of some grapevines growing in the field under a Mediterranean environment. Agric. For. Meteorol. 51, 107–121.

Winkel, T., Rambal, S., 1993. Influence of Water Stress on Grapevines Growing in the Field: From Leaf to Whole-Plant Response. Funct. Plant Biol. 20, 143–157.

Wookey, P.A., Atkinson, C.J., Mansfield, T.A., Wilkinson, J.R., 1991. Control of Plant Water Deficits Using the "Snow and Tingey System" and Their Influence on the Water Relations and Growth of Sunflower. J. Exp. Bot. 42, 589–595.

Zhang, J., Davies, W.J., 1989. Sequential Response of Whole Plant Water Relations to Prolonged Soil Drying and the Involvement of Xylem Sap ABA in the Regulation of Stomatal Behaviour of Sunflower Plants. New Phytol. 113, 167–174.

Zsófi, Z., Gál, L., Szilágyi, Z., Szü Cs, E., Marschall, M., Nagy, Z., Bálo, B., 2009. Use of stomatal conductance and pre-dawn water potential to classify terroir for the grape variety Kékfrankos. Aust. J. Grape Wine Res. 15, 36–47.

3 DO$_3$SE model parameterisations for additional or young forest tree species

3.1 Evergreen tree species

Parameterisation of the O$_3$ stomatal flux model DO$_3$SE for Mediterranean evergreen species is based on the parameterisation for mature holm oak (*Quercus ilex*) trees (see Table III.11 in Chapter 3 of the Modelling and Mapping Manual). **Table 3.1** contains the parameterisation for young holm oak trees grown at two experimental sites in Spain (Alonso et al., 2013; Calatayud et al., 2011) and one experimental site in Italy (Gerosa et al., 2015) that could be applied for local scale assessments of O$_3$ impacts on Holm oak. Table 3.1 also contains the parameterisation for additional evergreen tree species, i.e. for mature Scots pine (*Pinus sylvestris*) for application in the Atlantic region (Büker et al., 2015) and for young evergreen tree species in the Mediterranean region for Aleppo pine (*Pinus halepensis*; modified from Elvira et al., 2007), carob tree (*Ceratonia siliqua*; Alonso et al., in prep.), olive (*Olea europaea*; Alonso et al., 2013), strawberry tree (*Arbutus unedo*; Gerosa et al., pers. comm., to be included in Alonso et al., in prep.) and kermes oak (Quercus coccifera; Elvira et al., 2004). The parameterisation for the Mediterranean evergreen species is from experiments used to derive flux-based critical levels for Mediterranean evergreen species (see Table III.12 and Figure III.12 in Chapter 3 of the Modelling and Mapping Manual) and represents the physiology of young trees that were grown under well-watered conditions. The parameterisation for young trees grown in experimental conditions might be slightly different from the parameterisation for mature trees grown under natural conditions. An overview of the references is provided in **Table 3.2** (mature Scots pine) and **3.3** (young Mediterranean evergreen species).

Table 3.1 *Parameterisation of the O$_3$ stomatal flux model for mature Scots pine and for young Mediterranean evergreen species.*

Parameter	Units	Forest evergreen tree species parameterisation - POD$_1$SPEC[i]								
Region		Atlantic	Mediterranean							
Forest type		Conifer evergreen	Conifer evergreen	Broadleaf evergreen	Broadleaf evergreen	Broadleaf evergreen	Broadleaf evergreen	Broadleaf evergreen	Broadleaf evergreen	Broadleaf evergreen
Tree species[ii]	Common name	Scots pine	Aleppo pine	Carob tree	Olive	Strawberry tree	Kermes oak	Holm oak		
	Latin name	*Pinus sylvestris*	*Pinus halepensis*	*Ceratonia siliqua*	*Olea europaea*	*Arbutus unedo*	*Quercus coccifera*	*Quercus ilex* Ebro Delta (Spain)	*Quercus ilex* ssp ballota Valencia (Spain)	*Quercus ilex* ssp ilex Curno (Italy)
g_{max}	mmol O$_3$ m^{-2} PLA s^{-1}	190	230	220	340	155	240	235 ssp ilex 200 ssp ballota	210	235
f_{min}	fraction	0.1	0.025	0.015	0.033	0.1	0.08	0.11	0.02	0.02

light_a	-	0.006	0.013	0.009	0.009	0.009	0.009	0.007	0.012	0.009
T_{min}	°C	0	10	7	7	5.5	5	10	1	2
T_{opt}	°C	20	27	23	27	30	25	30	23	23
T_{max}	°C	36	38	39	42	40	40	41	39	38
VPD_{max}	kPa	0.6	1.0	1.5	2.2	3.5	2.2	2	2.2	2.2
VPD_{min}	kPa	2.8	3.2	3.3	4	8.5	4	4.5	4.0	4.0
ΣVPD_{crit}	kPa	-	-	-	-	-	-	-	-	-
PAW_t[iii]	%	-	-	-	-	-	-	-	-	-
SWC_{max}	% volume	-	-	-	-	-	-	-	-	-
SWC_{min}	% volume	-	-	-	-	-	-	-	-	-
SWP_{max}	MPa	-0.7	-1[ii]	-	-	-1.4	-0.5[ii]	-0.5[ii]	-	-
SWP_{min}	MPa	-1.5	-3[ii]	-	-	-4.8	-2.5[ii]	-2.5[ii]	-	-
f_{O3}	fraction	-	-	-	-	-	-	-	-	-
Astart_FD	day of year	f_{Temp}[iii]	1	1	1	1	1	1	1	1
Aend_FD	day of year	f_{Temp}[iii]	365	365	365	365	365	365	365	365
Leaf dimension	cm	0.8	0.2	4.5	1.5	4.5	2.0	3.0	3.0	3.0
Canopy height[iv]	m	20	15	6	6	6	2	20	20	20
f_{phen_a}	fraction	0.8	1	1	0.4	1	1	1	1	1
f_{phen_b}	fraction	(1.0)	1	1	1	1	1	1	1	1
f_{phen_c}	fraction	1.0	0.4	0.4	1	1	0.6	1	1	1
f_{phen_d}	fraction	(1.0)	1	1	1	1	1	1	1	1
f_{phen_e}	fraction	0.8	1	1	0.4	1	1	1	1	1
$f_{phen\_1\_FD}$	no. of days	40	0	0	50 (after delay of 120 days)[v]	-	0	-	-	-
$f_{phen\_2\_FD}$	no. of days	(200)	115	90	70	-	110	-	-	-
$f_{phen\_3\_FD}$	no. of days	(200)	120	60	35	-	95	-	-	-
$f_{phen\_4\_FD}$	no. of days	40	0	0	0	-	0	-	-	-
LIM_{start_FD}	year day	-	65	120	260	-	80	-	-	-
LIM_{send_FD}	year day	-	365	320	365	-	340	-	-	-

The values in brackets represent "dummy" values required for DO$_3$SE modelling purposes. "-" = parameterisation not required for this species.

[i] The parameterisation for Scots pine is for mature trees. The parameterisations for evergreen Mediterranean species is for young trees grown under experimental conditions used to derive critical levels and represent seedling physiology under well-watered conditions.

[ii] Pre-dawn leaf water potential (LWP) was used as surrogate for soil water potential.

[iii] f_{temp}: growing season is assumed to occur when air temperatures fall within T_{min} and T_{max} thresholds of f_{temp} relationship. Actual data are recommended if available!
[iv] Average height for adult trees.
[v] Please note that for *Olea europaea*, the increase (duration = 50 days) of the early year phenology (fphen = 0.4) to full phenology (fphen = 1) only starts at day of year 120! For the accumulation period from day of year 1 to day of year 120, a fphen of 0.4 should be assumed.

Table 3.2   *References for the parameterisation of the DO$_3$SE model for mature Scots pine in the Atlantic region.*

Species	Region	Parameter	References
Scots pine (*Pinus sylvestris*)	Atlantic	g_{max} [value – mmol O_3 m^{-2} PLA s^{-1}]	Beadle et al.(1985) [175]; Sturm et al. (1998) [171]; Whitehead et al. (1984) [188]
		f_{min}	Körner et al. (1995)
		light_a	Beadle et al. (1985); Ng (1979); Sturm et al. (1998)
		T_{min}, T_{opt}, T_{max}	Beadle et al. (1985); Ng (1979); Sturm et al. (1998)
		VPD_{min}, VPD_{max}	Beadle et al. (1985); Ng (1979); Sturm et al. (1998); Whitehead et al. (1984)
		SWP_{min}, SWP_{max}	Ng (1979); Sturm et al. (1998)
		f_{phen}	Körner et al. (1995)

Table 3.3   *References for the parameterisation of the DO$_3$SE model for young Mediterranean evergreen species.*

Region	Species	References
Mediterranean	**Aleppo pine (*Pinus halepensis*)**	Modified from Elvira et al., 2007
	Carob tree (*Ceratonia siliqua*)	Alonso et al. (in prep)
	Olive (*Olea europea*)	Alonso et al. (in prep)
	Strawberry tree (*Arbutus unedo*)	Alonso et al. (in prep)
	Kermes oak (*Quercus coccifera*)	Elvira et al. (2004)
	Holm oak (*Quercus ilex*)	Ebro Delta: Alonso et al. (2013); Valencia: Calatayud et al. (2011); Curno: Gerosa et al. (2015)

3.2 Broadleaf deciduous tree species

Table 3.4 contains the parameterisation of DO₃SE for mature temperate oak (Atlantic region), poplar species (Boreal and Continental region) and beech in the Mediterranean region. The references for these species are provided in **Table 3.5.**

Table 3.4 *Parameterisation of the O_3 stomatal flux model for mature temperate oak, poplar species and Mediterranean beech.*

Para-meter	Units	Forest broadleaf deciduous tree species parameterisation - POD₁SPEC		
Region		Atlantic	Boreal, Continental (Atlantic, Pannonian, Steppic)	Mediterranean
Forest type		Broadleaf deciduous		
Tree species	Common name	Temperate oak	Poplar	Beech
	Latin name	*Quercus robur/petraea*	*Populus spec.*	*Fagus sylvatica*
g_{max}	mmol O_3 m⁻² PLA s⁻¹	255	440	155
f_{min}	fraction	0.06	0.1	0.02
light_a	-	0.003	0.007	0.006
T_{min}	°C	0	11	4
T_{opt}	°C	20	27	21
T_{max}	°C	35	36	37
VPD_{max}	kPa	1.0	2.1	1.0
VPD_{min}	kPa	3.25	3.7	4.0
ΣVPD_{crit}	kPa	-	-	-
PAW_t	%	-	-	-
SWC_{max}	% volume	-	-	-
SWC_{min}	% volume	-	-	-
SWP_{max}	MPa	-0.5	-0.05	-2.0
SWP_{min}	MPa	-1.2	-1.25	-3.8
f_{O3}	fraction	-	-	-
Astart_FD	day of year	Latitude model	Latitude model	Latitude model
Aend_FD	day of year	Latitude model	Latitude model	Latitude model
Leaf dimension	cm	5	10	7
Canopy height	m	20	20	20
f_{phen_a}	fraction	0	0	0
f_{phen_b}	fraction	(1.0)	(1.0)	(1.0)
f_{phen_c}	fraction	1.0	1.0	1.0
f_{phen_d}	fraction	(1.0)	(1.0)	(1.0)
f_{phen_e}	fraction	0	0	0
$f_{phen\_1\_FD}$	no. of days	20	20	15
$f_{phen\_2\_FD}$	no. of days	(200)	(200)	(200)
$f_{phen\_3\_FD}$	no. of days	(200)	(200)	(200)
$f_{phen\_4\_FD}$	no. of days	30	20	20
LIM_{start_FD}	year day	-	-	-
LIM_{send_FD}	year day	-	-	-

The values in brackets represent "dummy" values required for DO₃SE modelling purposes. "-" = parameterisation not required for this species.

Table 3.5   *References for the parameterisation of the DO$_3$SE model temperate oak, poplar species and Mediterranean beech.*

Species	Parameter	References
Temperate oak	g$_{max}$ [value – mmol O$_3$ m^{-2} PLA s^{-1}]	*Quercus petraea*: Breda et al. (1995) [228]; Epron & Dreyer (1993) [177]; Breda et al. (1993a) [233]; Breda et al. (1993b) [275]; *Quercus robur*: Epron & Dreyer (1993) [198]; Breda et al. (1993b) [325]; Dolman & Van den Burg (1988) [264]
	f$_{min}$	Breda et al. (1993b)
	light_a	Breda et al. (1995); Dolman & Van den Burg (1988)
	VPD$_{min}$, VPD$_{max}$	Dolman & Van den Burg (1988)
	SWP$_{min}$, SWP$_{max}$	Epron & Dreyer (1993); Breda et al (1993a); Breda et al. (1993b); Vivin et al. (1993)
	f$_{phen}$	Breda et al. (1993b); Breda et al. (1995)
Poplar species	g$_{max}$ [value – mmol O$_3$ m^{-2} PLA s^{-1}]	Ceulemans et al. (1989) [313]; Manzanera and Martínez-Chacón (2007) [160]; Marzuoli et al. (2009) [575]; Oliver et al. (2012) [343]; Tricker et al. (2009) [228]; Voltas et al. (2006) [631, 520, 631, 440]; (Zhang et al., 1999) [226]; Le Thiec (pers. comm.)
	f$_{min}$	
	light_a	Ceulemans et al. (1989); Manzanera and Martínez-Chacón (2007); Marzuoli et al. (2009)
	T$_{min}$, T$_{opt}$, T$_{max}$	Marzuoli et al. (2009)
	VPD$_{min}$, VPD$_{max}$	Marzuoli et al. (2009)
	SWP$_{min}$, SWP$_{max}$	As for Continental beech
	f$_{phen}$	As for Continental beech; f$_{phen\_e}$ from Marzuoli et al. (2009)
	Leaf dimension	As for Continental beech
	Canopy height	As for Continental beech
Mediterranean beech	g$_{max}$ [value – mmol O$_3$ m^{-2} PLA s^{-1}]	Raftoyannis & Radoglou (2002) [156]; cf. Körner et al. (1979) [100; 140]; Nunn et al. (2005) [147]; Matyssek et al. (2004) [132]; Aranda et al. (2000) [183]
	T$_{min}$, T$_{opt}$, T$_{max}$	Damesin & Rambal (1998); Rico et al (1996)
	VPD$_{min}$, VPD$_{max}$	Grassi & Magnani (2005); Aranda et al (2000); Damesin & Rambal (1998); Rico et al (1996)
	SWP$_{min}$, SWP$_{max}$	Aranda et al. (2000); Damesin & Rambal (1998); Rico et al. (1996); Mediavilla & Escudero (2003); Grassi & Magnani (2005)

3.3 References

Alonso, R., Elvira, S., González-Fernández, I., Calvete, H., García-Gómez, H., Bermejo, V. (2013). Drought stress does not protect *Quercus ilex* L. from ozone effects: results from a comparative study of two subspecies differing in ozone sensitivity. Plant Biology 16: 375-384.

Aranda, I., Gil, L., Pardos, A.J. (2000). Water relations and gas exchange in *Fagus sylvatica* L. and *Quercus petraea* (Mattuschka) Liebl. In a mixed stand at their southern limit of distribution in Europe. Trees 14: 344-352.

Beadle, C.L., Neilson, R.E., Talbot, H., Jarvis, P.G. (1985). Stomatal conductance and photosynthesis in a mature scots pine forest. I. Diurnal, seasonal and spatial variation in shoots. J. of Appl. Ecol. 22: 557-571.

Breda, N., Cochard, H., Dreyer, E. and Granier, A. (1993a). Water transfer in a mature oak stand (*Quercus petraea*): seasonal evolution and effects of a severe drought. Canadian Journal Of Forest Research 23:1136-1143.

Breda, N., Cochard, H., Dreyer, E., Granier, A. (1993b). Field comparison of transpiration, stomatal conductance and vulnerability to cavitation of *Quercus petraea* and *Quercus robur* under water stress. Annales des Sciences Forestieres 50: 571-582.

Breda, N., Granier, A., Aussenac, G. (1995). Effects of thinning on soil and tree water relations, transpiration and growth in an oak forest (*Quercus petraea* (Matt.) Liebl.) Tree Physiology 15: 295-306.

Büker, P., Feng, Z., Uddling, J., Briolat, A., Alonso, R., Braun, S., Elvira, S., Gerosa, G., Karlsson, P.E., Le Thiec, D., Marzuoli, R., Mills, G., Oksanen, E., Wieser, G., Wilkinson, M., Emberson, L. D. (2015). New flux based dose-response relationships for ozone for European forest tree species. Environmental Pollution 206: 163-174.

Calatayud, V., Cerveró, J., Calvo, E., García-Breijo, F.-J.,Reig-Armiñana, J., Sanz, M.J. (2011). Responses of evergreen and deciduous *Quercus* species to enhanced ozone levels. Environmental Pollution 159: 55-63.

Ceulemans, R., Hinckley, T.M., Impens, I. (1989). Stomatal response of hybrid poplar to incident light, sudden darkening and leaf excision. Physiol. Plant. 75: 174-182.

Damesin C., Rambal S., Joffre R. (1998). Co-occurrence of trees with different leaf habit: a functional approach on Mediterranean oaks. Acta Oecologica 19: 195-204.

Dolman, A.J., van den Burg, G.J. (1988) Stomatal behaviour in an oak canopy. Agricultural and Forest Meteorolgy. 43: 99-108.

Elvira, S., Alonso, R., Gimeno, B.S. (2007). Simulation of stomatal conductance for Aleppo pine to estimate its ozone uptake. Environmental Pollution 146: 617-623.

Elvira, S., Bermejo, V., Manrique, E., Gimeno, B.S. (2004). On the response of two populations of *Quercus coccifera* to ozone and its relationship with ozone uptake. Environmental Pollution 146: 617-623.

Epron, D., Dreyer, E. (1990). Stomatal and non-stomatal limitation of photosynthesis by leaf water deficits in three oak species: a comparison of gas exchange and chlorophyll a fluorescence data. Annals of Forest Science 47: 435-450.

Gerosa, G., Fusaro, L., Mongo, R., Finco, A., Fares, S., Manes, F., Marzuoli, R. (2015). A flux-based assessment of above and below ground biomass of Holm oak (Quercus ilex L.) seedlings after one season of exposure to high ozone concentrations. Atmospheric Environment 113: 41-49.

Grassi G., Magnani F. (2005). Stomatal, mesophyll conductance and biochemical limitations to photosynthesis as affected by drought and leaf ontogeny in ash and oak trees. Plant, Cell and Environment 28: 834-849.

Körner, CH., Perterer, J., Altrichter, CH., Meusburger, A., Slovik, S., Zoschg, M. (1995). Ein einfaches empirisches Modell zur Berechnung der jahrlichen Schadgasaufnahme von Fichten- und Kiefernadeln. Allg. Forst- und Jagzeitung 165: 1-9.

Körner, C., Scheel, J. A., Bauer, H. (1979). Maximum leaf diffusive conductance in vascular plants. Photosynthetica 13**:** 45-82.

Manzanera, J.A., Martínez-Chacón, M.F (2007). Ecophysiological competence of Populus alba L., Fraxinus angustifolia Vahl., and Crataegus monogyna Jacq. used in plantations for the recovery of riparian vegetation. Environ. Manage. 40: 902–912.

Marzuoli, R., Gerosa, G., Desotgiu, R., Bussotti, F., Ballarin-Denti, A. (2009). Ozone fluxes and foliar injury development in the ozone-sensitive poplar clone Oxford (*Populus maximowiczii* × *Populus berolinensis*): A dose-response analysis. Tree Physiol. 29: 67-76

Matyssek, R., Wieser, G., Nunn, A. J., Kozovits, A. R., Reiter, I. M., Heerdt, C., Winkler, J. B., Baumgarten, M., Häberle, K. H., Grams, T. E. E., Werner, H., Fabian, P., Havranek, W. M. (2004). Comparison between AOT40 and ozone uptake in forest trees of different species, age and site conditions. Atmospheric Environment 38**:** 2271-2281.

Mediavilla, S., Escudero, A.E. (2003). Stomatal responses to drought at a Mediterranean site: a comparative study of co-occurring woody species differing in leaf longevity. Tree Physiology 23: 987–996.

Ng, P. (1979) response of stomata to environmental variables in *Pinus sylvestris* L. PhD Thesis. University of Edinburgh.

Nunn, A., Kozovits, A. R., Reiter, I. M., Heerdt, C., Leuchner, M., Lütz, C., Liu, X., Löw, Winkler, J. B., Grams, T. E. E., Häberle, K.-H., Werner, H., Fabian, P., Rennenberg, H., Matyssek, R. (2005). Comparison of ozone uptake and sensitivity between a phytotron study with young beech and a field experiment with adult beech (*Fagus sylvatica*). Environmental Pollution 137: 494-506.

Oliver, R.J., Taylor, G., Finch, J.W. (2012). Assessing the impact of internal conductance to CO2 in a land-surface scheme: Measurement and modelling of photosynthesis in *Populus nigra*. Agric. For. Meteorol. 152: 240–251.

Raftoyannis, Y. and Radoglou, K. (2002). Physiological responses of beech and sessile oak in a natural mixed stand during a dry summer. Annals of Botany 89: 723-730.

Rico M., Gallego H.A., Moreno G., Santa Regina I. (1996). Stomatal response of Quecus pyrenaica Willd to environmental factors in two sites differing in their annual rainfall (Sierra de Gata, Spain. Annales des Sciences Forestières 53: 221-234.

Sturm, N., Kostner, B., Hartung, W., Tenhunen, J.D. (1998). Environmental and endogenous controls on leaf- and stand-level water conductance in a Scots pine plantation. Annales des Sciences Forestieres 55: 237-253.

Tricker, P.J., Pecchiari, M., Bunn, S.M., Vaccari, F.P., Peressotti, A., Miglietta, F., Taylor, G. (2009). Water use of a bioenergy plantation increases in a future high CO2 world. Biomass Bioenergy 33: 200–208.

Vivin, P., Aussenac, G. and Levy, G. (1993). Differences in drought resistance among 3 deciduous oak species grown in large boxes. Annales des Sciences Forestieres 50: 221-233.

Voltas, J., Serrano, L., Hernández, M., Pemán, J. (2006). Carbon isotope discrimination, gas exchange and stem growth of four Euramerican hybrid poplars under different watering regimes. New For. 31: 435–451.

Whitehead, D., Jarvis, P.G., Waring, R.H. (1984). Stomatal conductance, transpiration, and resistance to water uptake in a *Pinus sylvestris* spacing experiment. Can. J. For. Res. 14: 692-700.

Zhang, H., Morison, J.I., Simmonds, L.P. (1999). Transpiration and water relations of poplar trees growing close to the water table. Tree Physiology 19: 563-573.

4 The EMEP MSC-W model: handling soil moisture impacts on O₃ fluxes

David Simpson

EMEP MSC-W, Norwegian Meteorological Institute, Oslo, Norway & Dept. Earth & Space Sciences, Chalmers University of Technology, Gothenburg, Sweden

4.1 Introduction

This short document briefly describes the way in which soil water (SW) is used in the O_3 deposition and flux calculations of the EMEP MSC-W chemical transport model (Simpson et al., 2007, 2012). We present some problems associated with the availability of robust SW data, and then the solution adopted for EMEP – the soil moisture index (SMI). The basic role of SW is to modify the stomatal conductance (g_s) of the overlying vegetation, with this role being expressed as a factor f_{SW}, which modifies g_s along with the other factors of the so-called DO_3SE module as implemented in EMEP (Emberson et al., 2001; Simpson et al., 2012).

The standard EMEP model is described in detail in Simpson et al. (2012), with updates documented in Simpson et al. (2016, and refs therein). Calculations of stomatal O_3-uptake and POD_Y make use of the stomatal conductance algorithm (now commonly referred to as DO_3SE) originally presented in Emberson et al. (2000, 2001), which depends on temperature, light, humidity, soil moisture and plant phenology. Calculation of non-stomatal sinks, in conjunction with an ecosystem specific calculation of vertical O_3 profiles, is an important part of this calculation as discussed in Tuovinen et al. (2004, 2009) or Simpson et al. (2003). The methodology and robustness of the calculations of O_3 deposition and stomatal conductance have been explored in a number of publications (Tuovinen et al. 2004, 2007, 2009; Emberson et al., 2007; Klingberg et al., 2008; Büker et al., 2012). Meteorological data for the EMEP model are provided at 3 hourly resolution from the European Centre for Medium Range Weather Forecasting Integrated Forecasting System (ECMWF-IFS) model (http://www.ecmwf.int/research/ifsdocs/), with sub 3-hourly meteorology estimated by the EMEP model. As well as the standard air parameters (temperature, humidity, etc.) and surface fluxes (of momentum, heat), the soil moisture index (SMI, described below) are taken from these IFS data; we used SMI values appropriate to ca. 1m rooting depth.

4.2 Soil moisture – the problems in large-scale modelling

There are many rather serious problems with the specification of SW for use in any regional modelling study. These include:

- SW values are below-ground, and hence not verifiable, except at an extremely limited number of sites in Europe. Indeed, the SW modelling study of Büker et al. (2012) was able to obtain data from just eight European (and two American) sites, and these data were scattered across several years, and for different depths and metrics.

- The relationship between the incoming amount of precipitation (in mm, say), volumetric soil water (m3/m3) and soil water pressure SWP (Pa) is extremely non-linear, with values calculated for SWP being very sensitive to assumptions about soil characteristics. This sensitivity, and the lack of any ability to verify the result, is a dangerous combination to feed into regional scale calculations of SW impacts.

- In any case, real soils are not homogeneous, but display differing textures and characteristics on a range of scales, all of which invalidate the equations usually used to convert from incoming precipitation to SWP. In a rather common example of this,

where possible, water will flow down cracks in the soil, rather than diffusing in the manner preferred by simple models.

- Further, plants are also not homogeneous, and they adapt to conditions. Plants undergoing water-stress will increase root depths, or shed leaves.

- In fact, many plants in dry areas will have roots which are sufficiently deep that they can access ground water. For such plants, SW is not a limiting factor for stomatal conductance.

The difficulties of estimating soil water metrics are well known (e.g. Albergel et al., 2012; Batjes, 1996; Miller et al., 2007; Samaneigo et al., 2013), with the conclusion being that one cannot estimate SW accurately in large-scale models. Instead, we must establish methods that get SW effects 'about-right', with a realistic view of the limitation associated with this parameter.

4.3 Soil moisture in the EMEP model

Soil water effects have been tested in the EMEP model since the late 1990s (e.g. Simpson et al., 2003), and included operationally around 2010 (Simpson et al., 2012). EMEP uses the soil moisture index (SMI) provided by the ECMWF model (www.ecmwf.int). SMI is designed to be robust in the face of the variations in, and lack of reliable data on, soil characteristics – this recognises that *no* model can accurately predict SW across large areas (e.g. Wipfler et al., 2011).

The basic equation used for SMI is:

$$S_{\mathrm{MI}} = (\mathrm{SW} - \mathrm{SW}_{\mathrm{min}})/(\mathrm{SW}_{\mathrm{max}} - \mathrm{SW}_{\mathrm{min}})$$

The f_{SW} values used in EMEP-DO$_3$SE are a very simple function of SMI, which itself is a simple scaling between the field capacity (FC) and permanent wilting point (PWP) of the vegetation **(Figure 4.1)**.
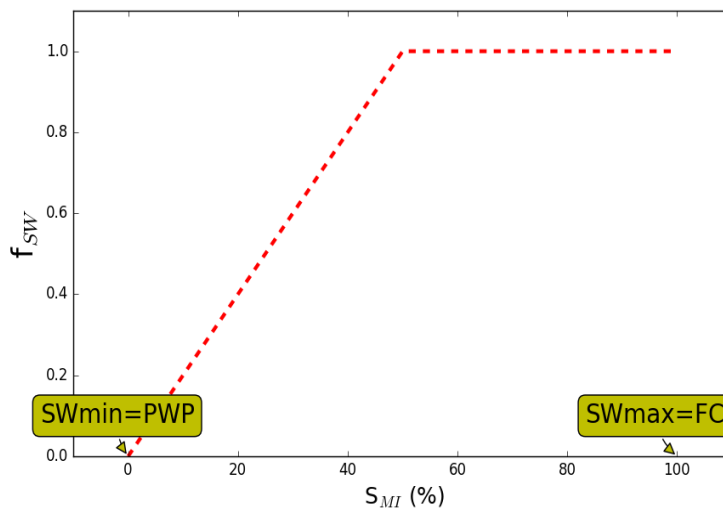
Figure 4.1   *The soil water factor, f_{SW}, used in the EMEP model as a function of SMI values.*

The ECMWF values of SMI, PWP and FC are per grid square, and thus not specific to any particular vegetation or soil.

4.4 Examples

Figure 4.2 shows examples of SMI and f_{SW} as calculated in the EMEP model from the ECMWF data for four sites, for locations and periods corresponding to the study of Büker et al (2012). For the purposes of illustration, values are given for both deep soils (ca. 1m) and shallow soil (10cm). Although EMEP-DO$_3$SE only uses the deep-soil values, the difference between the two provides some indication of the uncertainty and robustness, and also an indication of the range of values that might be seen by real vegetation. For example, many forests in Sweden lie upon shallow soils, often less than 50cm deep, and indeed most of the measurements found in Büker et al. (2012) also ranged between 10 and 50cm. The most obvious feature of these plots is the dramatic effect of SW on f_{SW} for the Spanish sites. Of course, the impact of these low f_{SW} factors on the calculated stomatal conductance and hence O$_3$ fluxes will often be mitigated also by simultaneous reductions in the phenology, humidify and (sometimes) temperature factors of EMEP-DO$_3$SE, so more investigation is required in order to place these examples into context. Figure 2.2 also illustrates nicely though that the f_{SW} value is very sensitive sometimes to the assumptions made concerning deep or shallow soil levels, especially at the Spanish sites.

(a) Asa, Sweden, 2000   (b) Hortenkopf, Germany, 2003

(c) Miraflores, Spain, 2005   (d) Prades, Spain, 2003
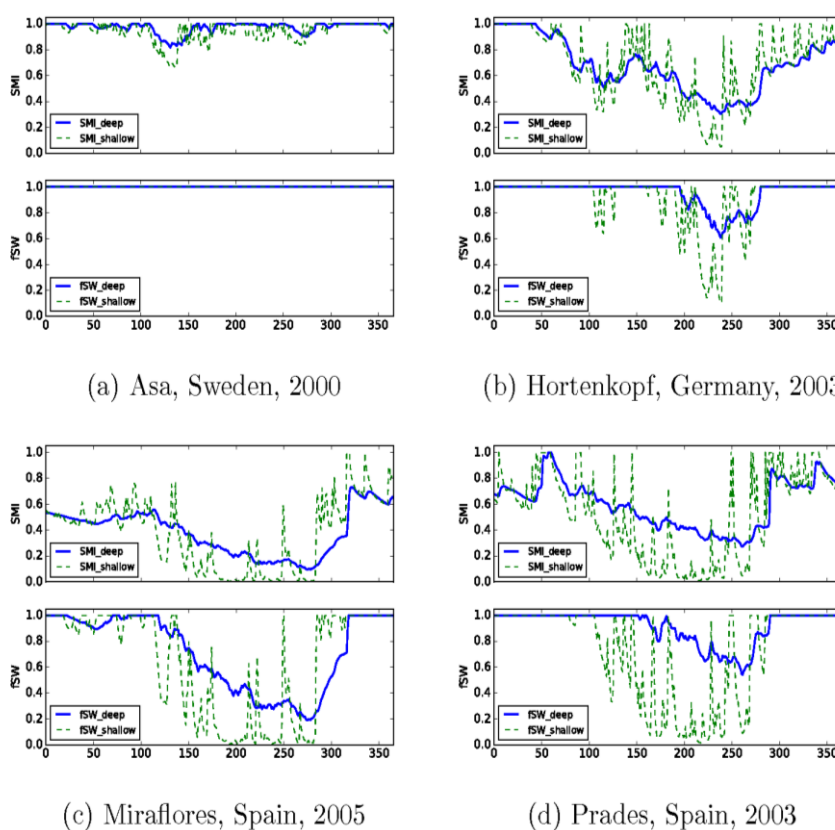
Figure 4.2   *Calculations of SMI (top of each subfigure) and f_{SW} (bottom) for four sites. Solid lines represent calculations for deep-soils, dashed are for shallow soils (see text).*

Recently, ICP Vegetation and EMEP/MSC-West have started a collaborative project to try to validate and improve the SMI methodology with detailed measurements of soil moisture at sites in soil moisture limited areas, particularly in the Mediterranean. The aim of the project is to improve large scale flux-based O$_3$ risk assessments, including application in integrated assessment modelling (POD$_Y$IAM) in soil limited regions.

4.5 Conclusions

This short document outlines the way soil water is handled in the EMEP model's calculations of O_3 fluxes, as well as gives some background to the choices made. The estimation of soil water and its impacts is very complex and fraught with uncertainty, however, and much more work is required to evaluate the chosen methods and their impacts against observational data, and to establish methods of dealing with SW which are as robust as possible given the limitations of available monitoring data.

4.6 References

Albergel, C.; de Rosnay, P.; Balsamo, G.; Isaksen, L. & Munoz-Sabater, J., Soil Moisture Analyses at ECMWF: Evaluation Using Global Ground-Based In Situ Observations, *Journal of Hydrometeorology,* 13, 1442-1460, 2012

Batjes, N. H., Development of a world data set of soil water retention properties using pedotransfer rules, *Geoderma,* 71, 31 – 52, 1996

Büker, P.; Morrissey, T.; Briolat, A.; Falk, R.; Simpson, D.; Tuovinen, J.-P.; Alonso, R.; Barth, S.; Baumgarten, M.; Grulke, N.; Karlsson, P. E.; King, J.; Lagergren, F.; Matyssek, R.; Nunn, A.; Ogaya, R.; Penuelas, J.; Rhea, L.; Schaub, M.; Uddling, J.; Werner, W. & Emberson, L. D., DO3SE modelling of soil moisture to determine ozone flux to forest trees, Atmos. Chem. Physics, 2012, 12, 5537-5562, 2012.

Emberson, L.; Simpson, D.; Tuovinen, J.-P.; Ashmore, M. & Cambridge, H. Towards a model of ozone deposition and stomatal uptake over Europe, The Norwegian Meteorological Institute, Oslo, Norway, 2000

Emberson, L.; Wieser, G. & Ashmore, M. Modelling of stomatal conductance and ozone flux of Norway spruce: comparison with field data Environ. Poll., 109, 393-402, 2000

Emberson, L.; Ashmore, M.; Simpson, D.; Tuovinen, J.-P. & Cambridge, H. Modelling and mapping ozone deposition in Europe Water, Air and Soil Pollution, 130, 577-582, 2001

Emberson, L. D.; Büker, P. & Ashmore, M. R. Assessing the risk caused by ground level ozone to European forest trees: A case study in pine, beech and oak across different climate regions Environ. Poll., 147, 454-466, 2007

Klingberg, J.; Karlsson, P. E.; Karlsson, G. P.; Hu, Y.; Chen, D. & Pleijel, H. Variation in ozone exposure in the landscape of southern Sweden with consideration of topography and coastal climate Atmos. Environ., 47, 252-260, 2012

LRTAP, 2015. In: Mills, G., et al. (Eds.), Chapter 3 of the LRTAP Convention Manual of Methodologies for Modelling and Mapping Effects of Air Pollution Available at. http://icpvegetation.ceh.ac.uk/., 2015

Miller, G. R.; Baldocchi, D. D.; Law, B. E. & Meyers, T. An analysis of soil moisture dynamics using multi-year data from a network of micrometeorological observation sites Adv. Water Resources, 30, 1065-1081, 2007

Mills, G.; Pleijel, H.; Braun, S.; Büker, P.; Bermejo, V.; Calvo, E.; Danielsson, H.; Emberson, L.; Grünhage, L.; Fernández, I. G.; Harmens, H.; Hayes, F.; Karlsson, P.-E. & Simpson, D. New stomatal flux-based critical levels for ozone effects on vegetation Atmos. Environ., 45, 5064 – 5068, 2011a

Mills, G.; Hayes, F.; Simpson, D.; Emberson, L.; Norris, D.; Harmens, H. & Büker, P. Evidence of widespread effects of ozone on crops and (semi-) natural vegetation in Europe (1990-2006) in relation to AOT40- and flux-based risk maps Global Change Biology, Blackwell Publishing Ltd, 17, 592-613, 2011b

Samaniego, L.; Kumar, R. & Zink, M., Implications of Parameter Uncertainty on Soil Moisture Drought Analysis in Germany, *Journal of Hydrometeorology,* 14, 47-68, 2013

Simpson, D.; Tuovinen, J.-P.; Emberson, L. & Ashmore, M. Characteristics of an ozone deposition module II: sensitivity analysis Water, Air and Soil Pollution, 143, 123-137, 2003

Simpson, D.; Benedictow, A.; Berge, H.; Bergström, R.; Emberson, L. D.; Fagerli, H.; Flechard, C. R.; Hayman, G. D.; Gauss, M.; Jonson, J. E.; Jenkin, M. E.; Nyri, A.; Richter, C.; Semeena, V. S.; Tsyro, S.; Tuovinen, J.-P.; Valdebenito, A. & Wind, P. The EMEP MSC-W chemical transport model -- technical description Atmos. Chem. Physics. 12, 7825-7865, 2012

Simpson, D.; Tsyro, S. & Wind, P. Updates to the EMEP/MSC-W model, in Transboundary particulate matter, photo-oxidants, acidifying and eutrophying components. Status Report 1/2016, The Norwegian Meteorological Institute, Oslo, Norway, 129-138, 20165, 2016

Simpson, D.; Emberson, L.; Ashmore, M. & Tuovinen, J. A comparison of two different approaches for mapping potential ozone damage to vegetation. A model study Environ. Poll., 146, 715-725, 2007

Tuovinen, J.-P.; Simpson, D.; Ashmore, M.; Emberson, L. & Gerosa, G. Robustness of modelled ozone exposures and doses Environ. Poll., 146, 578-586, 2007

Tuovinen, J.-P.; Emberson, L. & Simpson, D. Modelling ozone fluxes to forests for risk assessment: status and prospects Annals of Forest Science, 66, 401, 2009

Tuovinen, J.-P.; Ashmore, M.; Emberson, L. & Simpson, D. Testing and improving the EMEP ozone deposition module Atmos. Environ., 38, 2373-2385, 2004

Tuovinen, J.-P.; Emberson, L. & Simpson, D. Modelling ozone fluxes to forests for risk assessment: status and prospects Annals of Forest Science, 66, 401, 2009

Wipfler, E.L., Metselaar, K., van Dam, J.C., Feddes, R.A., van Meijgaard, E., van Ulft, L.H., van den Hurk, B., Zwart, S.J. & Bastiaanssen, W.G.M., Seasonal evaluation of the land surface scheme HTESSEL against remote sensing derived energy fluxes of the Transdanubian region in Hungary Hydrol. Earth Sys. Sci., 15, 1257-1271, 2011

5   O₃ flux-effect relationships for the net annual increment in trees

Patrick Büker[1], Lisa Emberson[1], Harry Harmens, Gina Mills, Sabine Braun[3], Per Erik Karlsson[4]

[1] Stockholm Environment Institute – York, University of York, UK
[2] ICP Vegetation Programme Coordination Centre, Centre for Ecology & Hydrology, Bangor, UK
[3] Institut für Angewandte Pflanzenbiologie (IAP), Schönenbuch, Switzerland
[4] IVL Swedish Environmental Research Institute, Gothenburg, Sweden

5.1 Introduction

The O₃-induced **change in total biomass** provides a measure of a tree's response to a certain O₃ concentration or dose integrated over the length of the entire exposure period (typically multiple years or even decades). While this response parameter has been widely used for the derivation of dose-response and flux-effect relationships for O₃ risk assessment approaches (and is ideal for single-year exposures such as for crops and grasslands), it is less suitable for the characterisation of O₃ effects on forest tree species whose life span is typically several decades. For this receptor an approach that takes into account the O₃ effect on annual growth is ideally required.

One solution to obtain flux-effect relationships for the O₃ influence on forest growth rates is to re-analyse the existing biomass relationships, converting the effect variable from percentage reduction in total biomass to percentage reduction in net annual increment (NAI). NAI (m³) is defined as the average annual volume over the given reference period of gross increment (i.e. the total increase of growing stock during a given time period) less that of natural losses on all trees to a minimum diameter at breast height (d.b.h.) of 0 cm (FOREST EUROPE, UNECE and FAO, 2011).

5.2 Methodology

For this approach, firstly the initial biomass (i.e. that at the start of the fumigation period) has to be derived for a specific experiment (we did this for trees used in the experiments included in Büker et al. (2015), where usually only the age of the tree at the beginning of the exposure period and the age and biomass at the point of harvest is recorded. This can be achieved by using a method developed by Sabine Braun given in the Annex (**Section 3.5**). With the derivation of the initial biomass the existing dose-response relationships data that describe the influence of single or multi-seasonal O₃ fumigation or filtration experiments on forest tree biomass could be re-analysed.

The O₃ treatment effect on biomass growth rates can then be estimated as the difference between this starting biomass (at onset of fumigation) and the final biomass under O₃ and control treatments. In our example, this effect was allocated to half-yearly increments so that the O₃ effect on NAI was a constant percentage, irrespective of age of tree or NAI size. For each experimental dataset this gives the value by which NAI is reduced (% reduction in NAI) due to a particular O₃ treatment, which is described as a seasonal average POD$_Y$SPEC value (i.e. the total experimental POD$_Y$SPEC value divided by the number of seasons (e.g. 6 months)). The % reductions in NAI for each experiment and treatment can then be pooled and a linear regression drawn through the data to give species-specific or species group (PFT) relative NAI dose-response relationships for O₃.

5.3 NAI-based flux-effect relationships for trees

Using the database from Büker et al. (2015), **Figures 5.1** and **5.2** show the NAI-based dose-response relationships for Norway spruce and Scots pine as well as beech and birch, respectively.
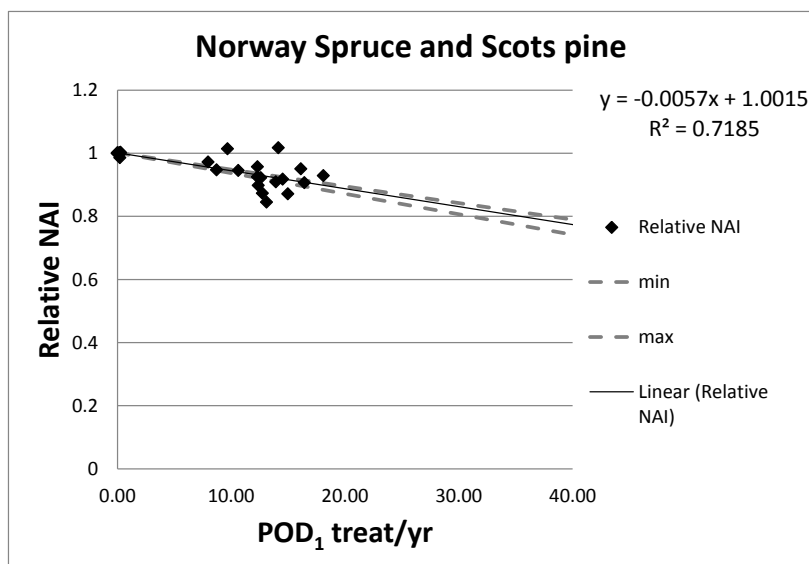
Norway Spruce and Scots pine

$y = -0.0057x + 1.0015$
$R^2 = 0.7185$

Figure 5.1   *NAI-based flux-effect relationship for Norway spruce and Scots pine.*

Beech/Birch

$y = -0.0093x + 0.9461$
$R^2 = 0.5866$
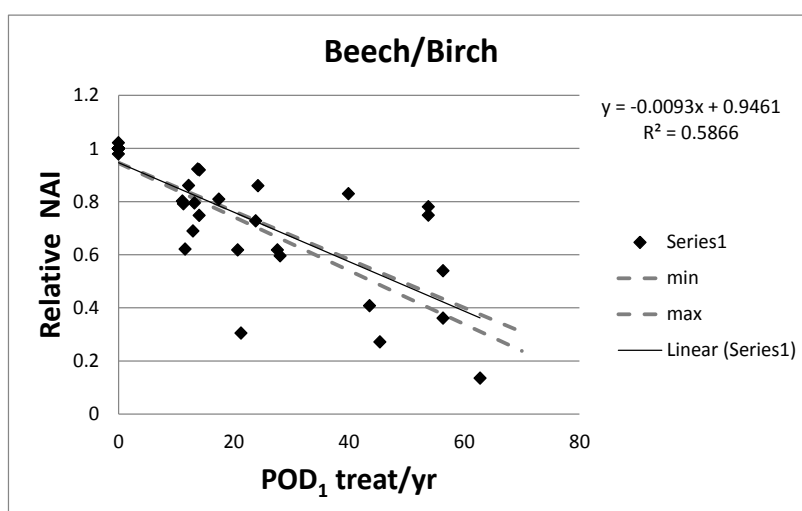
Figure 5.2   *NAI-based flux-effect relationship for beech and birch.*

5.4 References

Büker, P., Feng, Z., Uddling, J., Briolat, A., Alonso, R., Braun. S., Elvira, S., Gerosa, G., Karlsson, P.-E., Le Thiec, D., Marzuoli. R., Mills, G., Oksanen, E., Wieser, G., Wilkinson, M., Emberson, L. (2015). New flux-based dose-response relationships for ozone for European forest tree species. Environmental Pollution 206, 163-174.

FOREST EUROPE, UNECE and FAO (2011). State of Europe's Forests 2011. Status and Trends in Sustainable Forest Management in Europe. 344pp.

5.5 Appendix: Estimate of initial biomass from O₃-fumigation experiments

Sabine Braun

Institute for Applied Plant Biology

Dataset

Controls from fumigation experiments (carbon-filtered air if available, non-filtered air otherwise). Experiments with unclear or missing definition of initial age were deleted.

Variable names used

INITIALAGE: Initial age

ENDAGE: End age (LA: log(ENDAGE))

LBIOM: log biomass at end of the experiment

An overview over the dataset is given in **Figure 5.3**. Some data points showed to be outlying and were excluded in the data analysis:

- all *Populus* data (reason not known);
- *Betula pendula* from Ostad (very large pots);
- *Picea abies* and *Fagus sylvatica* from Zugerberg (small pots).
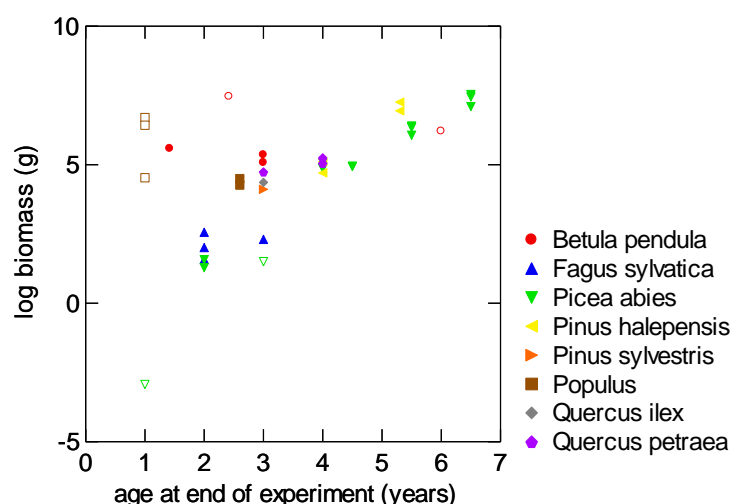
Figure 5.3   *Dataset used for the analysis. Empty symbols: data not considered (outliers).*

Starting point

Tree biomass $= y_0\big(1 - exp(-y_1 . tree\ age)\big)^{\left(\frac{1}{1-y_2}\right)}$ [1]

with y0=1, y1=0.03 and y2=0.65

For analysis with a regression model, constants y0 and y1 were taken as proposed (1 and 0.03, respectively). The expression (1-exp(-0.03*endage)) was calculated for each observation, renamed into the a new variable (C) and log transformed (LC).

After log transformation the formula looks like this:

log biomass = log(C)*(1/(1-y2))

This equation can be analysed with a linear model, without constant, to give an estimate for the expression (1/(1-y2)):

Call:

lm(formula = LBIOM ~ LC - 1, data = doseresponsecf)

Residuals:

    Min   1Q Median   3Q   Max
-9.1489 -0.2835 0.9387 2.4046 4.4802

Coefficients:

   Estimate Std. Error t value Pr(>|t|)

LC -1.7648   0.1838 -9.604 1.36e-11 ***

Signif. codes: 0 '***' 0.001 '**' 0.01 '*' 0.05 '.' 0.1 ' ' 1

Residual standard error: 2.815 on 37 degrees of freedom

Multiple R-squared: 0.7137,   Adjusted R-squared: 0.706

F-statistic: 92.23 on 1 and 37 DF, p-value: 1.365e-11

> AIC(model0)

[1] 189.4961

Model 1: Initial model

The coefficient is -1.7648 which corresponds to a y2 value of 0.433. The plot of residuals against estimates reveals, however, serious problems with this regression. Instead of showing a cloud of points without structure there is a clear linear arrangement of the points (**Figure 5.4**). It turned out that the residuals are correlated with age.
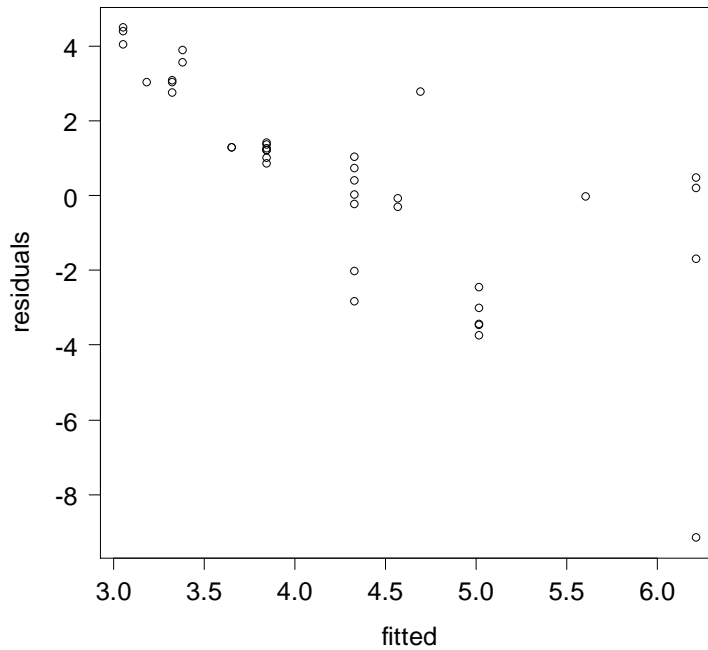
Figure 5.4 *Residual plot from the initial regression model.*

Modification of equation 1

Log biomass was almost linearly correlated with the age (Figure). Therefore a simple linear regression was applied. The intercept was omitted to ensure biomass 0 at age 0.

Call:

lm(formula = LBIOM ~ ENDAGE - 1, data = doseresponsecf)

Residuals:

```
   Min     1Q  Median     3Q    Max
-1.1310 -0.4615  0.1576  0.5750  1.6845
```

Coefficients:

```
       Estimate Std. Error t value Pr(>|t|)
ENDAGE  1.22339    0.03331   36.73   <2e-16 ***
---
```

Signif. codes: 0 '***' 0.001 '**' 0.01 '*' 0.05 '.' 0.1 ' ' 1

Residual standard error: 0.7659 on 26 degrees of freedom

Multiple R-squared: 0.9811,   Adjusted R-squared: 0.9804

F-statistic: 1349 on 1 and 26 DF, p-value: < 2.2e-16

> AIC(model8)

[1] 65.20422

Model 2: Simple model with end age as only predictor

The residual plot looks much better (Error! Reference source not found.) although there is still some pattern left. The values predicted from the model correlate well with the biomass data (**Figure 5.**). Although the inclusion of species into the model improved the model, it seems that this is rather an effect of the distribution of the species over the X-axis than real species differences. In the end the model without species was preferred.
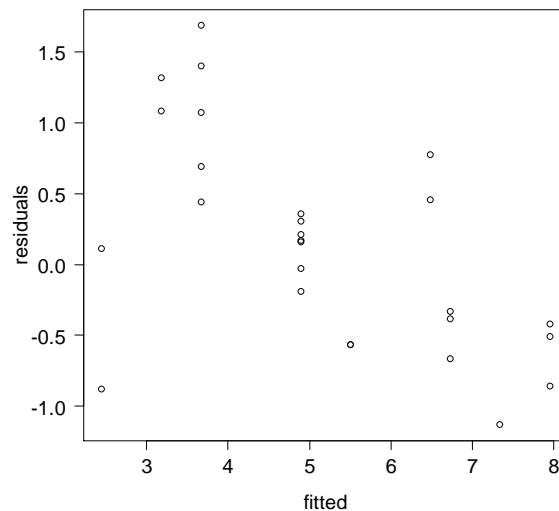
Figure 5.5   *Residual plot from the modified regression model.*

Residual analysis shows that the residuals for *Picea abies* are smaller than the others ($p<0.05$, **Figure 5.6**). Therefore a binary variable SPEC2 was created which takes values of 1 for *Picea abies* and of 0 for all others.

Model 3 shows the output. Species is no longer a significant predictor of the residuals.

Least Squares Means
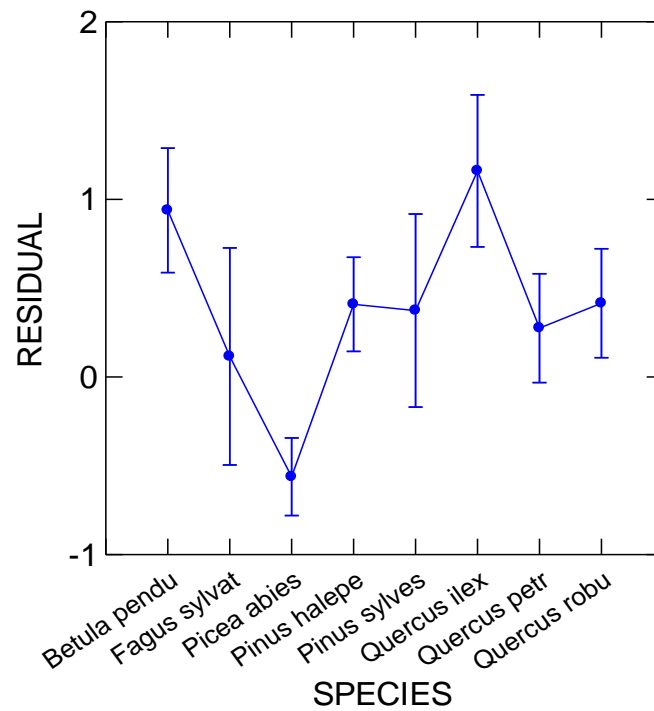
Figure 5.6 *Residuals from Model 2 against species.*

Call:

lm(formula = LBIOM ~ ENDAGE + ENDAGE:SPEC2 - 1, data = doseresponsecf)

Residuals:

Min	1Q	Median	3Q	Max
-1.75617	-0.17705	-0.06172	0.28538	1.37195

Coefficients:

	Estimate	Std. Error	t value	Pr(>|t|)	
ENDAGE	1.3276	0.0401	33.109	< 2e-16	***
ENDAGE:SPEC2	-0.1982	0.0553	-3.583	0.00143	**

Signif. codes: 0 '***' 0.001 '**' 0.01 '*' 0.05 '.' 0.1 ' ' 1

Residual standard error: 0.6349 on 25 degrees of freedom

Multiple R-squared: 0.9875,   Adjusted R-squared: 0.9865

F-statistic: 988 on 2 and 25 DF, p-value: < 2.2e-16

> AIC(model8)

[1] 56.01193

Model 3: Previous model with a binary variable for Picea abies.

The residuals still show some structure, so a mixed model is introduced with site as cluster. This procedure will also handle the problem of different pot sizes. Two outliers were removed. The residual plot looks good now (**Figure 5.7 and 5.8**).

```
     AIC     BIC   logLik
 71.19371 76.92966 -31.59685
```

Random effects:
 Formula: ~1 | EXPERIMENT.

```
        (Intercept)  Residual
StdDev:   1.395287 0.4437081
```

Fixed effects: LBIOM ~ ENDAGE + ENDAGE:SPEC2 - 1

```
              Value Std.Error DF   t-value p-value
ENDAGE       1.1599971 0.1095516 23 10.588593      0
ENDAGE:SPEC2 -0.5238286 0.1051257 23 -4.982879      0
```
 Correlation:
```
             ENDAGE
ENDAGE:SPEC2 -0.735
```

Standardized Within-Group Residuals:
```
     Min        Q1        Med         Q3        Max
-1.65270142 -0.50626091  0.07676185  0.47200336  2.53726027
```

```
              ENDAGE ENDAGE:SPEC2 (Intercept)
Donon        1.159997   -0.5238286   0.4145937
Ebro Delta   1.159997   -0.5238286   1.1303258
Headley      1.159997   -0.5238286   0.8940967
Kuopio       1.159997   -0.5238286   1.6498625
Ostad        1.159997   -0.5238286   2.8104975
Schönenbuch  1.159997   -0.5238286   0.2569469
Zugerberg    1.159997   -0.5238286  -0.5415212
```

Model 4: Output of the mixed regression.
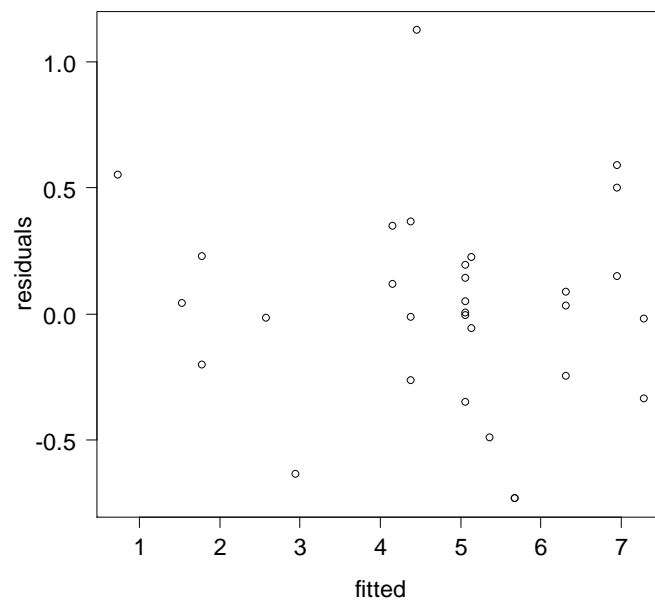
Figure 5.7   *Residual plot of*

Model 4.
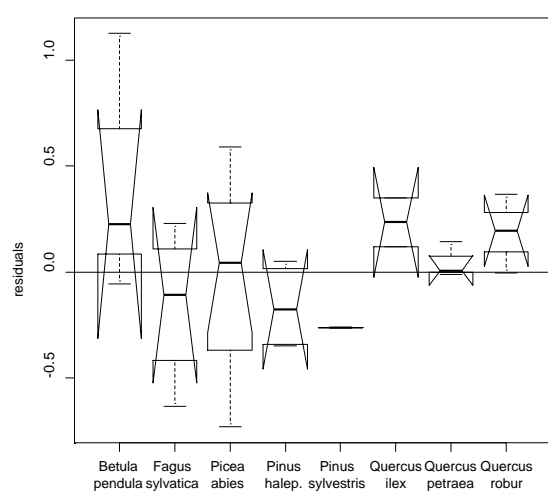
Figure 5.8   *Residual plot of*

Model 4 in relation to species.
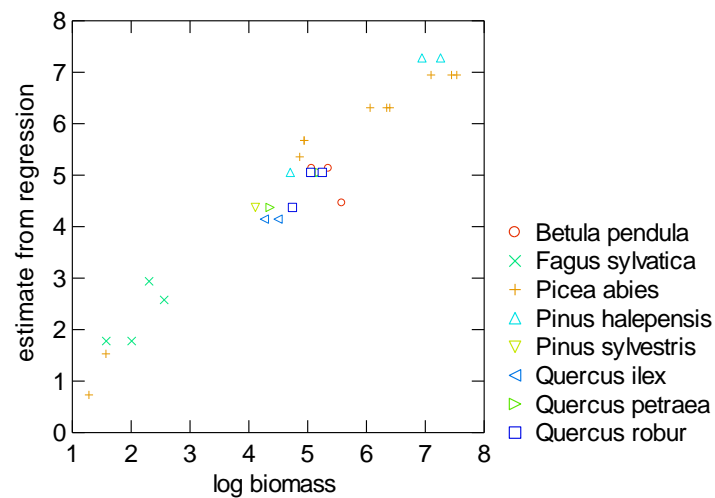
Figure 5.9   *Estimate of*

Model 4 vs. dependent variable.

Recommendations

For a general use, the resulting equations are:

For Picea abies:

$$biomass = e^{0.636*age}$$ [2]

For all others:

$$biomass = e^{1.160*age}$$ [3]

For the estimate of reference biomass within the single experiments, a site specific intercept is used according to the output of Model 4.

With formula 2 and 3 an estimate for initial biomass can be performed, with the following recommendations:

- In experiments with initial age 0 (seedlings) no correction is necessary. The final biomass data can be taken directly;

- In Birmensdorf, cuttings were used with an initial weight of 0.6 g. However, biomass data was only available for the 1990 experiment but according to the description of the experimental design this holds true also for the other experiments;

- It is recommended to calculate initial and final biomass with formula [2] and [3], take the ratio between the two and apply this factor to the effective final biomass of the charcoal-filtered treatments to get an estimate for the initial biomass.

6   Phenology, accumulation period and climate change: case-study in Germany

Ludger Grünhage[1] & Jürgen Bender[2]

[1] *Department of Plant Ecology, Justus-Liebig-University, Giessen, Germany*
[2] *Thünen Institute of Biodiversity, Braunschweig, Germany*

6.1 Phenology and accumulation period

The toxicological relevant accumulation period for wheat is defined as the time period 200 degree days before mid-anthesis to 700 degree days after mid-anthesis (CLRTAP 2010, 2015). There are basically two methods for estimating timing of mid-anthesis: phenological models and a latitude model (mid-anthesis = 2.57 · latitude + 40). For winter wheat in Central Europe mid-anthesis can be estimated using a temperature sum of 1024°C days after day 60 of the respective year (cf. Grünhage et al. 2011; LRTAP Convention, 2017). **Figure 6.1** illustrates that the current latitude model used does not predict timing of mid-anthesis accurately. Therefore, the latitude model for wheat should be revised or be replaced by an improved method for predicting the timing of mid-anthesis.

For beech, the start of the growing season is defined as the date of budburst/leaf emergence and the end of the growing season by the onset of dormancy; leaf discolouration is assumed to occur 20 days prior to dormancy (LRTAP Convention, 2017). Start and end of the growing season is estimated applying a latitude model which take into account the effect of height above sea level (a.s.l.) on plant phenology.
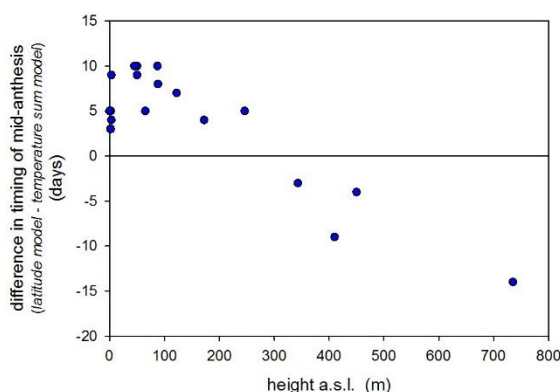

Figure 6.1   *Differences in timing of mid-anthesis of winter wheat estimated by the latitude model and the temperature sum model (1024°C days after yearday 60) for 19 monitoring stations in Germany in 2010 (Bender et al. 2015, modified).*

Figure 6.2 shows the differences in observed timing of the beginning of leaf unfolding (German Phenological Network) in the years 2001 – 2010 and timing of the start of the growing season (SGS) estimated by the latitude model:

$$DOY_{SGS} = 105 - (1.5 \cdot (50 - latitude)) + 10 \cdot height\ a.s.l.\ /\ 1000).$$

On average, timing of the start of the growing season is 5 days prior to beginning of leaf unfolding and is independent of the latitude (n = 12055, 95th percentile = 9 days, 5th percentile = –16 days).
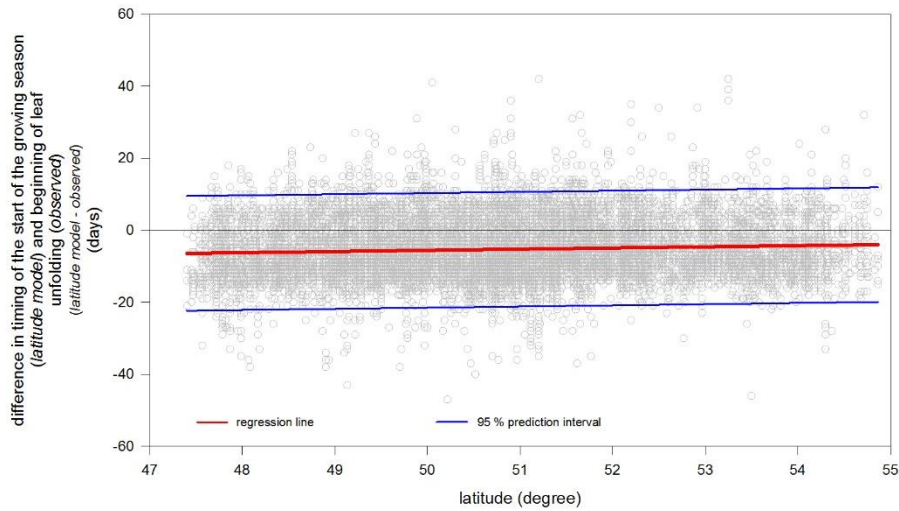
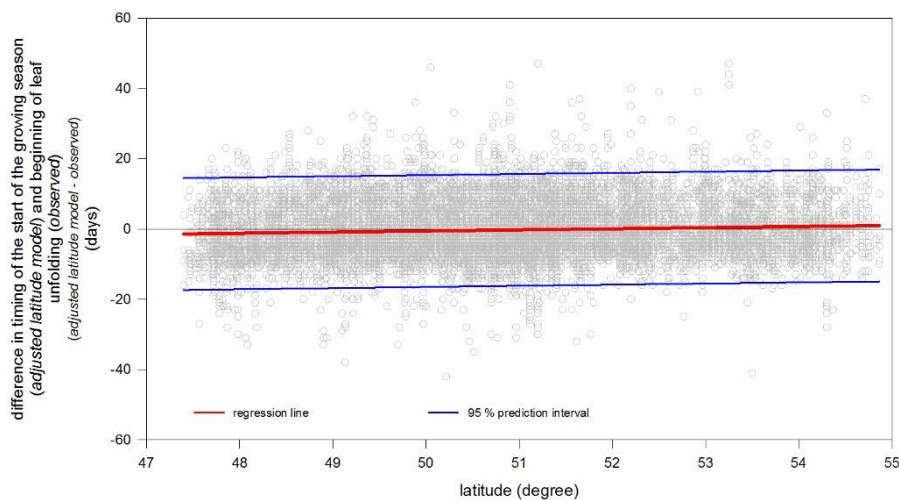**Figure 6.2**   *Differences in timing of the start of the growing season of beech estimated applying the CLRTAP latitude model and timing of observed beginning of leaf unfolding as a function of latitude (data source: German Phenological Network, DWD; time period 2001 – 2010).*

By adjustment of the yearday for the start of the growing season at latitude 50°N from 105 to 110,

DOY$_{SGS}$ = 110 – (1.5 · (50 – latitude)) + 10 · height a.s.l. / 1000

the fit between estimated and observed start of the growing season increased (n = 12055, 95th percentile = 14 days, 5th percentile = –11 days; **Figure 6.3**).

Figure 6.3   *Differences in timing of the start of the growing season of beech estimated applying the adjusted CLRTAP latitude model and timing of observed beginning of leaf unfolding as a function of latitude (data source: German Phenological Network, DWD; time period 2001 – 2010).*

For the onset of beech leaf discolouring,

43

$$DOY_{beech\ leaf\ discolouring} = (297 + (2 \cdot (50 - latitude)) - 10 \cdot height\ a.s.l. / 1000) - 20)$$

and thus for the length of the growing season there is a strong dependency on latitude for the differences between modelled and observed data (**Figure 6.4**; n = 11648, 95th percentile = 10 days, 5th percentile = –30 days).
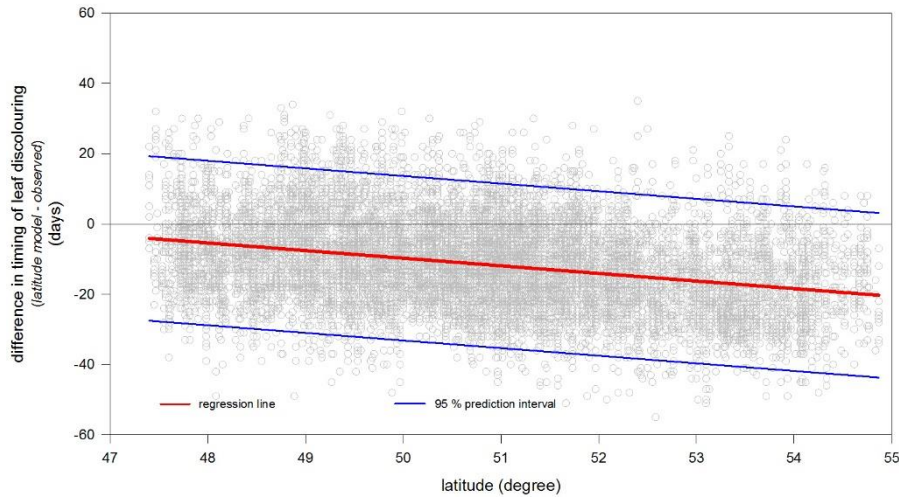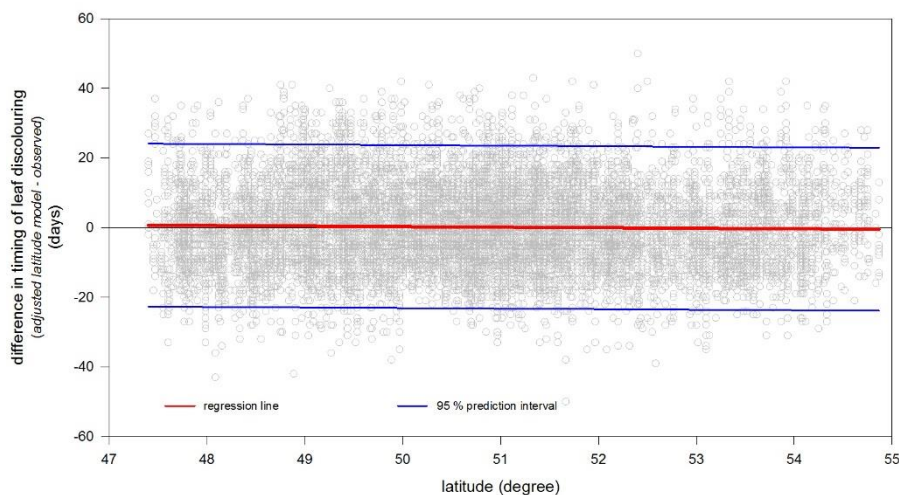

Figure 6.4   *Differences between observed and modelled timing of beech leaf discolouring as a function of latitude (data source: German Phenological Network, DWD; time period 2001 – 2010).*

By adjustment of the onset of dormancy from yearday 297 to yearday 307 at latitude 50°N and without considering the effect of latitude described in CLRTAP (2010, 2015) on the onset of dormancy,

$$DOY_{beech\ leaf\ discolouring} = (307 - 10 \cdot height\ a.s.l. / 1000) - 20)$$

the observed data fit sufficiently enough to the modelled ones (n = 11648, 95th percentile = 21 days, 5th percentile = –18 days; **Figure 6.5**).

Figure 6.5   *Differences between observed and modelled timing of beech leaf discolouring as a function of latitude (data source: German Phenological Network, DWD; time period 2001 – 2010).*

44

6.2 Phenology and climate change

Generally, increasing air temperature leads to an accelerated phenological development with the exception of timing of leaf discolouring and leaf fall (Menzel et al. 2006; **Figures 6.6** and **6.7**).

In comparison to the climate normal 1961–1990, the time period between heading and hard dough – as a proxy for the grain filling phase of winter wheat – has shortened continuously during the last 25 years (Figure 4.6). In the same time, the length of beech growing season increased (Figure 6.7).
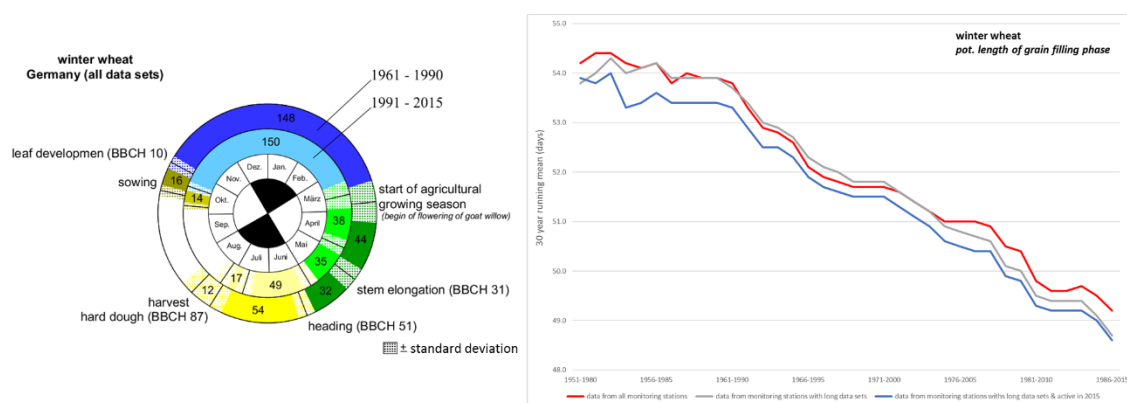
Figure 6.6   *Phenological clock for winter wheat in Germany and 30 year running mean for the potential length of the grain filling period (BBCH 51 – BBCH 87).*
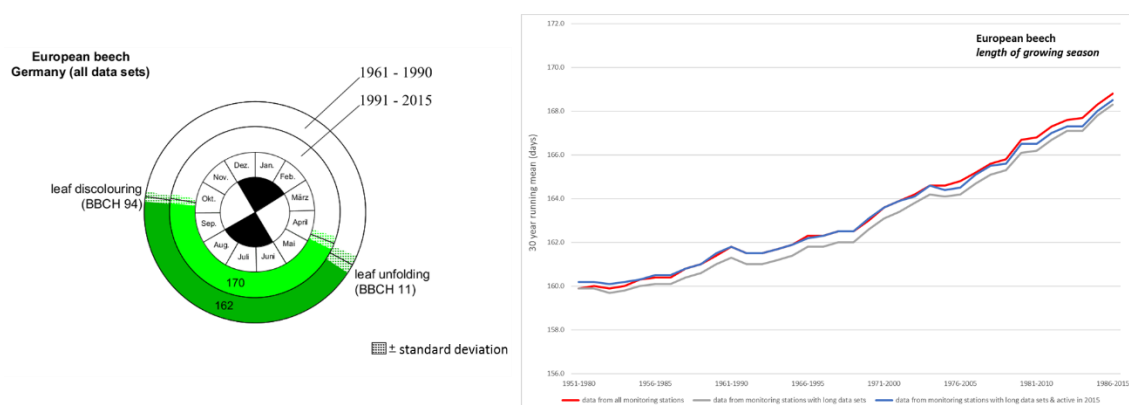

Figure 6.7   *Phenological clock for European beech in Germany and 30 year running mean for the length of the growing season (BBCH 11 – BBCH 94).*

The impact of future climate change on winter wheat and beech phenology was examined by Bender et al. (2015) by adding mean monthly anomalies with respect to 1971–2000 to daily climate data of 1997–2010 for the monitoring station Linden. The anomalies were averaged across a range of 13 projections for scenario A1B (similar to RCP6.0) and 3 projections for scenario E1 (similar to RCP2.6; for details see Bender et al. (2015), chapter 4.11).

As shown in **Figure 6.8**, increasing air temperature due to climate change leads to a further premature timing of mid-anthesis and a further shortening of the grain filling phase. This is in line with the described observations (Figure 6.6).
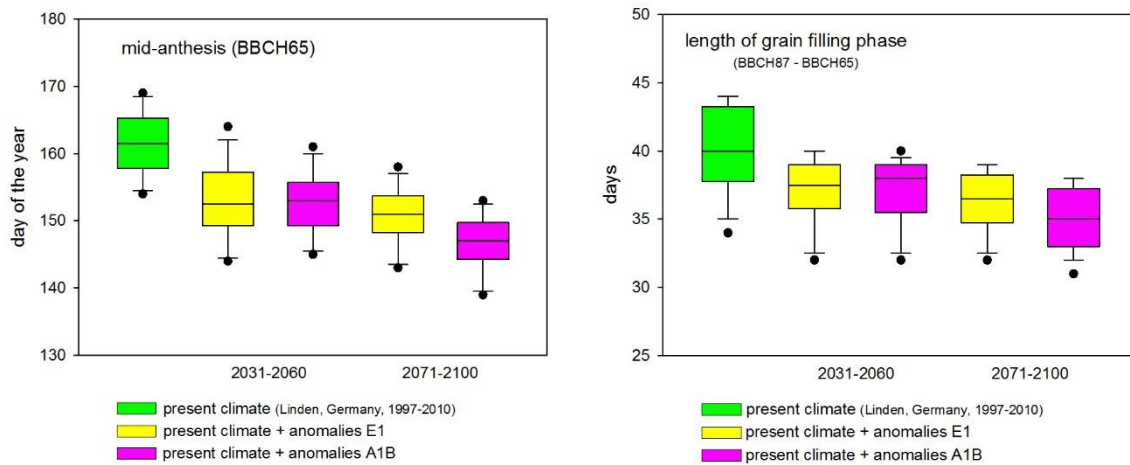

Figure 6.8   *Impact of increasing air temperature due to climate change on timing of mid-anthesis of winter wheat and on the length of the grain filling period (Bender et al. 2015, modified).*
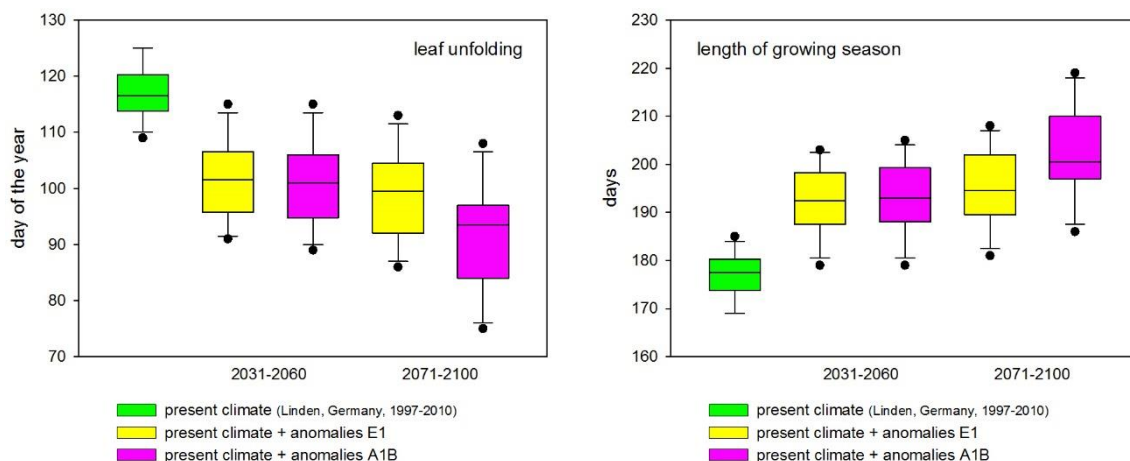

Figure 6.9   *Impact of increasing air temperature due to climate change on timing of beech leaf unfolding and on the length of the beech growing season (Bender et al. 2015, modified).*

As mentioned above, the observed accelerated development of beech phenology cannot be reflected by the latitude model. Therefore, the impact of increasing air temperatures due to climate change was estimated by Bender et al. (2015) by applying the thermal time model of Kramer (1994) for the timing of leaf unfolding assuming that the chilling requirement is fulfilled at February 1. As illustrated in **Figure 6.9**, the observed premature of timing of beech leaf unfolding and the lengthening of growing season will continue.

From the phenological literature it is well known, that timing of the end of dormancy depends on the weather conditions during the previous months. Therefore, assuming a fixed date for end of rest is too simple. More appropriate are so-called sequential models. Here it is assumed, that forcing temperatures are not effective unless the chilling requirement is fulfilled. Such a model is described, improved and tested against several other models by Kramer

(1994) for beech: the sequential-i model most accurately predicts the onset of growth (leaf unfolding) in the Netherlands and Germany. The beech latitude model for the onset of growth should be replaced.

Currently, no appropriate model for the timing of leaf discolouration is described in the phenological literature. Therefore, the beech latitude model for the end of the growing season should be retained.

Finally, the impact of increasing air temperature due to climate change on stomatal O_3 uptake of winter wheat and beech is summarized in **Figure 6.10**. For this purpose, O_3 concentrations were set constant to 60 ppb and no soil water limitation is assumed. Generally, increasing air temperature will lead to increased stomatal O_3 fluxes. The smaller enhancement for winter wheat can be attributed to the shortening of the accumulation period.
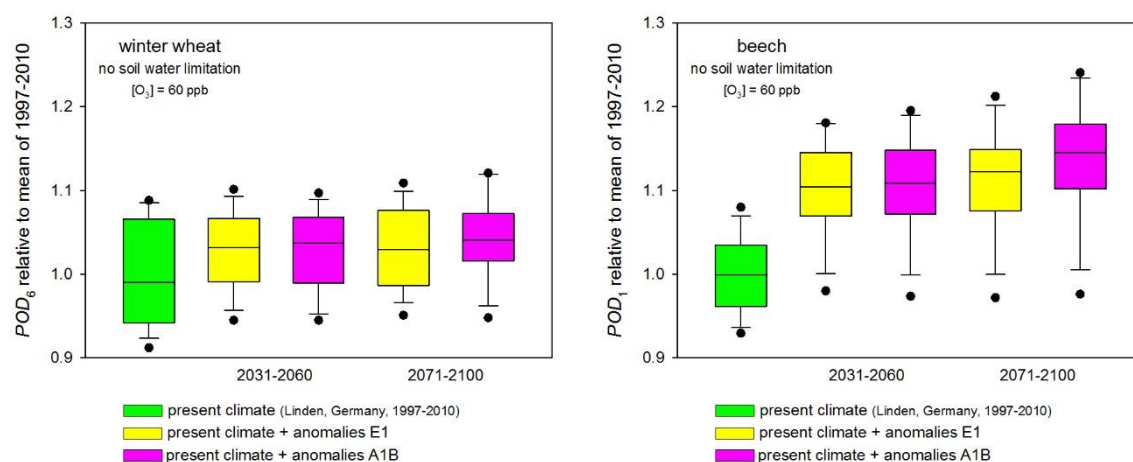

Figure 6.10   *Impact of increasing air temperature due to climate change on stomatal O_3 flux of winter wheat and beech (Bender et al. 2015, modified).*

6.3 Conclusions and recommendations

- The latitude model currently used in the Modelling and Mapping Manual does not predict timing of mid-anthesis accurately for wheat and should be revised or replaced by an improved methodology.

- After a small adjustment, timing of the start of the beech growing season according to the latitude model agreed sufficiently enough with the observed timing of the beginning of beech leaf unfolding in Germany (if the impact of increasing air temperature due to climate change on phenology is not considered).

- The latitude model does not predict the onset of beech leaf discolouring in Germany accurately. There is a strong dependency on latitude for the differences in timing of modelled and observed data. After adjustment, the latitude model agreed sufficiently enough with the observed timing of the beech leaf discolouring in Germany.

- Increasing air temperature due to climate change leads to a premature timing of mid-anthesis and a shortening of the time for grain filling for wheat. The phenological observations are in line with modelling results. Therefore, there is no need for a revision of the Modelling and Mapping Manual definition of the accumulation period for wheat in the near future.

- The impact of increasing air temperature cannot be taken into account by the current latitude model used for beech. Therefore, a more realistic O_3 risk assessment approach requires the application of an appropriate phenological model. For the onset of growth,

e.g. the sequential-i model of Kramer (1994) may be such an appropriate one. For the end of the growing season, the beech latitude model should be retained until a validated model is available.

● Increasing air temperature due to climate change will lead to increasing stomatal O_3 fluxes.

6.4 References

Bender, J., Bergmann, E., Weigel, H.-J., Grünhage, L., Schröder, M., Builtjes, P., Schaap, M., Kranenburg, R., Wichink Kruit, R., Stern, R., Baumgarten, M., Matyssek, R. (2015). Anwendung und Überprüfung neuer Methoden zur flächenhaften Bewertung der Auswirkung von bodennahem Ozon auf die Biodiversität terrestrischer Ökosysteme - Teil I. UBA-Texte 70/2015.

LRTAP Convention (2017). Mapping Critical Levels for Vegetation, Chapter III of Manual on methodologies and criteria for modelling and mapping critical loads and levels and air pollution effects, risks and trends. UNECE Convention on Long-range Transboundary Air Pollution.

Grünhage, L., Braden, H., Bender, J., Burkart, S., Lehmann, Y., Schröder, M. (2011). Evaluation of the ozone-related risk for winter wheat at local scale with the CRO_3PS model. Gefahrstoffe - Reinhaltung der Luft 71, 90-97.

Kramer, K. (1994). Selecting a model to predict the onset of growth of Fagus sylvatica. Journal of Applied Ecology 31, 172-181.

Menzel, A., Sparks, T.H., Estrella, N., Koch, E., Aasa, A., Ahas, R., Alm-kübler, K., Bissolli, P., Braslavská, O., Briede, A., Chmielewski, F.M., Crepinsek, Z., Curnel, Y., Dahl, Å., Defila, C., Donnelly, A., Filella, Y., Jatczak, K., Måge, F., Mestre, A., Nordli, Ø., Peñuelas, J., Pirinen, P., Remošová, V., Scheifinger, H., Striz, M., Susnik, A., van Vliet, A.J.H., Wielgolaski, F.-E., Zach, S., Zust, A. (2006). European phenological response to climate change. Global Change Biology 12, 1969-1976.

7   Budbreak of beech and birch in a changing climate

Sabine Braun[1], Stefan Müller[2], Per Erik Karlsson[3]

[1]*Institute for Applied Plant Biology, Schönenbuch, Switzerland*
[2]*Meteotest, Berne, Switzerland*
[3]*IVL Swedish Environmental Research Institute, Gothenburg, Sweden*

7.1 Background

O_3 uptake models for deciduous trees require a definition of the growing season when leaves are present to take up v. The time of leaf budbreak has, however, changed during the last 20 years as shown for beech (**Figure 7.1**) and birch (**Figure 7.2**). There are various models for calculating the timing of budbreak (Kramer, 1994b, Menzel, 1997). The aim of the present study was to find a way to estimate the start of the growing season for deciduous tree species which is able to predict not only the observed budbreak on an average but also to explain the observed time trend. Calculations were made for beech and birch.
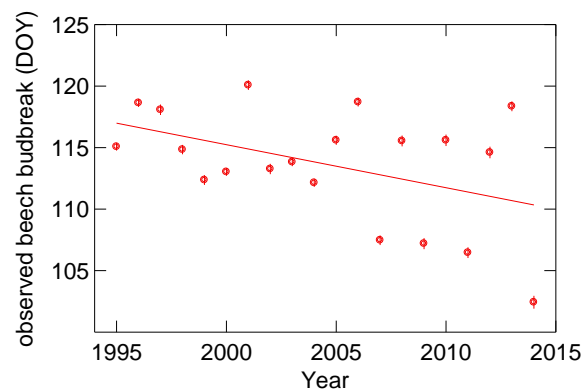

Figure 7.1   *Time of observed beech (Fagus sylvatica) budbreak in plots of the Pan European Phenology Project PEP725 (http://www.pep725.eu/index.php, 305 plots with 5268 observations). Bars: 95% confidence interval. Time trend is highly significant (p<0.001).*
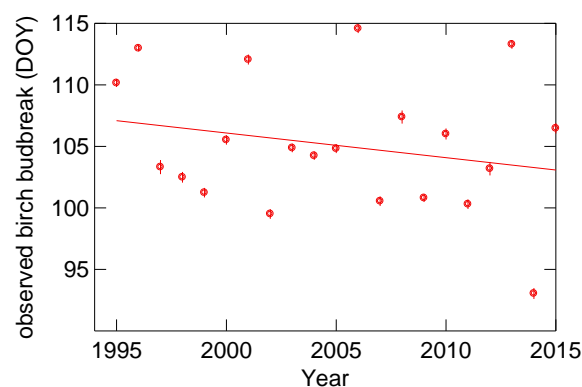

Figure 7.2   *Time trend of budbreak for birch in the same dataset as Figure 1 (263 plots with 4620 observations). Bars: 95% confidence interval. Time trend is highly significant (p<0.001).*

7.2 Dataset

Phenological observations from the Pan European Phenology Project PEP725 (http://www.pep725.eu/index.php) for beech and birch were used. Stage 11 (Leaf unfolding (first visible leaf stalk) was selected for data analysis as this was the most frequent stage represented in the data. For the Finnish birch sites it was stage 10 (mouse ear), for the Swiss birch sites stage 13 (leaf unfolding 50%). The dataset was too large for detailed data analysis, so in addition to the already available Swiss plots, 305 stations were selected according to the following criteria:

- Observations of beech phenology for as long as possible (more than a few years per station);

- Spatial distribution in a north-south corridor from UK over D to SLO and CRO and a southwest – northeast gradient in Germany to obtain a maximal variability of meteorology (**Figure 7.3**).

For the birch dataset another 18 Finnish datasets were included in the analysis.
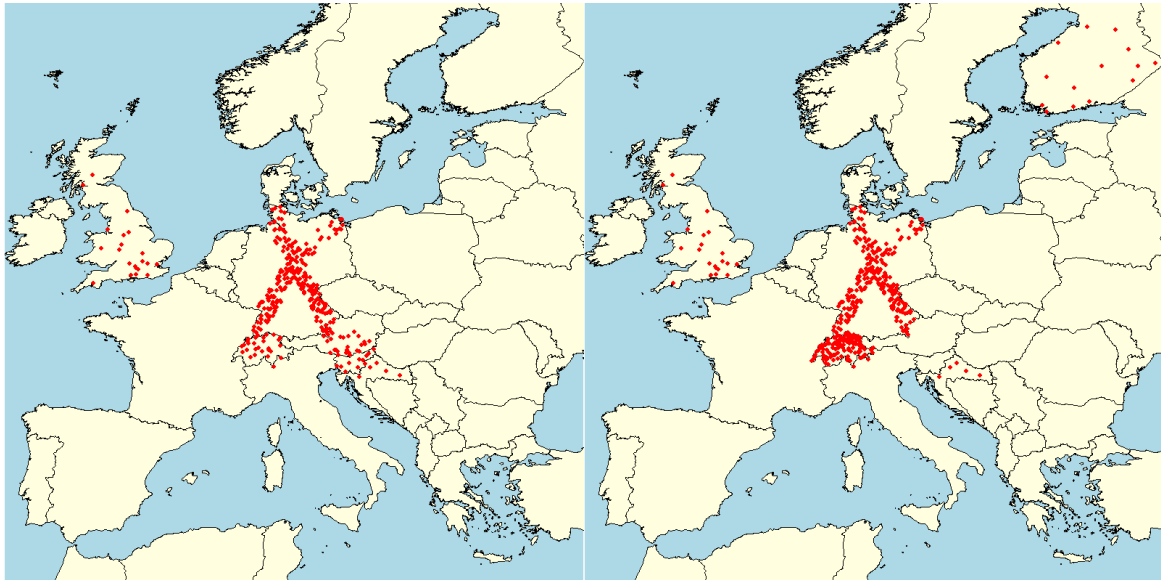

Figure 7.3   *Map of the selected phenology stations for Fagus sylvatica (left) and Betula sp. (right).*

The dataset comprises 332 plots with 5510 observations for beech and 418 plots with 6573 observations for birch. Budbreak data earlier than DOY 50 or later than DOY 180 in the birch dataset were considered as outliers and removed. Climate data based on the Global Surface Summary of the day (Globalsod) from NOAA (https://data.noaa.gov/dataset/global-surface-summary-of-the-day-gsod).

The aim of the data analysis presented here was to find a budbreak model which predicts the geographical and the temporal variations in observed budbreak well and at the same time is able to explain the observed time trend in budbreak. Thus, an important step of the data analysis was to regress the residuals against time. The models should also be applicable for mapping purposes, e.g. not contain variables which cannot be mapped.

7.3 Calculations using different models

Kramer model

Kramer (1994b) published a two stage budbreak model which separates a phase of endogenous and exogenous dormance. The endogenous dormance which does not allow budbreak at any time is stopped when a critical chilling (Ccrit) is reached. Then the rate of forcing is calculated. Budbreak occurs when the rate of forcing reaches the corresponding limit (Fcrit).

Rate of chilling = R_c

$$R_c = \begin{cases} 0 & T \leq T_{min} \\ \dfrac{T - T_{min}}{T_{opt} - T_{min}} & T_{min} < T \leq T_{opt} \\ \dfrac{T - T_{max}}{T_{opt} - T_{max}} & T_{opt} < T \leq T_{max} \\ 0 & T \geq T_{max} \end{cases} \qquad \textit{Equation 1}$$

Summing up of the chilling $= S_c$

$$S_C = \sum_{t_1}^{t} R_C \quad when: \quad S_C \geq C_{crit} \quad then \quad t_2 = t \quad \textit{Equation 2}$$

Response function (K)

$$K = \begin{cases} 0 & S_c < C_{crit} \\ 1 & S_c \geq C_{crit} \end{cases} \qquad \textit{Equation 3}$$

Rate of forcing (R_f)

$$R_f = \begin{cases} 0 & T \leq T_b \\ K \dfrac{1}{1 + e^{b(T+c)}} & T > T_b \end{cases} \qquad \textit{Equation 4}$$

with the variables:

R_c = rate of chilling [CU/day]

R_f = rate of forcing [FU/day]

S_c = state of chilling [CU]

S_f = state of forcing [FU]

T = temperature (daily average, °C)

t = time [day of the year, DOY]

		Fagus sylvatica	Betula sp. (D)
C_{crit}	threshold for the state of chilling	109	84.3
F_{crit}	threshold for the state of forcing	9.66	1.1
T_{min}	minimum temperature for chilling [°C]	-18	-15
T_{opt}	optimum temperature for chilling [°C]	-1.34	-10
T_{max}	maximum temperature for chilling [°C]	97	58.3
b	constant	-0.12	-0.13
c	constant	-20.54	-38
t_1	start of the endogenous dormance, set to November 1st (DOY 304)		

t₂ pushed above is in the document as:

t_2 = end of the endogenous dormance [DOY], set to DOY≥61 (March 1st)

t_3 = end of the exogenous dormance [DOY]

K = response function

The parameters used for beech are listed in **Table 7.1**. The initial constants for beech were taken from Kramer, 1994b, the constants for birch from Kramer, 1994a. All constants were optimized for maximum correlation with observed budbreak using a reduced dataset with 100 plots.

Table 7.1   *Parameters used for the calculation of budbreak of beech and birch.*

According to Sakalli and Simpson (2012) the temperature requirement for budbreak may vary depending on temperature. Therefore it was tested if the model could be improved by multiplication of the parameters listed in Table 1 with a factor representing the annual temperature, ranging from 0.8-1.2. This factor was calculated according to the following formula:

$$Tfak = (9.6 - Tm))/30$$

with Tm being the annual temperature of the year preceding the budbreak calculation. In the case of *Fagus sylvatic* (beech) *a*, a multiplication of Fcrit with this factor improved the regression slightly (from R2=0.41 to R2= 0.42). In all the other cases tested (all *Betula* (birch) and the remaining *Fagus* constants) no improvement was achieved. The regression of the residuals against time was not improved by this change.

The start of the rate of forcing calculation was restricted for beech to the time after March 1st (DOY 61) and for birch to DOY 32 (February 1st). The earliest observed budbreak was on day 68 and on day 51, respectively. It would be possible to change this restriction if necessary.

Kramer(1994a) has published also coefficients for other tree species which enables a wider application of his model. However, the coefficients given in this paper for *Fagus sylvatica* differ from the coefficients in Kramer, 1994b. They proved to be less suitable than the ones in Table 7.1 and are therefore not shown in **Table 7.2**. The application to the other species should, however, be tested with a similar dataset as presented here.
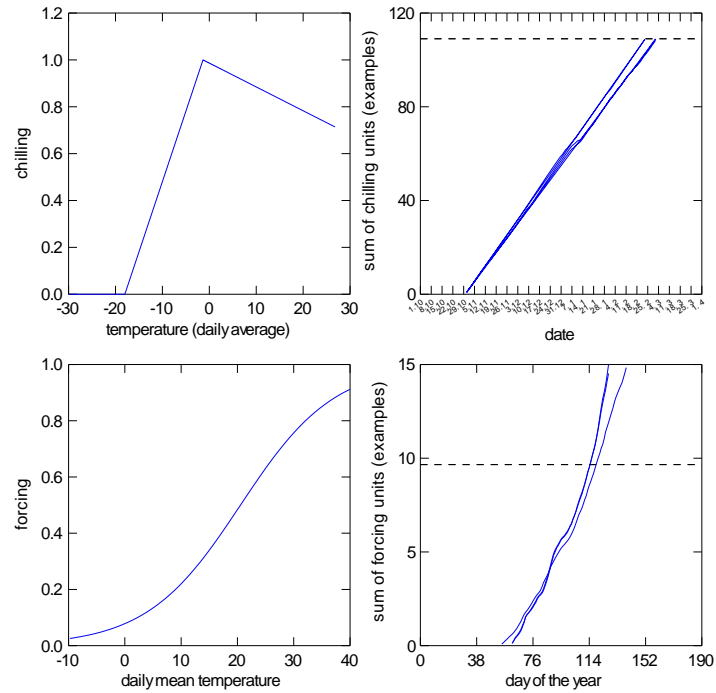
Figure 7.4   *Form of the response functions (left) and cumulative sum for a series of examples (right) for chilling (upper row) and forcing (lower row) in the budbreak calculation of Fagus with the Kramer model as used with the constants shown in Table 7.1. Dashed lines in the right graphs: limits for chilling (Ccrit) and forcing (Fcrit). The examples were PEP_ID numbers 68, 6863 and 19297.*
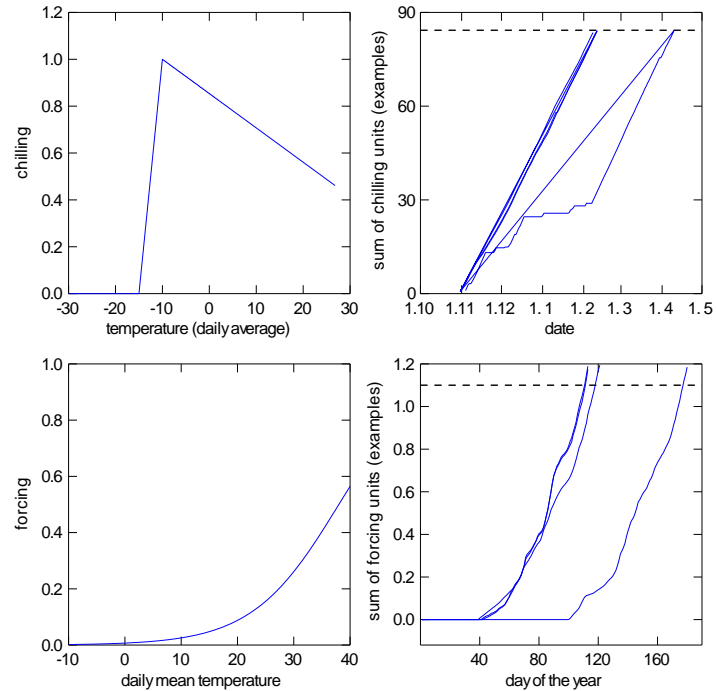

Figure 7.5   *Form of the response functions (left) and cumulative sum for a series of examples (right) for chilling (upper row) and forcing (lower row) in the budbreak calculation of Betula with the Kramer model as used with the constants shown in Table 7.1. One of the examples illustrates the effect of insufficient chilling. Dashed lines in the right graphs: limits for chilling (Ccrit) and forcing (Fcrit). The examples were PEP_ID numbers 68, 6863, 7178 and 19297.*

Table 7.2   *Coefficients for other tree species than beech (Kramer, 1994a).*

Species	T_{min}	T_{opt}	T_{max}	C_{crit}	b	c	F_{crit}
Larix decidua (D)	-13,2	-2,2	101,4	91,4	0,13	34,3	1,3
Betula pubescens (Nl)	-12,0	-0,9	37,8	99,4	0,19	18,3	5,4
Betula pubescens (D)	-10,3	-10,0	58,3	84,3	0,13	38,4	1,0
Tilia platyphylla (D)	-11,2	-2,8	98,6	91,5	0,15	33,9	1,2
Tilia cordata (D)	-51,5	3,2	49,9	106,7	0,11	39,1	2,0
Quercus rubra (Nl)	-11,5	-1,1	22,7	94,1	0,16	22,4	5,5
Quercus robur (D)	-11,4	-3,8	39,3	101,7	0,11	37,8	1,9
Quercus robur (Nl)	-20,6	-0,8	58,9	112,2	0,17	16,2	11,7
Fraxinus excelsior (D)	-20,4	-3,5	165,8	140,4	0,09	53,1	0,7
Quercus petraea (Nl)	-24,0	-0,2	113,8	129,0	0,17	15,3	12,7
Picea abies (D)	-11,4	0,1	16,3	82,5	0,14	35,9	1,6
Pinus sylvestris (D)	-13,8	-1,2	16,5	85,3	0,11	37,6	2,4

Menzel model

The Menzel model (Menzel, 1997) developed for beech (*Fagus sylvatica*) is a three stage phenological model. It calculates first chill days after November 1st, then a critical thermal time to be reached. After February 1st, a thermal time is accumulated. Budbreak occurs when this thermal time surpasses a set threshold.

Table 7.3   *Coefficients for the Menzel model.*

Art	T_bCD	T_bTT	a	b
Fagus sylvatica	9	6	1921.8931	-348.1324
Picea abies (early)	9	4	1848.1129	-316.974
Picea abies (late)	9	5	1615.5578	-274.0063
Pinus sylvestris	9	5	1394.5225	-222.7066
Larix decidua	7	3	1372.4707	-245.535
Quercus robur	9	4	1747.9219	-298.3638
Quercus petraea	9	3	1740.8994	-282.1039

Starting from November 1st the „chill days" with a temperature below a specific cold threshold (CD, **Table 7.3**) are cumulated, according to equation 7.

$$CD = \sum_{t1}^{t} 1 \quad when : T \leq T_b CD \qquad\qquad \text{Equation 5}$$

With:

CD =   chill days

t1   =   starting day (DOY=304)

T_bCD   temperature threshold for chill days (Table 3)

Afterwards the critical thermal time (TT_{crit}) which has to be exceeded to reach the phenological stage is calculated according to equation 8:

$$TT_{crit} = a + b \cdot \ln(CD) \quad \text{Equation 6}$$

With:

TT_{crit} =   critical thermal time to be reached for budbreak

CD =   chill days

a, b =   constants from Table 3

Starting at the end of the endogenous dormance set to Feb. 1st, the thermal time (TT) surpassing a specific threshold (T_bTT) is cumulated according to equation 9:

$$TT = \sum_{t2}^{t}(T - T_b TT) \quad wenn: T \geq T_b TT \qquad\qquad \text{Equation 7}$$

with:

TT =   thermal time

T   =   temperature (daily average)

T_bTT =   threshold for the thermal time (Table 3)

t2   =   starting day (DOY=32, end of the endogenous domancy)

Budbreak is reached when the actual thermal time (TT) exceeds the critical thermal time (TT_{crit}) according to equation 10:

$$TT \geq TT_{crit} \qquad\qquad \text{Equation 8}$$

Chuine model

Chuine (2000) presented a budbreak model which bases, similar to the Kramer model, on a chilling and a forcing stage. The forcing equation has the same form as in the Kramer model but chilling occurs only at temperatures below a certain threshold. Fu et al. (2012) calibrated this model for a variety of tree species. The coefficients given in the Chuine and in the Fu paper differ somewhat. So the model was also optimized for maximum correlation with observed budbreak. The optimum coefficients obtained are listed in

Table *7.4.*

Rate of chilling = R_c

$$R_c = \begin{cases} \dfrac{1}{1+e^{ca*(T-cc)^2+cb(T-cc)}} \\ 0 \qquad\qquad\qquad T>T_{max} \; or \; T<T_{min} \end{cases}$$

Equation 9

summing up of the chilling $=S_c$

$$S_c = \sum_{t_0}^{t} R_c \quad when: \quad S_c \geq C* \quad then \quad t=t_1$$

Equation 10

Rate of forcing (R_f)

$$R_F = \begin{cases} 0 & T \leq T_b \\ K\dfrac{1}{1+e^{fb(T+fc)}} & T>T_b \end{cases}$$

Equation 11

summing up of the forcing $=Sf$

$$S_F = \sum_{t_1}^{t} R_F \quad when: \quad S_F \geq F* \quad then \quad t=t_2$$

Equation 12

Table 7.4 *Coefficients used in the Chuine model.*

	ca	cb	cc	fb	fc	C*	F*
Fagus	0.49	11.1	3.27	-0.3	12	90	20
Betula	0.54	11	2.66	-6.1	7.07	70	12

Simple temperature sum

A temperature sum for average daily temperatures exceeding 5 °C starting on January 1st (DOY=1) was calculated:

$$TSUM_5 = \sum_{DOY=1}^{Tsum<45} ((\max(T-5),0)$$

Equation 13

Budbreak of birch occurs when this temperature sum exceeds 45.

As a covariate for beech temperature sum was cumulated from DOY=1 to the budbreak date calculated with the Kramer model.

Temperature sum after Sakalli & Simpson

Sakalli and Simpson (2012) presented a temperature sum for calculation of birch budbreak. This model assumes that the temperature sum >5°C needed for budbreak is higher in warm regions than in cold regions. The critical sum is defined as:

$$D_{u,i} = \propto - \beta_i$$

56

Equation 14

$D_{u,i}$ is the required number of days for the start of the unfolding of the leaves for a given ordinal day i, α (=39) and β(=0.2) are empirical constants, and SGS is defined as the first day where a number $D_{u,i}$ of previous days have daily average temperatures exceeding 5°C.

Different values for α were tested. The best regression was obtained with α=30 while a β of 0.2 proved to be best.

Latitude Model

The latitude model was applied according to the recommendation of the Mapping Manual:

$$SGS_{lat} = (LAT - 50) * 1.5 + \left(\frac{ALT}{100}\right) + 105$$

Where:

LAT: Latitude in degrees

ALTITUDE: Altitude in meters

As altitude values were not available for all stations, the dataset for this analysis was slightly reduced (5070 instead of 5190 for beech, 6311 instead of 6404 for birch).

Drought

Potential evapotranspiration was calculated from daily averages of temperature and humidity according to Romanenko (1961), with the modification by Xu and Singh (1998). The formula for daily evaporation sums (in mm) was:

$$ETP = \frac{0.0021*(25+T)^2*(100-RH)}{30.4}$$

Equation 15

with:

T: temperature (daily average, °C)

RH: relative humidity (daily average %)

Climatic water balance CWB was then calculated:

$$CWB = PREC - ETP$$

Equation 16

with:

PREC: precipitation (mm)

The climatic water balance was cumulated during various periods before or after the calculated budbreak date.

End of the growing season

Predicting leaf discoloration is more difficult than predicting budbreak (Estrella and Menzel, 2006). A very simple approach was made with the same dataset as for budbreak calculation. The following covariates were included in the analysis:

- annual mean temperature
- monthly temperature September (mean and minimum daily average)
- monthly temperature October (mean and minimum daily average)
- monthly temperature November (mean and minimum daily average)
- minimum climatic water balance

The stage "50% discoloration" was analyzed for both beech and birch.

Statistical analysis

The data were analyzed in R using the function lmer (package lme4, Bates et al., 2015), with site ID as cluster. Dependent variable was observed budbreak. The following parameters were included as independent variables:

- Latitude;
- Budbreak calculated by the Menzel model;
- Budbreak calculated by the Kramer model;
- Temperature sum >5°C;
- Average temperatures various time periods (not used in the final model);
- Climatic water balance cumulated over 5, 10, 15, 20, 25 or 30 days preceding the budbreak according to the best model.

All variables, including the dependent variable, were centered, i.e. the mean was subtracted. The quality of the models was judged by the AIC and by analysis of the regression of the residuals against year, where the R^2 should be as small as possible. The results of all models are presented with a plot of observed budbreak vs. modelled and a plot of residuals vs. time. Both plots contain loess smoothers (black lines) to illustrate local trends and give a robust information on trends. The former plot includes also the result of a linear regression as red line and the 1:1 line as green line. The plots do not include information on the clustering while the regression model included site as clusters.

To calculate R^2 from the mixed model, the predicted values for level 0 of the model were regressed against observed values using a normal linear regression.

7.4 Results for different models

Simple temperature sum model

Temperature sum was applied differently for beech and birch: for birch budbreak was assumed when temperature sum exceeded 45. For beech no such threshold has been defined. Thus temperature sum was therefore cumulated up to the day of observed budbreak. On an average, beech budbreak occurred when temperature sum >5°C exceeded 160 degree days. Thus, for further calculations a threshold of 160 was used for beech. This model performed not very well (**Figure 7.6**). In birch the model performed slightly better, but still unsatisfactory. The residuals show still a trend after the year 2006 (**Figure 7.7**).
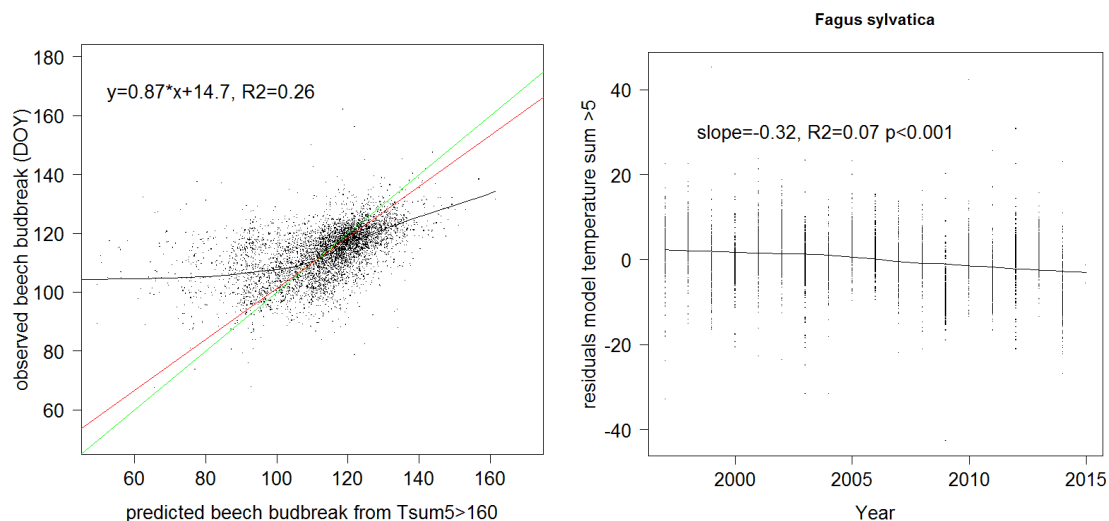
Figure 7.5   *Performance of the temperature sum model for beech. Left: Observed vs. predicted budbreak, right: plot of residuals against time. Black line: loess smoother, red line: linear regression.*
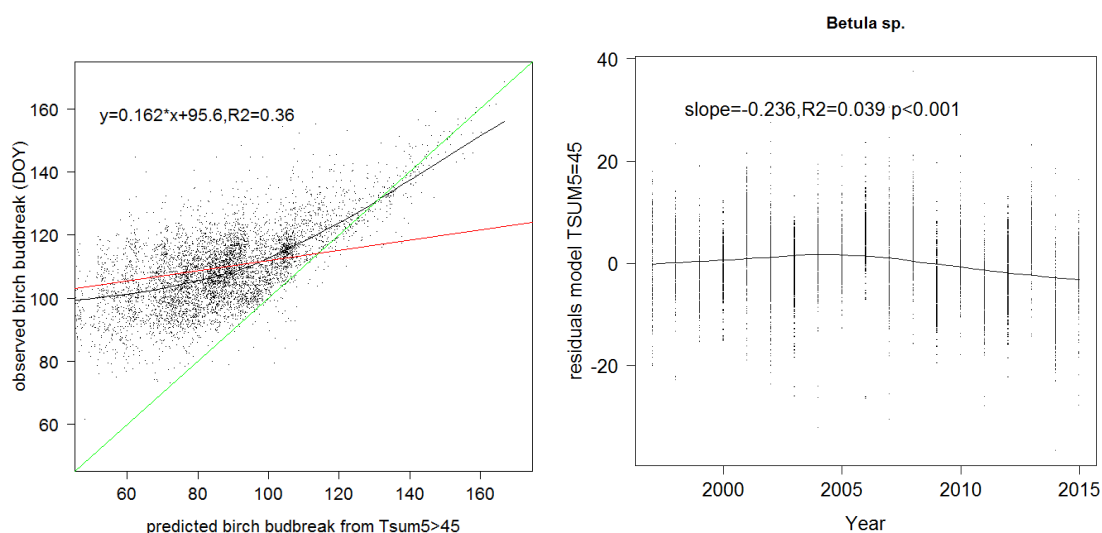

Figure 7.6   *Performance of the temperature sum model for birch. Left: Observed vs. predicted budbreak, right: plot of residuals against time. Black line: loess smoother, red line: linear regression.*

Temperature sum after Sakalli & Simpson

The Sakalli & Simpson model was developed for birch, so only the birch results are shown in **Figure 7.8**. With an R^2 of 0.12 the model did not perform well.
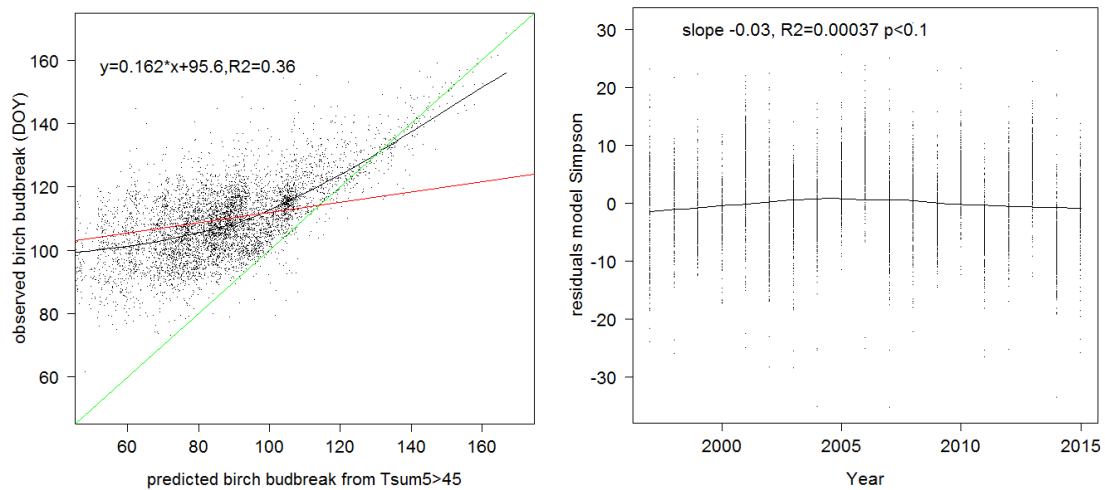
Figure 7.7 *Performance of the Sakalli&Simpson model for birch. Left: Observed vs. predicted budbreak, right: plot of residuals against time. Black line: loess smoother, red line: linear regression.*

Menzel model

The Menzel model is specific for *Fagus sylvatica* so it was applied for beech only. It gave better predictions than a temperature sum model but the residuals still show a clear regression against time (**Figure 7.9**).
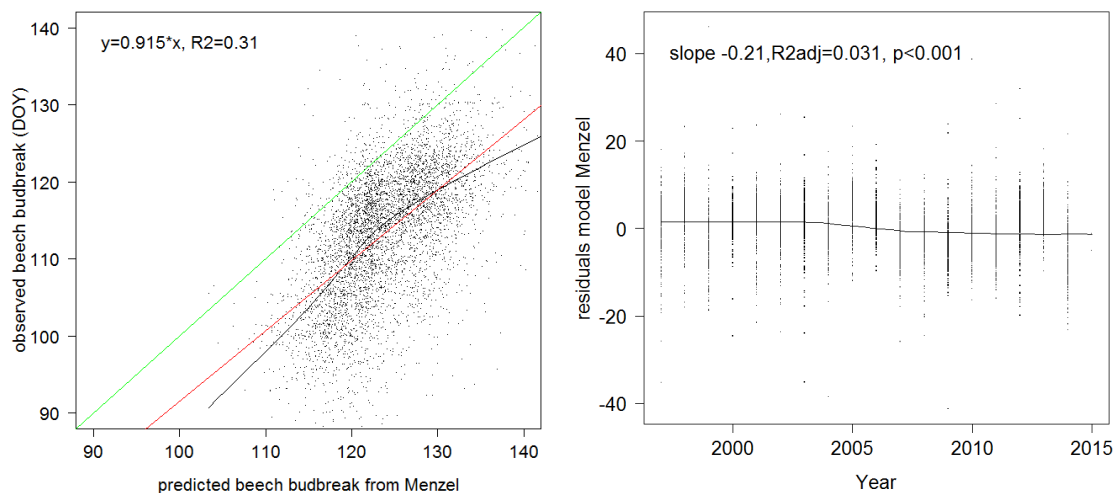

Figure 7.8 *Performance of the Menzel model for beech. Left: Observed vs. predicted budbreak, right: plot of residuals against time. Black line: loess smoother, red line: linear regression.*

Kramer model

The Kramer model performed rather well for beech and birch, both in terms of the AIC and in the R^2 (**Table 7.5** and **7.6**) but the residuals were still correlated with time (**Figure 7.10** and **7.11**). The model was better for birch than for beech but in birch the slope is below 1.
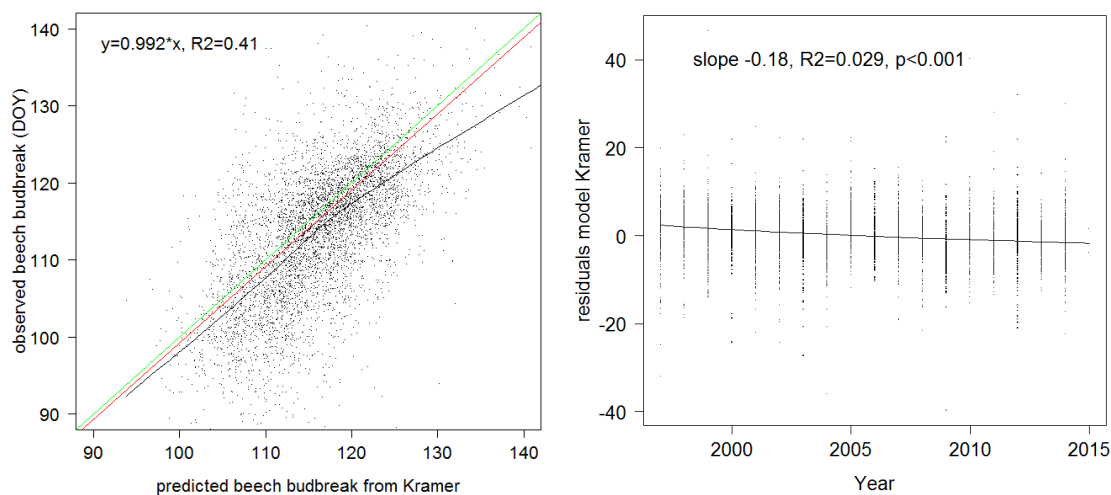
Figure 7.9 *Performance of the Kramer model for beech. Left: Observed vs. predicted budbreak, right: plot of residuals against time. Black line: loess smoother, red line: linear regression.*

Table 7.4 *Regression coefficients for the Kramer model for beech.*

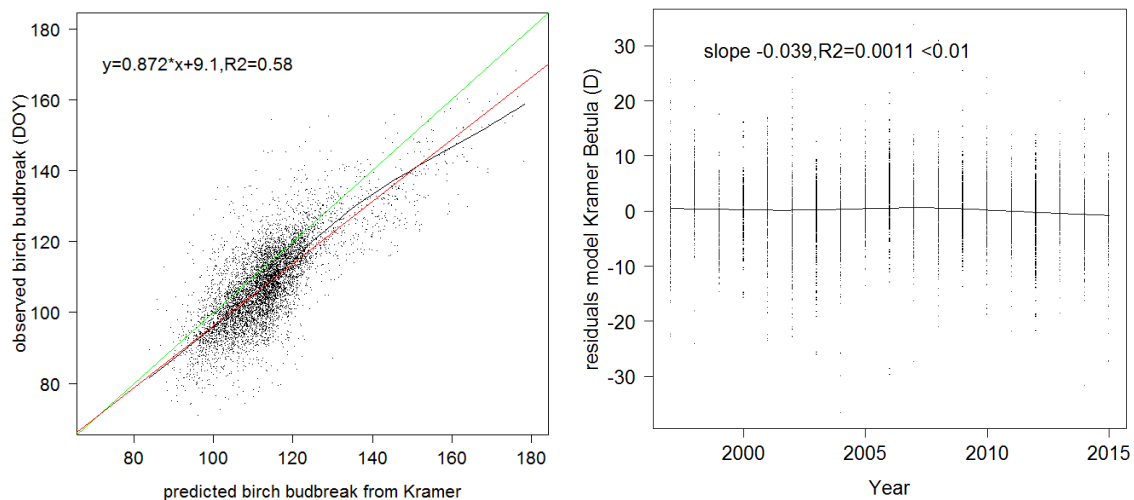| Budbreak	beech				
	Estimate	Std..Error	t.value	p.z	mean
observed bubreak					113.33
modelled Kramer	0.991	0.016	61.631	0.0000	116.1

Figure 7.10 *Performance of the Kramer model for birch. Left: Observed vs. predicted budbreak, right: plot of residuals against time. Black line: loess smoother, red line: linear regression.*

Neither annual average temperature, latitude nor climatic water balance improved clearly the regression between observed budbreak and budbreak modelled with the Kramer model.

61

Table 7.5   *Regression coefficients for the Kramer model for birch.*

	Estimate	SE	t.value	p.z	mean
observed budbreak					108.03
modelled Kramer	0.8727	0.01241	70.353	0.0000	113.33

Chuine model

In the Chuine model it happened often that the chilling limit was not reached and therefore no budbreak was calculated. This reduced the dataset in an unpredictable way and made comparisons impossible. After 14 optimization steps the Chuine model was therefore abandoned.

Latitude model

The variance explained by the latitude is 13% for beech (**Figure 7.12**) and 30% for birch (**Figure 7.13**). The difference between beech and birch is mainly due to the larger spread of the data range by inclusion of the Finnish birch plots. As the relation has been derived with observed budbreak data, the slope of the regression is close to 1. But the variation of the budbreak data predicted with the latitude model is much smaller than the variation of the observed data.
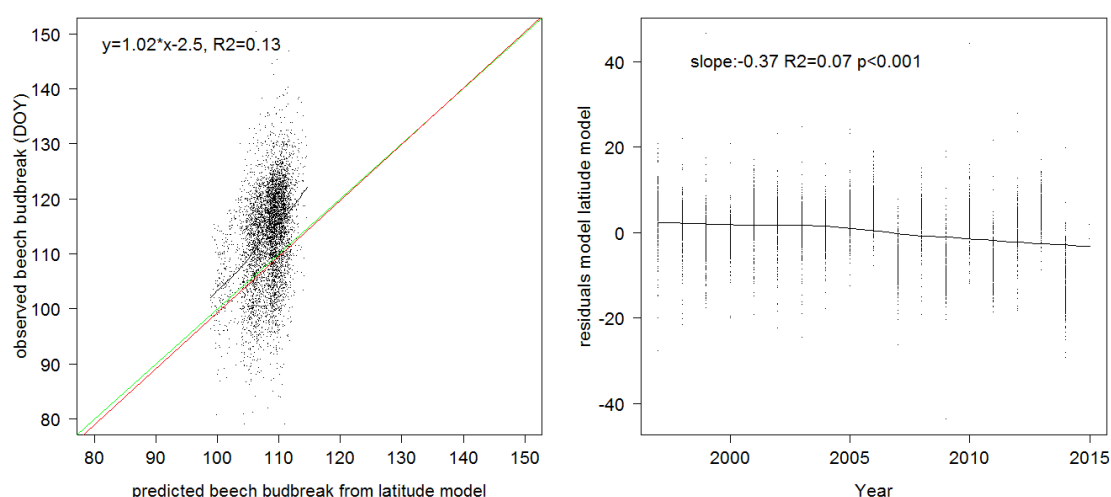

Figure 7.11   *Performance of the latitude model for beech. Left: Observed vs. predicted budbreak, right: plot of residuals against time.*
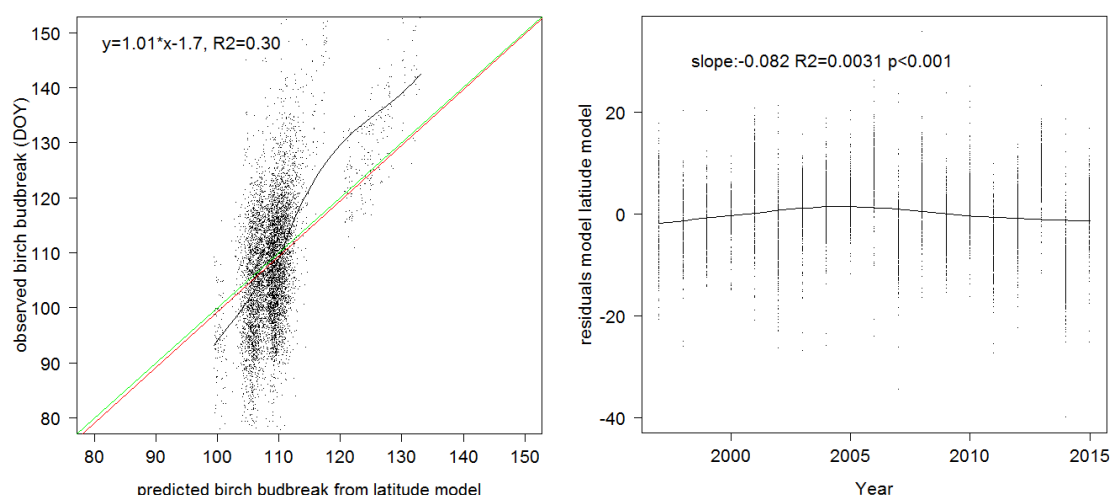
62

Figure 7.13 *Performance of the latitude model for birch. Left: Observed vs. predicted budbreak, right: plot of residuals against time.*

End of the growing season

<u>Beech</u>

Significant covariates were annual average temperatures, the average temperatures of September, October and November, the minimum temperature in November, the minimum water balance of the whole growing season and latitude (**Table 7.6**). The relations were not linear, the introduction of a polynom (using the function poly) improved the model.

As shown in **Figure 7.14** the performance of this model is bad. R^2 is only 0.14, and the spread of the estimated values is much smaller than the observed data. The slope of 1 which is suggested by the loess smoother is an artefact of the fact that validation was made with the same dataset as the derivation. The latitude model according to the Mapping Manual is even worse than the regression model (**Figure 7.15**) with only 1% of the variance explained.

Table 7.6 Output of the regression model for leaf discoloration of beech

|	poly	Estimate	Std..Error	t.value	p.z
average annual temperature	1	98.937	26.147	3.784	0.000
	2	57.629	14.193	4.061	0.000
T Sept	1	180.735	26.604	6.794	0.000
	2	-13.307	14.095	-0.944	0.345
T Oct	1	62.654	28.111	2.229	0.026
	2	54.020	15.198	3.554	0.000
T Nov	1	44.723	33.649	1.329	0.184
	2	-15.509	17.750	-0.874	0.382
minimum temperature Nov	1	-52.244	27.969	-1.868	0.062
	2	16.986	18.619	0.912	0.362
water balance	1	-31.152	16.171	-1.926	0.054
	2	-11.851	12.763	-0.929	0.353
Latitude	1	85.379	13.053	6.541	0.000
	2	7.426	12.736	0.583	0.560

63
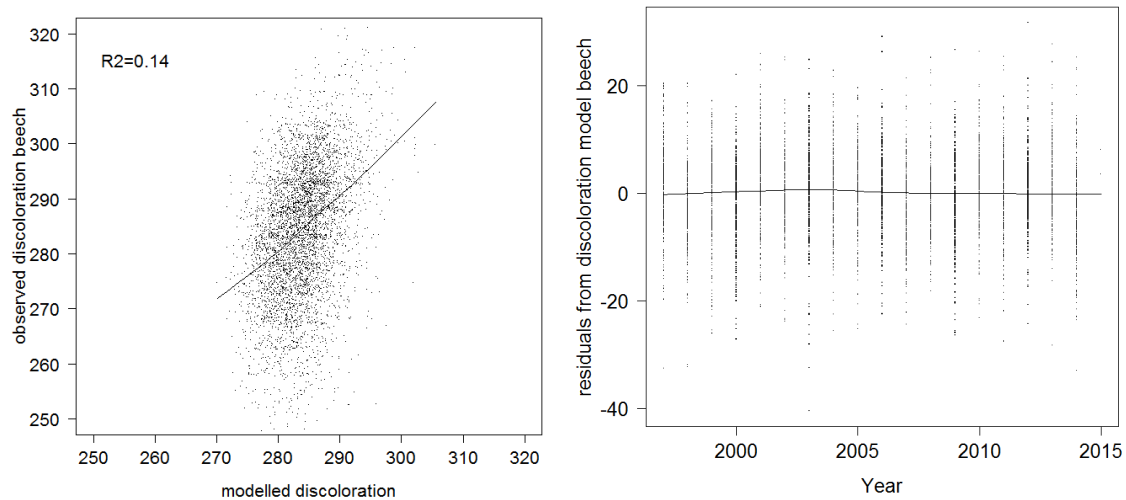
Figure 7.14 *Performance of the regression model for leaf discoloration in beech. Left: modelled vs. observed values. Right: Plot of residuals against years.*
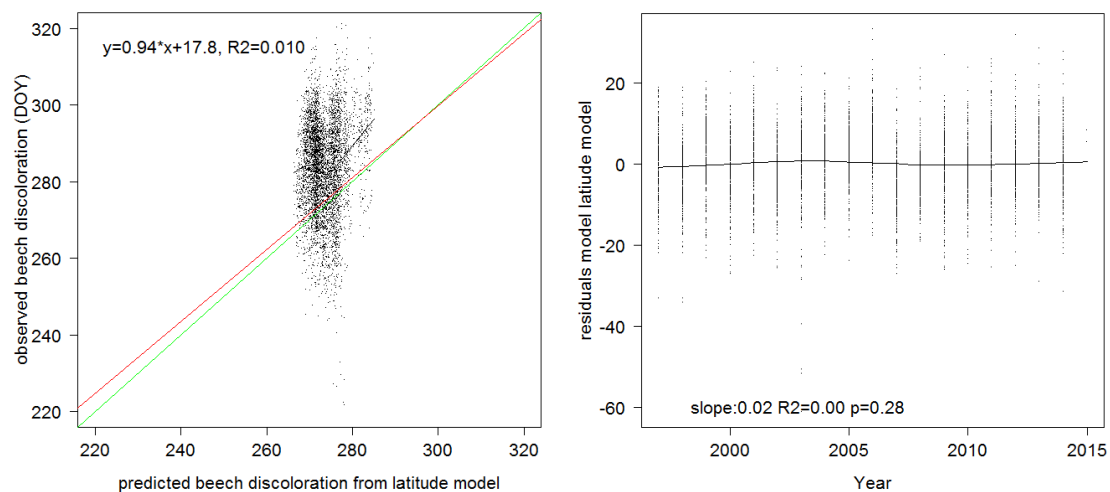

Figure 7.15 *Performance of the latitude model for leaf discoloration in beech. Left: modelled vs. observed values. Right: Plot of residuals against years.*

Birch

The birch dataset does not include the Finnish sites as no data on leaf discoloration and on humidity were available. In birch, monthly temperatures of September and October, the minimum climatic water balance and latitude were significant predictors for leaf discoloration. In addition, annual temperature and the minimum water balance were significant predictors. As in beech polynoms were calculated. **Table 7.7** shows the coefficients of the model, **Figure** the plot of modelled vs. observed values. The model is even worse than the beech model, with only 8% of the variance explained. The latitude model explains even less, 4%, of the variance (**Figure**).

64

Table 7.7   *Output of the regression model for leaf discoloration of birch.*

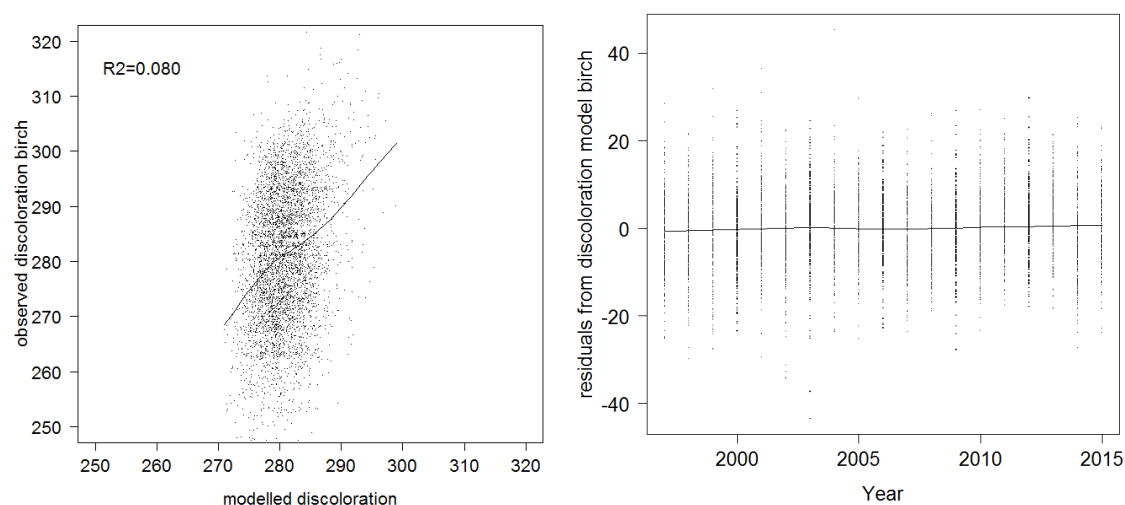|	poly	Estimate	Std..Error	t.value	p.z
	1	93.92	26.623	3.528	0.000
T Sept	2	56.30	15.033	3.745	0.000
	1	76.95	24.315	3.165	0.002
T Oct	2	-8.00	14.204	-0.563	0.573
	1	-128.15	15.696	-8.165	0.000
water balance	2	-26.77	13.330	-2.009	0.045
	1	-130.99	12.726	-10.293	0.000
Latitude	2	-9.03	13.481	-0.670	0.503

Figure 7.16   *Performance of the regression model for leaf discoloration in birch. Left: modelled vs. observed values. Right: Plot of residuals against years.*
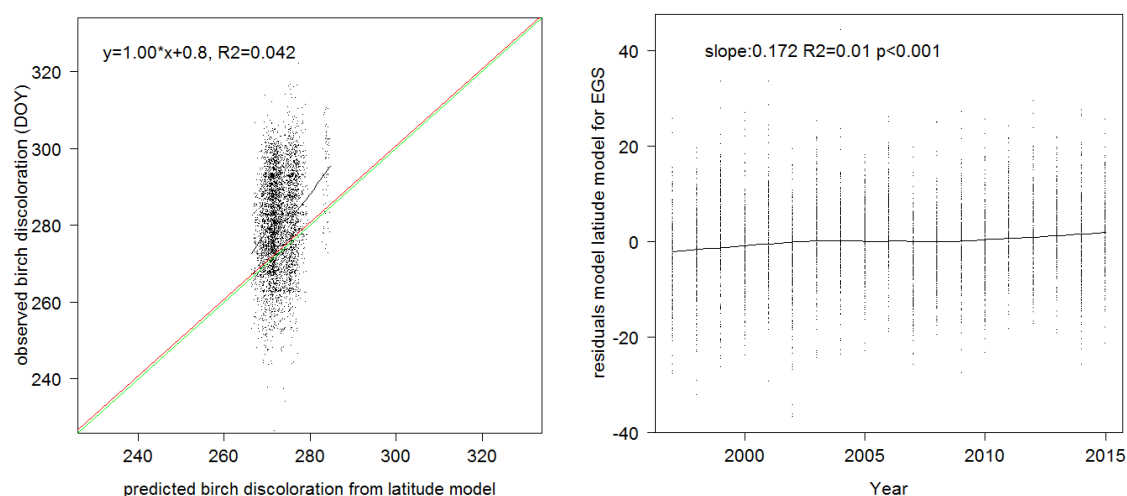

Figure 7.17   *Performance of the latitude model for leaf discoloration in birch. Left: modelled vs. observed values. Right: Plot of residuals against years.*

65

7.5 Conclusions

- Budbreak of beech and birch has shifted to earlier dates during the last 20 years. This justifies the evaluation of a more dynamic procedure than the latitude model as a tool to model future O_3 uptake periods as the latitude model cannot handle changes in climate.

- Various budbreak models were tested with a large dataset from the Pan European Phenology Project PEP725 (332 beech and 418 birch plots). Their performance was assessed using a regression of the residuals against time.

- From the models tested for beech and birch, the Kramer budbreak model performed best (**Table 7.9**). The two stage Kramer model explained 41% and 58% of the variance in budbreak date for beech and birch respectively. The slope of observed vs. modelled budbreak is close to 1 in beech. In birch it is 0.87, suggesting that early or late budbreak dates will be modelled less accurately. The beech model, however, is not able to fully explain the time trend of budbreak whereas in the birch model the time trend of the residuals is quite small.

- Parameters are published also for other tree species which enables a generalisation but it is recommended to test the parameterisation against observed budbreak data.

- The temperature sum models did not yield any usable predictions for budbreak of beech and birch. Also the proposed models for the end of the growing season are not good enough to allow a use for mapping purposes.

Table 7.9   *Summary of the performance of budbreak models for beech and birch.*

Model	*Fagus sylvatica* (beech)			*Betula sp.* (birch)		
	R^2 adj	Slope	time trend residuals	R^2 adj	Slope	time trend residuals
Menzel	0.31	0.91	-0.21			
Kramer	0.41	0.99	-0.18	0.58	0.87	-0.04
Simple temperature sum	0.26	0.87	-0.32	0.36	0.16	-0.24
Temperature sum Sakalli & Simpson				0.12	0.16	-0.03
Latitude model	0.13	1.02	-0.37	0.3	1.01	-0.08
Observed time trend			-0.37			-0.09

7.6 References

Bates, D., Maechler, M., Bolker, B., Walker, S., 2015. Fitting Linear Mixed-Effects Models Using lme4. Journal of Statistical Software 67, 1-48.

Chuine, I., 2000. A Unified Model for Budburst of Trees. Journal of Theoretical Biology 207, 337-347.

Estrella, N., Menzel, A., 2006. Responses of leaf colouring in four deciduous tree species to climate and weather in Germany. Climate Research 32, 253-257.

Fu, Y.H., Campioli, M., Demar+®e, G., Deckmyn, A., Hamdi, R., Janssens, I.A., Deckmyn, G., 2012. Bayesian calibration of the Unified budburst model in six temperate tree species. International Journal of Biometeorology 56, 153-164.

Kramer, K., 1994a. A modelling analysis of the effects of climatic warming on the probability of spring frost damage to tree species in The Netherlands and Germany. Plant Cell Environ 17, 367-377.

Kramer, K., 1994b. Selecting a Model to Predict the Onset of Growth of Fagus sylvatica. Journal of Applied Ecology 31, 172-181.

Menzel, A., 1997. Phänologie von Waldbäumen unter sich ändernden Klimabedingungen - Auswertung der Beobachtungen in den Internationalen Phänologischen Gärten und Möglichkeit der Modellierung von Phänodaten. 1-147 pp.

Romanenko, V.A., 1961. Computation of the autumn soil moisture using a universal relationship for a large area. Kiev.

Sakalli, A., Simpson, D., 2012. Towards the use of dynamic growing seasons in a chemical transport model. BG 9, 5161-5179.

Xu, C.Y., Singh, V.P., 1998. Dependence of evaporation on meteorological variables at different time-scales and intercomparison of estimation methods. Hydrol Process 12, 429-442.

8   Estimating O₃-sensitivity periods for trees in Fennoscandia

Per Erik Karlsson[1], Sabine Braun[2], Håkan Pleijel[3], Jenny Klingberg[3, *], Åslög Dahl[3], Göran Wallin[3], Magnuz Engardt[4], Kjell Bolmgren[5], Anne Tolvanen[6]

[1]*IVL Swedish Environmental Research Institute, Gothenburg, Sweden*
[2]*Institute for Applied Plant Biology, Schönenbuch, Switzerland*
[3]*University of Gothenburg, Sweden*
[4]*Swedish Meteorological and Hydrological Institute, Sweden*
[5]*Swedish University of Agricultural Sciences, Sweden*
[6]*Natural Resources Institute Finland (Luke) and University of Oulu, Finland*

*Present address: Gothenburg Botanical Garden, Sweden

Summary

- The time period during the year when forest trees are susceptible for O₃ exposure, the O₃ sensitivity period, O₃SP, may be defined for deciduous trees as the period between leaf budburst and autumn leaf coloration, while for evergreen coniferous trees it should be based on the period of active leaf gas exchange.

- The start and end of O₃SP were assessed for deciduous (European Silver birch) and coniferous (Norway spruce) trees in Fennoscandia.

- The latitude model, currently used in the LRTAP Modelling and Mapping Manual, has a limited capacity to predict yearly values for the timing of the onset of budburst of birch at 6 sites in Sweden and at 17 sites Finland (R^2 0.62, slope 2.4), and it strongly underestimated the day-of-year (doy) for bud burst of birch at northern latitudes, compared to what has been observed.

- A modification of the latitude model did to some extent improve the predictions of budburst of birch (R^2 0.63, slope 0.85).

- A temperature sum (T_{sum}) model, accumulating daily mean temperatures above 5 °C up to a limit of 45 degree*days, predicted budburst of birch in Sweden and Finland relatively well, with an R^2 of 0.83 and a slope of 0.88.

- The two-stage Kramer model, used with default parameterisation from Germany, strongly overestimated the doy for budburst by 20-30 days at northern latitudes, but otherwise provided a relatively strong correlation between predicted and observed doy for budburst (R^2 0.71, slope 0.76).

- **For Fennoscandia, it might be appropriate to use the simple T_{sum} model parameterized for birch to predict the timing of start of the O₃ sensitivity period for deciduous forests.**

- For the timing of autumn leaf coloration there were increasing trends for doy at all sites.

- There were some weak correlations between the doy for autumn leaf coloration and the mean temperature across the months July and August, in particular in the southern geographical region of Sweden and Finland.

- **A satisfying model to predict the end of the O₃SP for deciduous trees species in Fennoscandia still has to be developed.**

- In stands in Northern Sweden, the gas exchange of mature Norway spruce trees started well before the predicted start of growing season, both when predicted with the Modelling and Mapping Manual latitude model as well as when predicted as the time when 24-h mean temperatures exceeded 5°C.

- **The latitude model used within the Modelling and Mapping Manual to estimate the onset of the O₃SP for coniferous tree species in Fennoscandia clearly needs to be replaced. The solution is not to use a simple application as when 24-h mean temperatures exceeded 5°C.**

- **For predicting the timing of the end of the O₃SP during autumn in Fennoscandia, there are currently no satisfactory methods available for coniferous tree species.**

8.1 Introduction

The time period during the year when forest trees may be susceptible to O_3 exposure, the O_3 sensitivity period (O₃SP, Klingberg et al., 2014), may be defined for deciduous trees as the period between leaf bud burst and leaf autumn coloration, while for evergreen coniferous trees it should be based on the period of active leaf gas exchange.

The aim of this document was to review the performance of different methods to estimate the timing of the leaf budburst and leaf autumn coloration for deciduous trees as well as the period of active gas exchange for coniferous trees in Fennoscandia. A further aim was to describe the significance of climate induced changes in the phenology for the methods to estimate the O₃SP. Finally, the aim was to make suggestions for improvements concerning the estimations.

A special emphasis is given to the timing of the spring budburst of deciduous tree species in Fennoscandia. In Chapter 7, methods are described to estimate the timing of budburst for beech and birch over large parts of Europe north of the Alps.

O_3 has to be taken up through the stomata of leaves in order to have negative impacts on physiology and growth of forest trees. Leaf O_3 uptake, i.e. the stomatal O_3 flux, is considered as the most appropriate index to estimate vegetation O_3 exposure (Mills et al., 2011). Relevant O_3 exposure indices for vegetation should be calculated for the period during the year when the vegetation is sensitive to O_3 impacts. It has been suggested to use a more general concept of an O_3 sensitive period, O₃SP, (Klingberg et al., 2014) instead of the terms "accumulation period, phenology and growing season" currently used in the Modelling and Mapping Manual (LRTAP Convention, 2017). Traditionally O₃SP has been considered to coincide with the growing season. However it is in fact not known if O_3 may have an impact on deciduous trees e.g. during the process of bud swelling before the bud burst or after the onset of autumn leaf coloration.

O₃SP at northern latitudes are getting longer (Karlsson et al., 2007) and are starting earlier during spring. Of particular interest at northern latitudes is the overlap between high O_3 concentrations during spring and the initiation of the O₃SP. This is illustrated in **Figure 8.1** with data from Esrange, located in northern Sweden (Lat 67°45´, Long 20°15´). The monthly mean daytime O_3 concentrations calculated over two different five-year periods, 1990-1994 and 2006-2010 were plotted separately for each month of the year. In addition, the length of growing season for the nearby site Ätnarova is illustrated for the same two five-year periods. The monthly mean daylight O_3 concentrations at Esrange had a maximum in April. Furthermore, it was higher during spring for the latter five-year period compared to the earlier period. At these northern latitudes, the growing season started later in the year for the period 1990-1994, compared to the period 2006-2010. Hence the start of the growing season and the high O_3 concentrations during spring are progressively increasing to overlap.
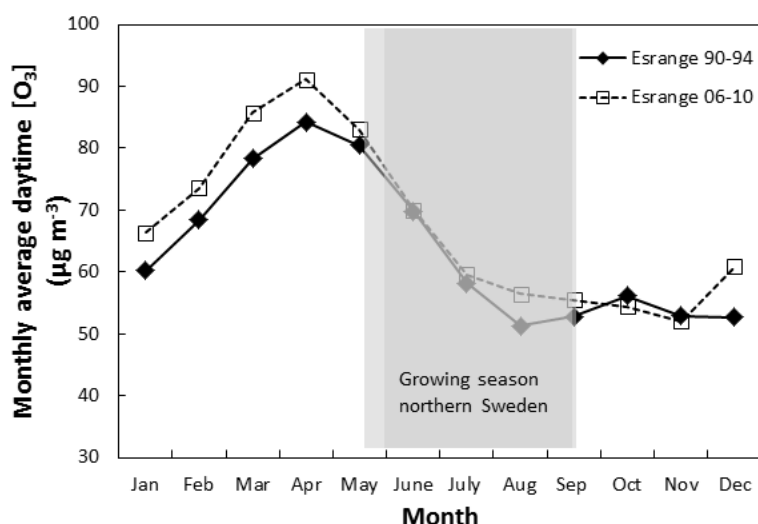
Figure 8.1   *The monthly mean daytime O₃ concentrations calculated over two different five-year periods, 1990-1994 and 2006-2010 for the site Esrange, positioned in northern Sweden (Lat 67°45´, Long 20°15´). In addition the mean start and end of growing season for the nearby site Ätnarova is shown for the two five-year periods with two different grey areas. The dark grey area indicates the mean growing season for 1990-1994 while the lighter grey area indicates the mean growing season 2006-2010. The start of growing season was calculated as the occasion when the daily mean air temperature exceeded 5°C for five consecutive days and vice versa for the end of the growing season. For the period 1990-1994 the growing season lasted between day-of-year (doy) 151-256, for the period 2006-2010 between doy 139-261. Klingberg et al., in preparation.*

8.2 Changes in the phenology of trees in northern Europe

The earlier onset of spring budburst and the later onset of autumn leaf coloration was demonstrated e.g. by Olsson (2014), see **Figure 8.2**. The average day of year (doy) for budburst and leaf colouring was assessed for more than 1,000 trees in Austria, Germany and the United Kingdom between 1950 and 2012, with data from the Pan European Phenology Project, see further below. Overall, budburst advanced 4-5 days/decade and the autumn leaf coloration was delayed by 4-5 days/decade.
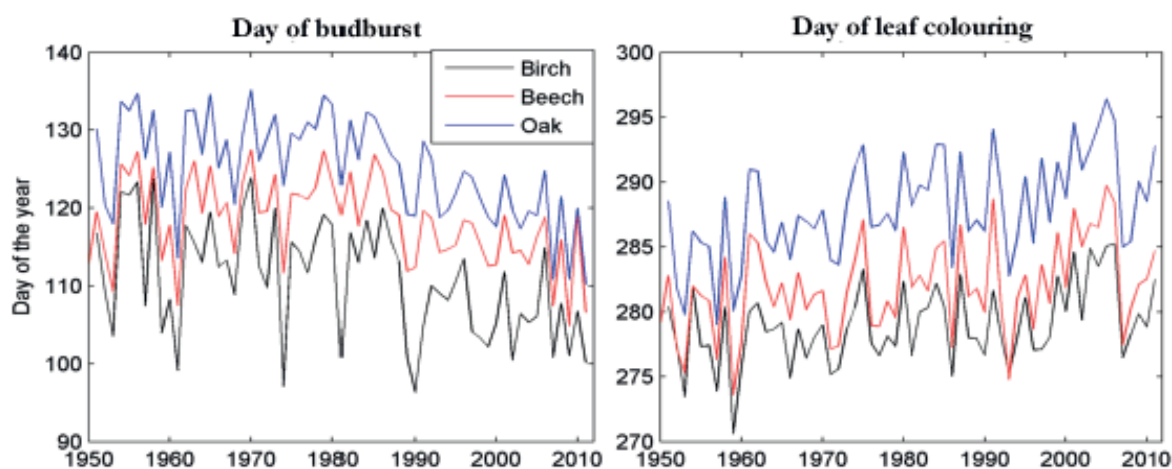

Figure 8.2   *Average day of year of budburst and leaf colouring for over a 1,000 trees in Austria, Germany and the United Kingdom between 1950 and 2012. From Olsson (2014).*

Menzel et al. (2006) used long-term, ground-based, ocular inspection observations to determine that autumn leaf coloration in Europe was delayed by 1.3 days per decade between 1971 and 2000. However, these trends were not unidirectional as only some individual sites demonstrated significantly delayed senescence, while others showed senescence dates that advanced and a large fraction of sites did not change significantly over time.

8.3 The physiological basis for deciduous tree budburst and leaf coloration

For birch in northern Europe, budburst is synchronized with flowering and hence the onset of the pollen season. Hence, there is a lot of research interest in being able to predict the onset of flowering of birch, due to the significance for pollen allergy. The synchronization is less evident for beech and oak. A comprehensive overview of the physiological basis for tree budburst and leaf coloration was provided by Olsson (2014). Existing models are to different extent capable of capturing the spring budburst or autumn leaf coloration for deciduous trees over large regions, such as northern Europe (Olsson, 2014). Uncertainties in model structure due to lack of scientific understanding are of more importance than uncertainties in phenology and climate data. Today there is no "ready-to use" model to apply for spring budburst and autumn coloration for birch and beech over large geographical areas such as e Fennoscandia.

Spring budburst

In northern tree species, budburst is controlled by both air temperature and the photoperiod. The role of the photoperiod for the budburst of beech was clearly demonstrated in an experimental study in the botanical garden of Munich, southern Germany. The light environment was manipulated by using light-tight and translucent plastic bags around the twigs (Zohner & Renner, 2015). Under constant 8-h days, budburst in beech outdoors was delayed by 41 days as compared to twigs receiving natural light conditions in translucent bags, under the environmental conditions prevailing in the botanical garden of Munich. Furthermore, long photoperiods advanced budburst for one-third of the species investigated in an experimental study by Laube et al. (2014).
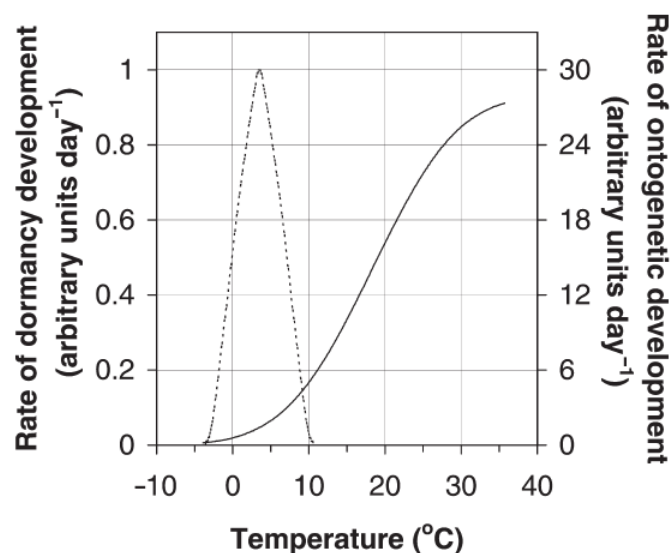

Figure 8.3   *Examples of chilling and forcing temperature responses. The efficiency of different temperatures to contribute to the chilling response is illustrated with the dotted curve and the left y-axis. The efficiency of different temperatures to contribute to the forcing response is illustrated with the solid curve and the right y-axis. From Linkosalo et al, 2000.*

Temperature controls budburst through two different processes; 1. Dormancy (inverse "readiness"), "chilling temp sum"; 2. Forcing temperatures,"warming temp sum". Increased chilling length, within certain limits, advanced budburst for almost all investigated species (Laube et al., 2014). Generally, in models the impact of temperature is calculated as temperature sums, with chilling temperature efficiency as an optimum curve and forcing temperatures above a base temperature, as illustrated in **Figure 8.3**.

Autumn leaf coloration

The delay in the autumn coloration of vegetation in Europe is not as clear as the changes during spring (Menzel et al., 2006). Temperature-induced changes in senescence at high-latitude sites are likely to be constrained by the influence of photoperiod (Gill et al., 2015). Local meteorological factors such as wind, precipitation and solar radiation have been shown to affect dates of senescence (Liu et al, 2016).

8.4 General considerations for the O_3 sensitivity periods for trees

There are some general considerations that can be made regarding the revision of the methodology to estimate the O_3SP for trees in continental and northern Europe.

The main objectives with developing new methodology should be:

- To predict year-to-year variations in O_3 risk assessments:
  - There is a considerable yearly variation in the occurrence of high O_3 concentrations, in particular during spring at northern latitudes. It is important that O_3SP for a specific year is predicted correctly in order to include/ exclude these periods of high concentrations when relevant;
- To predict spatial variation in O_3 risk assessments:
  - The O_3SP varies greatly spatially across Europe, in particular with latitude and altitude, but also between coastal and inland climates etc.:
- To predict impacts of climate change:
  - Climate change is having impacts on tree phenology and hence the O_3SP. It is important that future changes can be predicted in a credible way.

Further issues are to what extent O_3SP should be used to make correct representations separately for different tree species or alternatively for more general generic groups of species. Furthermore, should the methodology be representative for the entire geographical area or alternatively make separate representations that are valid for different regions? Finally, it may be an advantage if the methodology is simple and easy to understand for non-experts.

8.5 The O_3 sensitivity period for deciduous tree species

Definition of O_3SP for deciduous tree species

The O_3SP for deciduous tree species is suggested to be defined as the time between onset of spring budburst and the onset of autumn leaf coloration. It is however recognized that it is unknown if O_3 has impacts outside this time period, e.g. during the process of bud swelling or during the later processes of leaf senescence.

The choice of a representative deciduous tree species for Fennoscandia involves several aspects. However, birch, *Betula pendula*, has a much larger geographical distribution over Fennoscandia, as compared to beech, *Fagus sylvatica* (**Figure 8.4**). Hence, the choice for Fennoscandia should be birch.
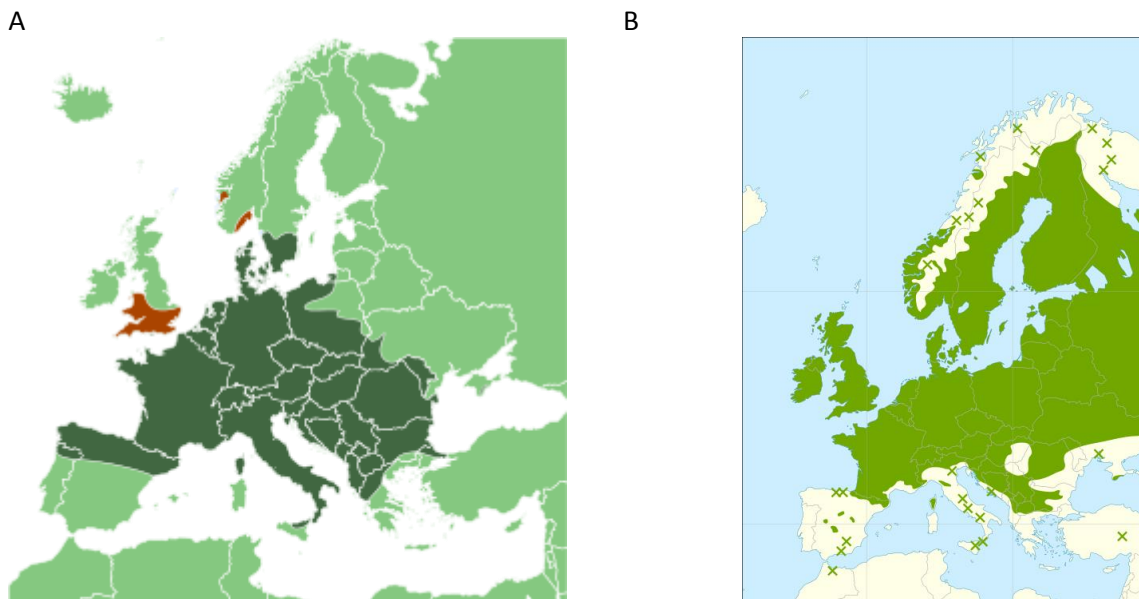
Figure 8.4 *Geographical distribution maps for beech, Fagus sylvatica, (A) and birch (B, Betula pendula). Source: Wikipedia.*

Methods to calculate the start of O₃SP for deciduous tree species

New attempts to describe the timing of spring budburst for beech and birch in Europe north of the Alps are described in a parallel document, Braun et al., 2017. In this section, we attempt to describe the timing of spring budburst for birch in Fennoscandia. We have started the analyses with a dataset for budburst of birch in Sweden and Finland. Some aspects of the timing of autumn leaf coloration are also included in these analyses.

Data description

Phenology data were obtained for *Betula* species from Pan European Phenology Project PEP725, (http://www.pep725.eu/). Furthermore, data were obtained from the Swedish Phenology Network. For budburst, the class bbch 10 was used (First leaves separated (mouse ear)) and for leaf autumn coloration the class bbch 94, (Autumnal colouring of leaves (50%)). The data include the species *Betula pendula* and *B. pubescence*, and the data for these two species were not separated.

The daily-mean temperatures from the sites in Finland were extracted from MESAN (Häggmark et al., 2000). MESAN is a system for mesoscale analyses of selected meteorological variables, including 2 m temperature, not readily provided by numerical weather forecast models. MESAN uses "Optimal interpolation" of observations of meteorological variables from a range of data sources together with a "Background field" from a meteorological weather forecast model to produce gridded fields of the variables in question. The daily-mean 2 m temperatures for the present study were extracted from the MESAN-grid encompassing each observation site and, for simplicity, averaged over data every three hours in GMT-time (the daily averages are thus not identical to the local time 24-hour averages, but shifted some 2 hours). The daily-mean temperatures from the sites in Sweden were obtained from geographically interpolated data supplied by SMHI, "Luftweb".

In the analysis of the onset of spring budburst, data were used for 17 sites in Finland which did not lack more than one year of data over the 15-year period 1997-2011, and for 6 sites in Sweden with three years data 2013-2016 (**Figure 8.5**). For analysis of autumn leaf colouration, data were used for 10 sites in Finland with one year or less missing data 2008-2013 and 15 sites in Sweden with at least 3 years data 2010-2015. Latitude for the sites ranged from 55 –

73

68 degrees, longitudes ranged from 12-31 degrees. However, for the analysis of the relations between autumn leaf colouration and mean temperatures, data was currently available for only four of the Finnish sites.
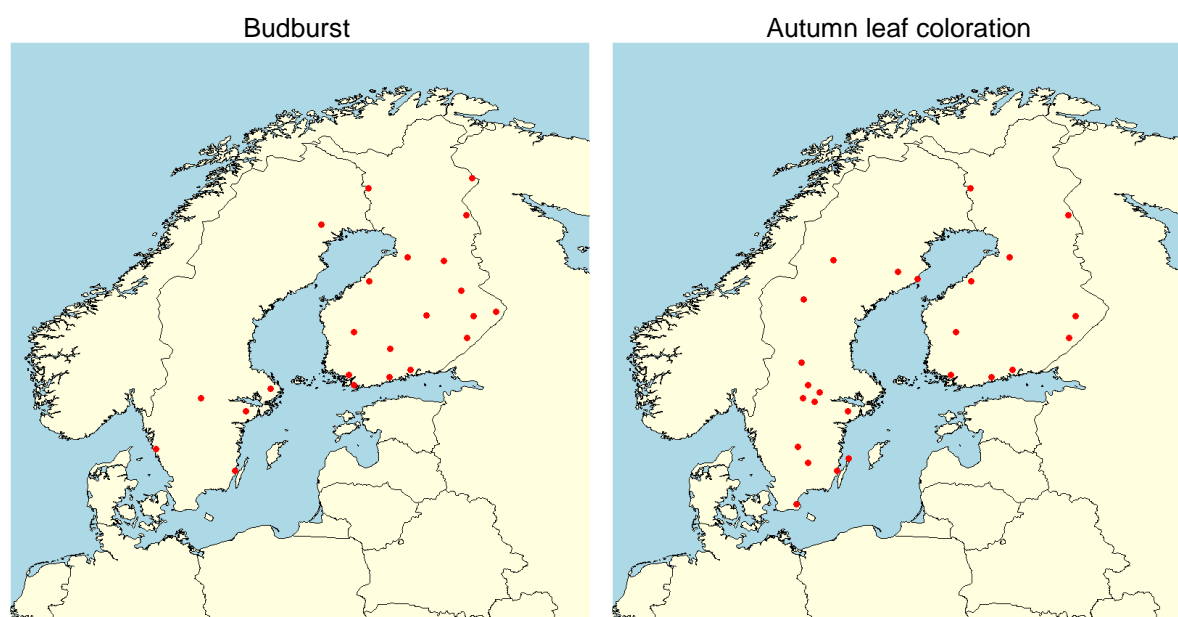
Budburst	Autumn leaf coloration

Figure 8.5   *Map over the different sites with information on the timing of budburst (left) and autumn leaf coloration (right) for birch in Finland and Sweden.*

General data analysis

The variation between data on spring budburst for all sites and years was considerable, but in many cases between-year variations were synchronized between sites (data not shown). For the mean values across the whole time period, 1997-2011 for Finland and 2013-2016 for Sweden, separately for each site, there were strong correlations for the timing of spring budburst with site latitude but not for autumn leaf coloration (**Figure 8.6**). The latter is a somewhat unexpected result. There were no correlations with longitude (data not shown).
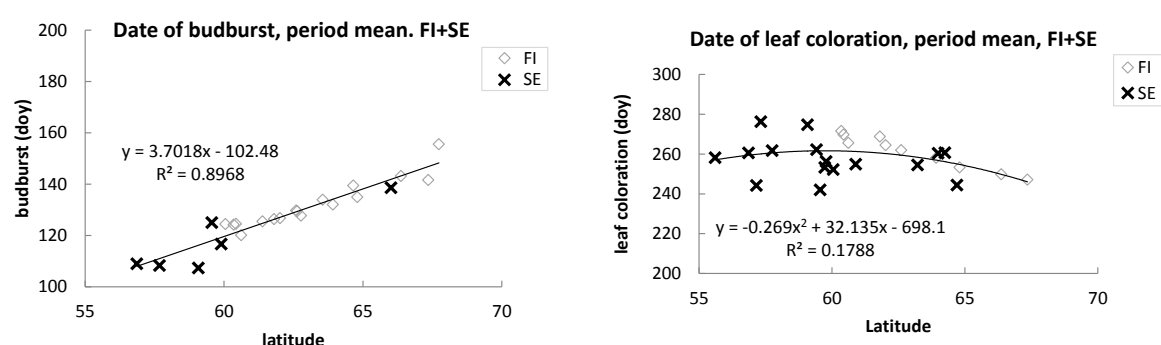

Figure 8.6   *The mean timing (day of year, doy) for budburst (BB_doy) and autumn coloration (AUT_doy) for sites with birch in Sweden and Finland, plotted against geographical position described by latitude.*

For mean values over long time periods, there are strong correlations for the timing of spring budburst with site latitude, but not for autumn leaf coloration for birch in Sweden and Finland.

In **Figure 8.7** time trends are shown for spring bud burst (left) and autumn leaf coloration (right), for birch in Finland, grouped according to four different latitude classes.

For budburst, the between-year variation was large and there were no clear trends over the period 1997-2011. This is in contrast to the results from the analysis by Olsson (2014, Figure 8.1). Earlier studies have demonstrated a significant advancement in the timing of the bud burst in the northern half of Finland (Poikolainen et al., 2016). This may not be shown if the data are analysed together for the whole country. The gradient from south to north for the timing of budburst is clear.

For doy for autumn coloration there were clear increasing trends for all latitude groups as well as across all sites. This is some conflict with the statement of Menzel et al. (2006), who observed no trend in leaf colouring, but in that study the majority of the observations were from Germany. As already shown in Figure 6.6, there was no clear relation between the timing of leaf autumn coloration and latitude for birch in Finland.

For the timing spring budburst for birch in Finland, there were no clear trends over the time period 1997-2011.

For the timing of autumn leaf coloration for birch in Finland there was a trend for later dates for all latitude groups.
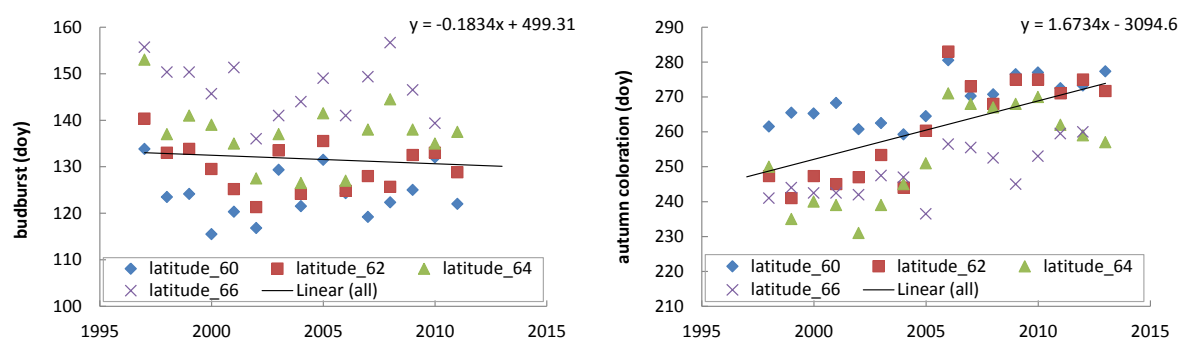

Figure 8.7   Time trends for spring bud burst (left) and autumn leaf coloration (right), for *Betula* sites in Finland, grouped according to four different latitude classes. Included are sites were data for budburst are missing <2 year, for autumn coloration <3 years. Latitude_60; latitudes 60-61.99, etc Latitude 66; latitudes >66. Black trend lines are added for regressions across all sites.

The correlations between budburst and autumn leaf coloration with temperature were analysed using T_{sum} based on 24h mean temperatures specific for the different sites:

Figure 8.8 shows the correlation between the mean accumulated T_{sum} >5°C since January at the time of observed budburst as mean values over the period 1997-2011, plotted against latitude for the 17 different sites with birch across Finland. Also shown is the standard deviation.

The accumulated T_{sum} >5°C at the day of the observed budburst was relatively similar for all sites independently of latitude, with a mean value of around 44 degree*days. The standard deviation was around 10-20 degree*days, demonstrating a considerable between-year variation, which however seem to be similar for all sites except one. Altitude was tested, but did not explain the difference in T_{sum} >5°C for a specific sites vs the mean for all sites.

Figure 8.8 *The accumulated temperature sum >5°C since January at the time of observed budburst, as a mean value across a 15-year period, plotted against latitude for 17 different sites with birch across Finland. The mean value and the standard deviation for each site over the period 1997-2011 are shown.*
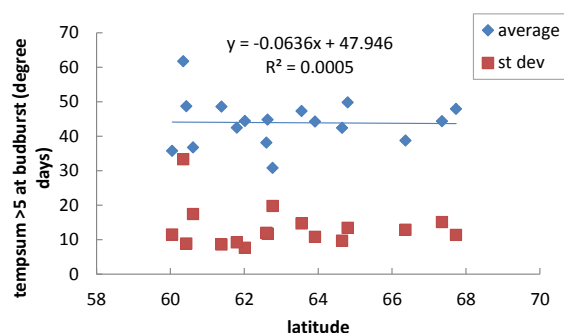
> **The accumulated temperature sum >5°C at the day of the observed budburst, as a mean value across a 15-year period, was relatively similar for all sites independently of latitude, with a mean value of around 44 degree days.**

Predicted vs observed timing of spring budburst of birch in Sweden and Finland – comparison of alternative models

In the current version of the Mapping Manual, the timing of the budburst (start of growing season, SGS) for deciduous trees in northern Europe is estimated with the "latitude model", which is defined as "SGS occurs at year day 105 at latitude 50°N, SGS will alter by 1.5 days per degree latitude earlier on moving south and later on moving north", i.e. SGS = 105 + ((lat-50)*1.5); SGS in day of year; lat in degrees

Prediction vs observations of the timing for the onset of budburst of birch in Sweden and Finland were compared using four different models:

1. The latitude model as described in the Modelling and Mapping Manual;
2. A modified version of the latitude model, according to SGS = 105 + (((lat*6)-340)*0.7);
3. A simple T_{sum} model, where daily mean temperatures were accumulated above 5°C and budburst was assumed to occur when the accumulated T_{sum} >45 degree days;
4. A version of the "Kramer model", including the impacts of T_{sum} both on a chilling period and on a forcing period. This model is described in detail in the companion paper Braun et al., 2017, as well as in Kramer (1994a,b). The parameterisation used was "birch D". In the Kramer model the forcing T_{sum} is accumulated over a base temperature of 0 °C.

There are several more models that can be tested (e.g. Linvill, 1990; Andersen, 1991, Sakalli and Simpson, 2012). The model by Sakalli & Simpson (2012) was tested in Chapter 7. It was less good compared to the T_{sum} models. More models might be tested in a later stage, as well as including observation data from Norway in the validation procedures.

Description of the Kramer model

The default Kramer model function for the rate of forcing (R_f, for explanation see Figure 8.3 above) is shown in **Figure 8.9** and compared to the corresponding function used for beech. The function gives much lower values for birch in the temperature range 0-10 °C, as compared to beech. At 10 °C, the value for birch is 0.02, while the value for beech is 0.48. The limit value for the accumulated R_f at budburst, F_{crit}, is set to 1.0 for birch and 9.66 for beech, but this difference is smaller than the difference in R_f values in the relevant temperature ranges.
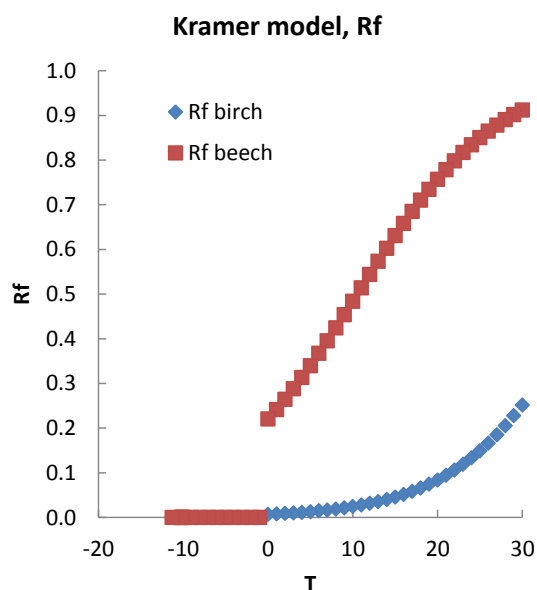
Figure 8.9 *Comparison of the value for R_f values for birch and beech calculated at different daily mean temperatures (T) by the Kramer model.*

Results from the comparisons

From the results shown in **Figure 8.10A**, it is clear that the latitude model had a limited capacity to predict yearly values for the timing of the onset of budburst, compared to what has been observed in Finland and Sweden. Observation ranged between doy 90-170 while the predictions from the latitude model only ranged between doy 110-130. It was possible to modify the latitude model to get the slope between observed and modelled values close to 1 and have an expanded range over the x-axis, as exemplified in **Figure 8.10B**, but the R^2 did not improve.

The simple T_{sum} model on the other hand, predicted doy for budburst almost with the same range as the yearly observations at the sites (**Figure 8.10C**), with an R^2 of 0.83 and a slope of 0.88.

The Kramer model applied with default parameterisation (from Germany) predicted the same range in between-year variation in the timing of budburst as was observed (**Figure 8.10D**), but the Kramer model systematically overestimated the doy for budburst by 20-30 days. It is likely that the function for the rate of temperature forcing, R_f, (Figure 6.9) yielded too low values in the relevant temperature range. This result contrasts with what was found by Braun et al., in Chapter 7.

The latitude model had a limited capacity to predict yearly values for the timing of the onset of budburst of birch in Sweden and Finland, compared to what has been observed. Even a modified version of the latitude model did not make satisfactory predictions of budburst.

A simple temperature sum model predicted budburst relatively well compared to observations, with an R^2 of 0.83 and a slope of 0.88.

The Kramer model, used with default parameterisation, gave a good prediction of the range of doy for the budburst of birch, but the model over-predicted the doy for budburst by 20-30 days, i.e. it predicted a later timing for the budburst.
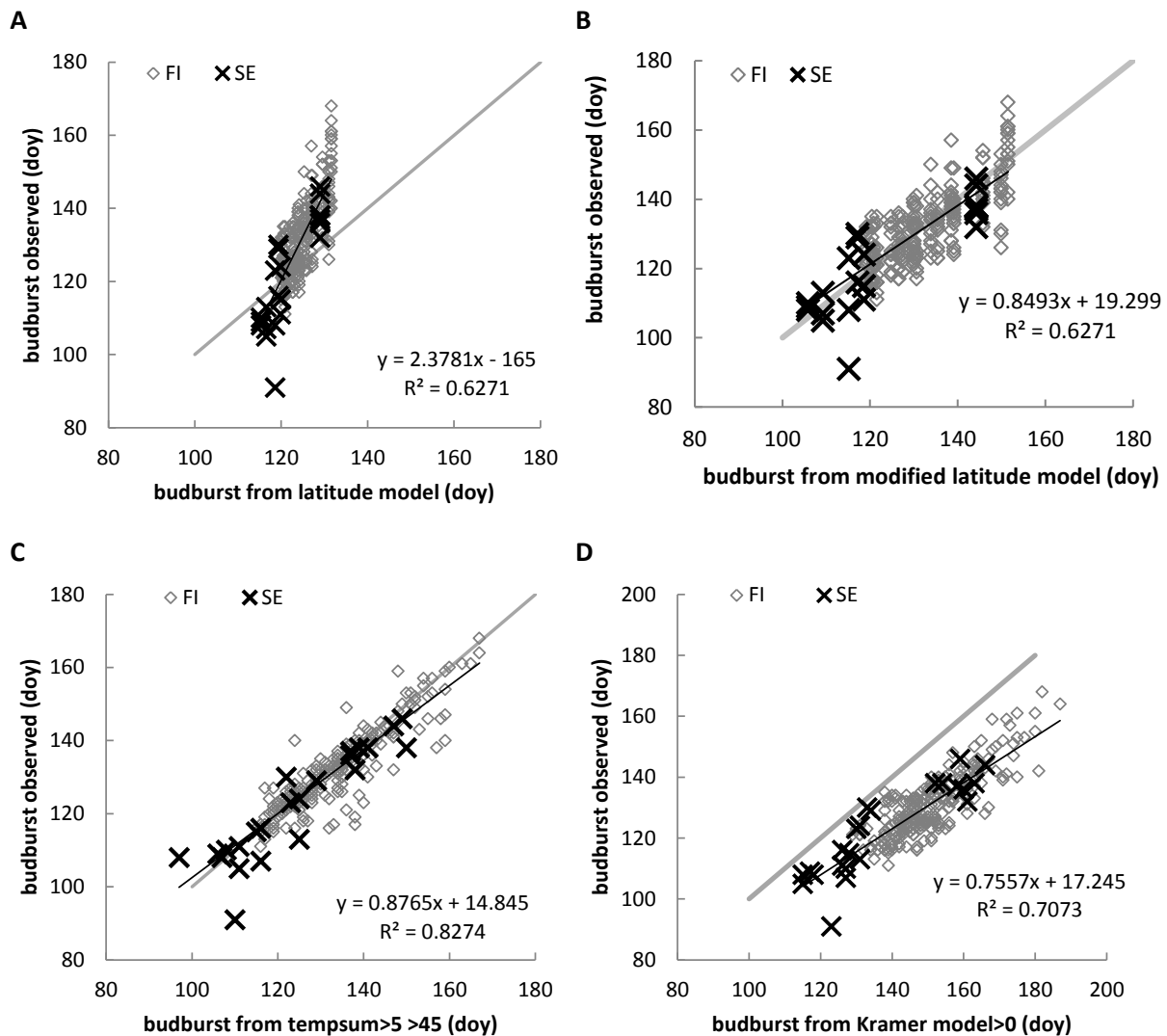
Figure 8.10 *Comparison of the prediction of the onset of budburst (day of year, doy) of birch in Sweden and Finland for the "latitude model" (A) and a model based on the accumulated daily temperature sum above 5°C since Jan 1st (C). In the temperature sum model it was assumed that budburst occur when the accumulated temperature sum >5 °C exceed 45 degree*days. In addition, the latitude model was modified (B) according to SGS = 105 + (((lat*6)-340)*0.7), in order to improve the correlation with observations. This modification was by no means optimized and should only be seen as an example. Finally, the timing of budburst was predicted with the Kramer model (D). The analysis was made with the annual data, 1997-2011 from 17 sites in Finland and 2013-2016 from 6 sites in Sweden. Only sites with a data loss of one year or less were used.*

Methods to calculate the end of O₃SP for deciduous tree species

Keskitalo et al. (2005) studied the process of senescence in free-growing aspen trees, *Populus tremula*, growing in Umeå, northern Sweden. They concluded that senescence was initiated solely by the photoperiod. Degradation of leaf constituents took place over an 18-d period.

There is today no generally accepted model to apply for autumn leaf coloration for deciduous trees. Liu et al. (2016) analysed the end-of-season (EOS) in northern China, determined from satellite data. They suggested that temperature during summer affects EOS in autumn. They

suggested to use the mean temperature 1-5 months prior to EOS. To improve the models, they suggested to in addition use precipitation sum and solar radiation 1–5 months prior to EOS. Delpierre et al. (2009) analysed the timing of temperate forest autumn leaf colouring in France 1997–2006. They suggested to use a model based on a one-way process triggered by photoperiod and progressing through a photoperiod-sensitive cold-degree day summation procedure.

Estrella & Menzel (2006) analysed the autumn leaf coloration dates for 4 deciduous tree species (horse chestnut, beech, birch, oak) in Germany (1951–2003). They concluded that a warm September (all species) and August (oak, birch) delayed autumn leaf coloration while a warm June (horse chestnut, oak) and May (horse chestnut) advanced autumn leaf coloration, even though the correlation coefficients were relatively weak. Autumn leaf coloration dates were not strongly related to the date when the daily mean temperatures decreased below 5 °C for five consecutive days. In conclusion, they stated that there is no complete and coherent model for the timing of observed autumn leaf coloration of deciduous trees in temperate zones.

However, Estrella & Menzel (2006) still suggested the following model for beech, based on mean monthly temperatures for June, August and September:

Beech leaf colouring [day of the year] = 264.86 + (–1.30 × mo_6 [°C]) + (1.04 × mo_8 [°C]) + (1.56 × mo_9 [°C]).

For birch, the number of dry days in September were incorporated alongside August and September mean temperatures.

Birch leaf colouring [day of the year] = 254 + (0.68 mo_8 [°C]) + (1.45 mo_9 [°C]) + (–0.35 ndry_9 [no. of days])

Preliminary analyses were made in this study of the leaf autumn coloration for 15 sites 2010-2015 with birch in Sweden and 4 sites 2008-2013 in Finland, for separate sites and years, correlating the doy for leaf coloration with the mean temperatures for the time period 1 July – 31 August (**Figure 8.11**). The sites were separated into three geographical classes depending on latitudes.
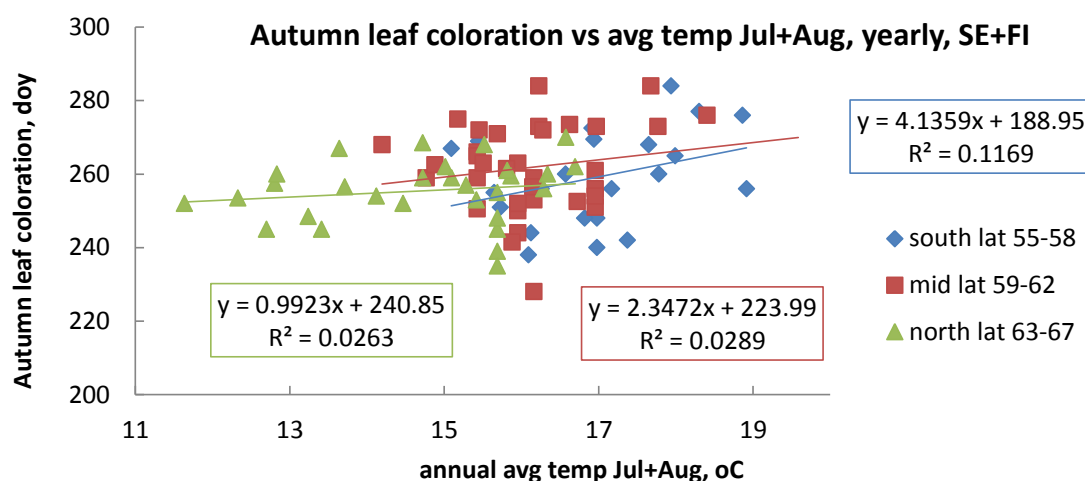

Figure 8.11 Comparison of the annual doy for observed leaf coloration, separately for each site, with the mean temperatures for the time period 1 July – 31 August for the same year and site. The sites were separated into three geographical classes depending on latitudes.

There were some weak indications that there might be a correlation of the doy for leaf autumn coloration with the corresponding mean temperature for the months July + August, in particular in the southern geographical region. In the northern region, there was no correlation what so

ever. The relation between autumn leaf coloration and the mean temperature for the months August + September was also tested, but gave worse results.

The analyses shown in Figure 6.11 represent a first step and need to be elaborated further. For autumn coloration there seems to be increasing temporal trends of doy for all latitude groups as well as across all sites (Figure 6.7), but this is not well explained by differences in the mean monthly temperatures for July + August (Figure 8.11).

8.6 The O_3 sensitivity period for evergreen coniferous tree species

Definition of O_3SP for coniferous tree species

The O_3SP for coniferous tree species is suggested to be defined as the period during the year with active leaf gas exchange.

Methods to calculate the start of O_3SP for coniferous tree species

In northern Europe the growing season has been suggested to start when the 24-hour mean temperature exceed a base temperature of approximately $5^{\circ}C$ (range 3.3 – 6.5 $^{\circ}C$ for different sites) during five consecutive days (Suni et al., 2003). This study was based on micro-meteorological measurements of canopy gas exchange for coniferous trees species in northern Sweden and Finland as well as Siberia.

However, other studies reveal a more complicated picture. Wallin et al. (2013) measured gas-exchange of 40-year-old Norway spruce trees with branch cuvettes in stands at Flakaliden in northern Sweden at 64.1° latitude. The trees were enclosed in "Whole-Tree Chambers" and were subject to combination treatments with ambient and elevated temperature and CO_2, respectively. Measurements were also made on adjacent trees without enclosure. Data on light saturated photosynthesis was reported but it can be assumed that there is a relatively close correlation between photosynthesis and stomatal conductance in these trees. Measurements were made during spring recovery from dormancy during three years 2002-2004. Results are shown in **Figure 8.12** for 2003, a year with spring temperatures similar to long-term average spring temperatures. The results from the other years were similar. It can be seen from the results that the recovery of gas-exchange from winter dormancy is non-linear over time and that the first recovery, up to 60% of summer maximum gas-exchange, occurs already more than a month before the calculated start of growing season (calculated as when the 24-h mean temperatures exceed $5^{\circ}C$ as well as calculated with the latitude model = doy126). It is also clear that the treatment with elevated temperature advanced the start of the gas-exchange to earlier dates. Measurements on trees without enclosure resembled those of the enclosed trees with ambient temperatures. The main conclusions made by the authors were that the photosynthetic recovery during spring to a large extent was related to air temperature and that intermittent frost events delayed the recovery.
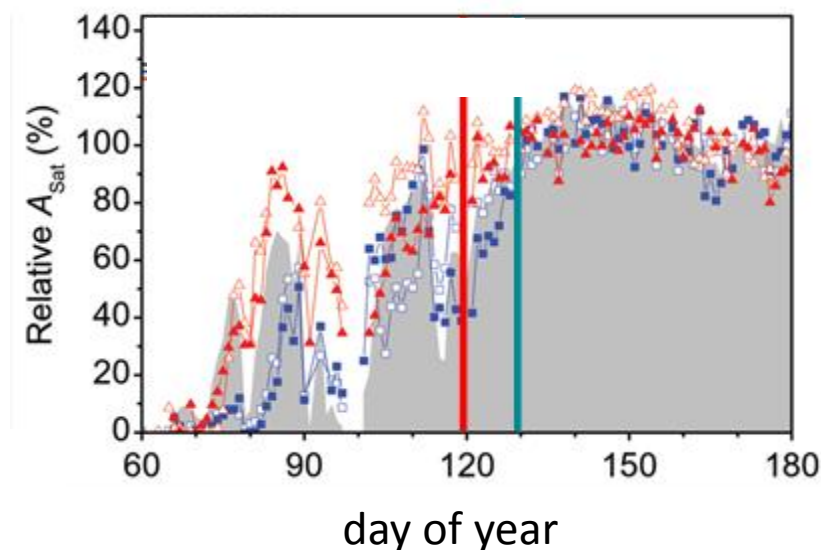
Figure 8.12   Light-saturated photosynthesis (% of June average) of 1-year-old shoots in 40-year old Norway spruce trees at Flakaliden in northern Sweden (latitude 64.1°) plotted against day of year (doy) on the x-axis. Data are for trees enclosed in "Whole-Tree Chambers" with ambient temperatures (Blue symbols) or with elevated temperatures (red symbols). Also show are data for trees not enclosed in chambers (grey field). Vertical thick lines indicate the timing of the start of the growing season calculated as when 24-h mean temperatures exceed 5 °C for five consecutive days in the chambers with ambient temperature (blue line) and elevated temperatures (red line). The start of growing season calculated with the latitude model is doy 126. Data is shown for the year 2003, but similar data were obtained for 2002 and 2004. For more details, see Wallin et al. (2013).

Hence, methods used within the Modelling and Mapping Manual to estimate the onset of the O₃ sensitivity period for coniferous tree species in northern Europe clearly needs revision and the solution is not a simple application as when 24-h mean temperatures exceeded 5°C. One approach, suggested by Klingberg et al. (2014), could be to define the O₃ sensitivity period based on daily calculations of stomatal conductance (g_{sto}) with the DO₃SE model approach, based on local meteorology. The start (end) of the O₃SP was suggested as the first (last) day of the year when the daily summed g_{sto} exceeded 30% of the theoretically maximum daily summed g_{sto} (g_{max} summed over 24 h).

It is evident that the start of the gas exchange of these mature Norway spruce trees in stands in Northern Sweden started well before the calculated start of growing season, either as when 24-h mean temperatures exceeded 5°C or as predicted with the latitude model.

Methods to calculate the end of O₃SP for coniferous tree species

There are, as far as we know, no methods to calculate the end of O₃SP for coniferous tree species.

8.7 Conclusions

Conclusions regarding potential methods to estimate O₃SP for trees in Fennoscandia:

Deciduous trees (birch), start of O₃SP: A satisfying model can most likely be developed within the next few years. A modified Latitude model may act as a "quick fix".

Deciduous trees (birch), end of O₃SP: A satisfying model can maybe be developed within the next few years.

Coniferous trees (spruce), start of O₃SP: A satisfying model can probably be developed within the next few years

Coniferous trees (spruce), end of O₃SP: As yet, there are no available models or even concepts. These have to be developed from scratch.

8.8 References

Andersen, T.B. 1991. A model to predict the beginning of the pollen season. Grana 30, 169-275.

Andersen, T.B. 1991. A model to predict the beginning of the pollen season. Grana 30, 169-275.

Braun, S., Müller, S., Karlsson, P.E. Budbreak of beech and birch in a changing climate. Scientific Background Document B accompanying Chapter 3 of the LRTAP Modelling and Mapping Manual. Available at the web page of ICP Vegetation, http://icpvegetation.ceh.ac.uk.

Delpierre, N., Dufrene, E., Soudani, K., Ulrich, U., Cecchini, S., Boe, J., Francois, C. 2009. Modelling interannual and spatial variability of leaf senescence for three deciduous tree species in France. Agricultural and Forest Meteorology 149, 938 – 948.

Estrella, N. Menzel, A. 2006. Responses of leaf colouring in four deciduous tree species to climate and weather in Germany. Clim Res 32, 253–267.

Gill et al., 2015. Changes in autumn senescence in northern hemisphere deciduous trees: a meta-analysis of autumn phenology studies. Annals of Botany doi:10.1093/aob/mcv055.

Häggmark, L., Ivarsson, K.-I., Gollvik, S. and Olofsson, P.-O. 2000. Mesan, an operational mesoscale analysis system. Tellus 52A, 2-20.

Karlsson, P.E., Tang, L., Sundberg, J., Chen, D., Lindskog, A. and Pleijel, H. 2007. Increasing risk for negative ozone impacts on vegetation in northern Sweden. Environmental Pollution 150, 96-106.

Keskitalo, J., Bergquist, G., Gardeström, P., Jansson, S. 2005. A Cellular Timetable of Autumn Senescence. Plant Physiology, 139, 1635–1648

Klingberg, J. M. Engardt, P. E. Karlsson, J. Langner, and H. Pleijel. 2014. Declining ozone exposure of European vegetation under climate change and reduced precursor emissions. Biogeosciences, 11, 5269–5283.

Kramer K. 1994a . A modelling analysis of the effects of climatic warming on the probability of spring frost damage to tree species in The Netherlands and Germany. Plant Cell Environ 17: 367-377.

Kramer K. 1994b. Selecting a Model to Predict the Onset of Growth of Fagus sylvatica. Journal of Applied Ecology 31: 172-181.

Laube, J., Sparks, t.H., Estrella, N., Höfler, J., Ankerst, D.P., Menzel, A. 2014. Chilling outweighs photoperiod in preventing precocious spring development. Global Change Biology 20, 170–182.

Linkosalo, Carter,T.R., Häkkinen, R., Hari, P. 2000. Predicting spring phenology and frost damage risk of Betula spp. under climatic warming: a comparison of two models. Tree Physiology 20, 1175–1182.

Linvill, 1990. Calculating Chilling Hours and Chill Units from Daily Maximum and Minimum Temperature Observations. HORTSCIENCE, VOL. 25, 14-16.

Liu, Q., Fu, Y.H., Zeng, Z., Huang, Li, M.X., Piao, S. 2016. Temperature, precipitation, and insolation effects on autumn vegetation phenology in temperate China. Global Change Biology 22, 644–655.

Menzel et al., 2006. European phenological response to climate change matches the warming pattern. Global Change Biology 12, 1969–1976.

Mills, G., Håkan Pleijel, Sabine Braun, Patrick Büker, Victoria Bermejo, Esperanzo Calvo, Helena Danielsson, Lisa Emberson, Ludger Grünhage, Ignacio González Fernández, Harry Harmens, Felicity Hayes, Karlsson, P.E., David Simpson. 2011. New stomatal fluxbased critical levels for ozone effects on vegetation. Atmospheric Environment 45, 5064-5068.

Olsson, C. 2014. Tree phenology modelling in the boreal and temperate climate zones : Timing of spring and autumn events. Thesis. Department of Physical Geography and Ecosystem Science, Lund University. ISBN 978-91-85793-43-3

Poikolainen, J. Tolvanen, A. Karhu, J., Kubin, E. 2016. Seventeen-year trends in spring and autumn phenophases of Betula pubescens in a boreal environment. Int J Biom 60, 1227-1236.

Sakalli, A., Simpson. D. 2012. Towards the use of dynamic growing seasons in a chemical transport model. Biogeosciences, 9, 5161–5179.

Suni, T., Berninger, F., Vesala, T., Markkanen, T., Hari, P., Makela, A., Ilvesniemi, H., Hanninen, H., Nikinmaa, E., Huttula, T., Laurila, T., Aurela, M., Grelle, A., Lindroth, A., Arneth, A., Shibistova, O. and Lloyd, J. 2003. Air temperature triggers the recovery of evergreen boreal forest photosynthesis in spring, Glob. Change Biol., 9, 1410-1426.

Wallin, G., Hall, M., Slaney, M., Räntfors, M., Medhurst, J. Linder, S. 2013. Spring photosynthetic recovery of boreal Norway spruce under conditions of elevated [CO2] and air temperature. Tree Physiology 33, 1177–1191.

Zohner, C. M., Renner. S. S. 2015. Perception of photoperiod in individual buds of mature trees regulates leaf-out. New Phytologist 208, 1023–1030.

9 Analysis of O₃ flux-effect relationships - the Random Effects Method

Christian Schindler[1)] and Sabine Braun[2)]

[1)] *Swiss TPH, University of Basel, Switzerland*
[2)] *Institute for Applied Plant Biology, Schönenbuch, Switzerland*

9.1 The Fuhrer method

For establishing dose-response and flux-effect relationships between O_3 and plant response, the results from experiments in open top chambers were used (Fuhrer et al., 1997). Such experiments have at least two treatments: a control which may contain some O_3 and one or several treatments with increased O_3. For control treatments containing O_3, Fuhrer et al. (1997) proposed to evaluate first the regression between plant response and O_3 and use the intercept of the regression line (i.e., the intersection with the y-axis) as estimate for the plant response among controls (**Figure 9.1**). This procedure allows estimating a confidence interval for the intercept. While it does not affect the slope of the regression, the calculation of the hypothetical control translates, however, the error of the regression line to the intercept. The Fuhrer method corrects the biomass from multiannual experiments with an exponent of 1/years but it does not consider the exponential distribution of the biomass data. The adjustment of multi-annual experiments used so far leads to a loss of statistical power as it reduces the spread of the data points over the two axes.
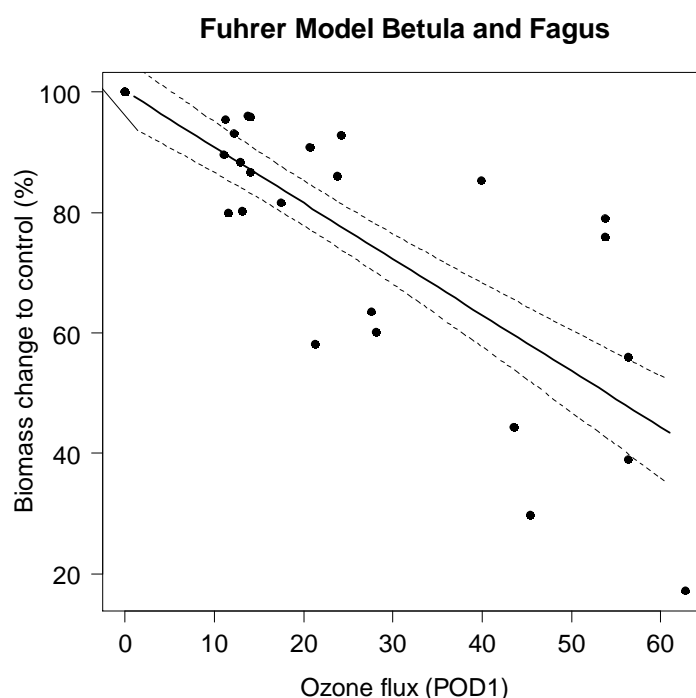
Fuhrer Model Betula and Fagus

Figure 9.12   *Flux-effect relationship for Betula sp. (birch) and Fagus sylvatica (beech) analysed with the Fuhrer method.*

Advantages of the Fuhrer method are:
- Relatively easy to apply;

- Comparison with Random Effects Method reveals similar slopes of the dose response relationships and critical levels (for the data that have been tested).

<u>Drawbacks of the Fuhrer method are</u>:

- Does not allow considering the exponential nature of the growth of young plants (problem for trees)

- Does not allow to account for the arrangement of the data in groups (experiments)

- Does not allow for a transformation of the dependent variable assuring normal distribution of the residuals.

9.2 The Random Effects Method

We propose here to analyze dose-response curves with more sophisticated regression methods which are more flexible and allow adaptations to specific datasets. The exponential transformation might not be necessary for crops but it is certainly needed for trees.

With an exponential growth model, the size of the tree i at time t can be described as:

$$s_i(t) = s_i(0) \times e^{(b_1 \times t - b_2 \times c_i \times t)}$$

with:

$s_i(t)$: size of tree i at time t

$c_1 = O_3$ exposure level of tree i.

If we assume that $s_i(0)$, b_1 and b_2 are constant across all trees of a given experiment then we obtain:

$$\frac{s_i(t)}{s_1(t)} = e^{-b_2 \times (c_i - c_1) \times t}$$

(tree number 1 with lowest value c_i being the reference)

Taking logarithm, one obtains:

$$ln\left[\frac{s_i(t)}{s_1(t)}\right] = -b_2 \times (c_i - c_1) \times t$$

So, b_2 can be estimated using a regression model

$$y_i = b \times x_i + error$$

with $y = ln[s_i(t)/s_1(t)]$ and $x_i = -(c_i - c_1)*t$

and without intercept term.

When extending the regression analysis across different experiments, it makes sense to assume that the effects of O_3 on growth vary slightly across experiments. This can be captured by a random component v added to b2 and satisfying:

1) v is constant within trees of the same experiment
2) v varies across experiments
3) v has a mean value of 0 across all experiments
4) v is normally distributed

This gives rise to a random effects model of the form:

$$y_{ij} = (b + v_j) \times x_i + error$$

where j denotes the number of the experiment.

We may further add a random intercept u_j for each experiment j, capturing slight deviations from our assumptions:

$$y_{ij} = u_j + (b + v_j) \times x_i + error$$

When the biomass of the controls is set to 1 and O_3 exposure is taken as difference in exposure between treatment and control (i.e., with exposure among controls being set to 0) the latter model is not necessary.

With this exponential model, the biomass change over the whole experiment can be analyzed in relation to the O_3 cumulated over the whole experiment.

In R, the presented model can be calculated with the packacke nlme (Pinheiro et al., 2016):

```
x <- (treatment_O₃ – reference_O₃) * duration exposure

y <- log(size_tree/size_tree₁)

EXP: experiment number
```

    (i)   without random effect of the intercept:
```
model <-nlme( y ~ (b + v)*x,   data=mydata, fixed=c(b~1), start=c(b=-
0.0035),  random= v~1|EXP)
```

    (ii)   with random effect of the intercept:
```
model <-nlme( y ~ u+(b + v)*x,   data=mydata, fixed=c(b~1), start=c(b=-
0.0035),  random= u+v~1|EXP)
```

If the log to the basis e is taken, then the slope b can be directly converted into an estimate of relative biomass loss in percent, i.e., by multiplying b with 100. This estimate is sufficiently

precise if b is small (e.g. <0.1). For larger values of b, 100*(exp(b)-1) should be taken. The confidence interval of b equals b ± SE*1.96. The relative biomass at $O_3=0$ is 1 as the logarithmic model has an intercept of 0 (**Figure 9.2**). With this method, the statistical uncertainty about the intercept is no longer relevant.

Errors in the control measurements may be taken into account by a random intercept u (bullet point ii).

The Critical Level has to be defined as a maximum tolerated biomass reduction. This has already been done for the current Critical Level for forest trees where annual biomass losses of 2% and 4% are accepted for Norway spruce and beech/birch, respectively.
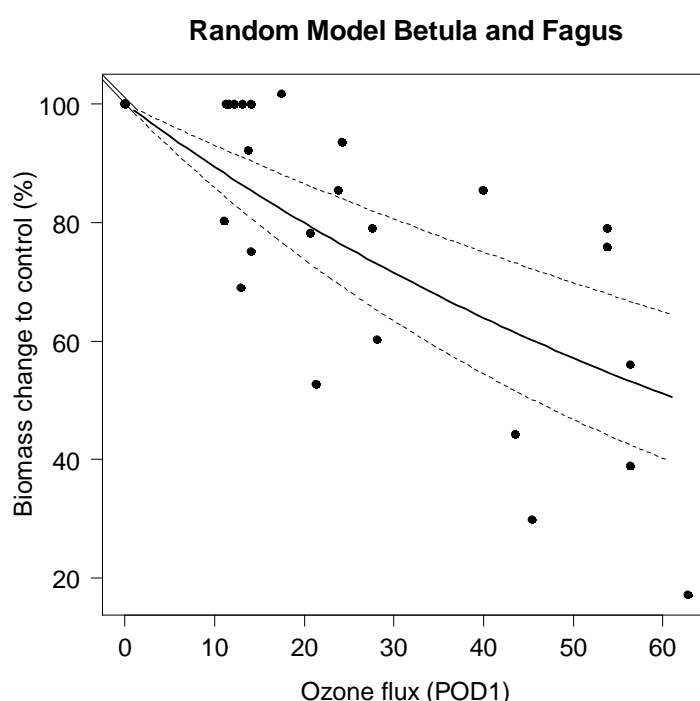
Random Model Betula and Fagus

Figure 9.13   *Dose response relationship for Betula sp. (birch) and Fagus sylvatica (beech) analysed with the Random Effects Model. The figure displays the exponential dose-response curve (solid line) and its 95%-confidence limits (dotted lines).*

Advantages of the Random Effects model are:

- Allows more flexible data analysis including exponential growth data, transformation of the dependent variable and correct adjustment of confidence intervals for arrangements of data in groups;
- Use of state of the art statistical methods.

Drawbacks of the Random Effects model are:

- More complex than the Fuhrer method;

87

- Requires certain statistical knowledge and experience with statistical software.

9.3 Comparison of both methods for O_3 effects on trees

Recalculations of the dose-response curves with the random effects method were based on the dataset used by Büker et al. (2015) with threshold 1 (POD_1). The comparison with results from the Fuhrer Method shows that the random effects model yields slightly more sensitive dose-response relationships than the Fuhrer approach (**Table 9.8 - 9.3**) while some standard errors are smaller and some larger. Larger standard errors can be explained by the non-consideration of the clusters in the Fuhrer procedure. A better performance of the random effects approach is, however, illustrated by comparing the plots of fitted vs. observed values (**Figure 9.14** and **9.4**). This can be explained by the better suitability of a log model for biomass, by the retention of multiannual data which increases the spread of the x-axis and by the better control of differences between experiments.

Table 9.8   *Coefficients calculated with the random effects approach.*

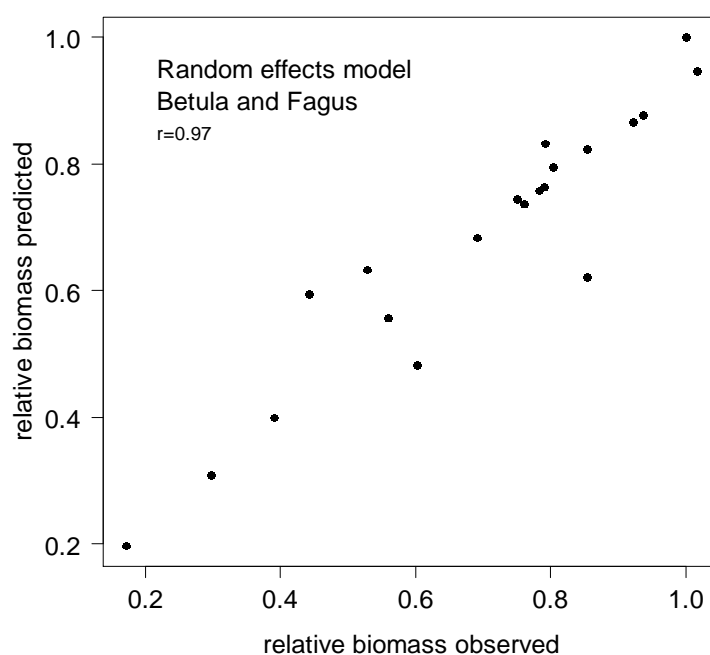|	slope	Std.Error	DF	t-value	p-value	groups	obs.
Betula, Fagus, Populus	-0.01153	0.00196	23	-5.89544	0.00000	18	41
Betula, Fagus	-0.01119	0.00208	19	-5.38621	0.00000	15	34
Quercus deciduous	-0.00269	0.00049	10	-5.49543	0.00030	6	16
Quercus ilex	-0.00221	0.00036	4	-6.16366	0.00350	2	6
Coniferous	-0.00268	0.00051	22	-5.25838	0.00000	18	40
Picea	-0.00258	0.00062	16	-4.19215	0.00070	13	29

Figure 9.14   *Plot of predicted vs. observed values of $ln(c_i(t)/c_1(t)$ for the Betula/Fagus dataset calculated with the Random Effects model*

Table 9.9   *Coefficients calculated with the Fuhrer approach.*

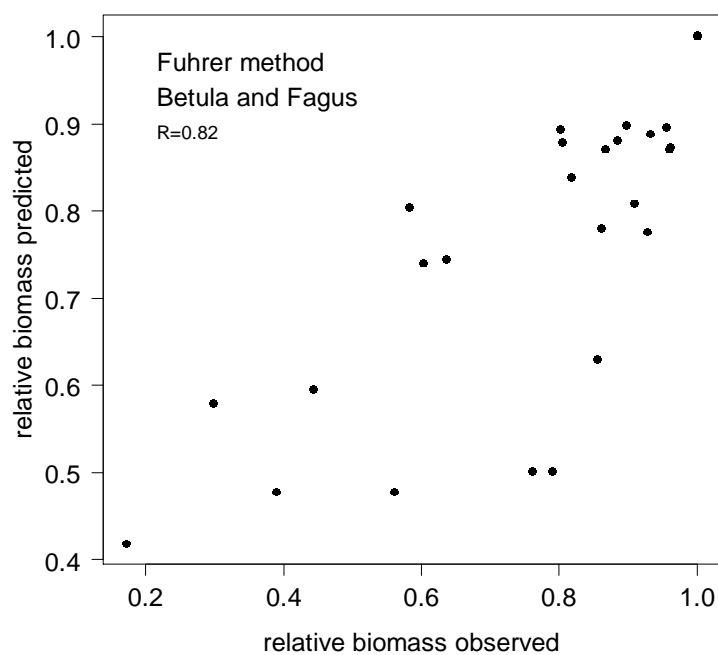|	intercept	SE intercept	slope	SE slope	p-value
Betula, Fagus, Populus	0.99375	0.03251	-0.00847	0.00104	0.00000
Betula, Fagus	1.00186	0.03190	-0.00930	0.00113	0.00000
Quercus deciduous	1.03254	0.01964	-0.00275	0.00044	0.00002
Quercus ilex	0.99938	0.01563	-0.00180	0.00061	0.04090
Coniferous	0.99878	0.00585	-0.00240	0.00037	0.00000
Picea	0.99837	0.00590	-0.00218	0.00059	0.00097

Figure 9.15   *Plot of predicted vs. observed relative biomass for the Betula/Fagus dataset calculated with the Fuhrer method.*

Table 9.10   *Estimates of POD$_1$ (mmol m^{-2} y^{-1}) values causing 5% biomass reduction including the 95% confidence interval.*

	random effects approach			linear model (Fuhrer approach)		
	average	95% confidence interval		average	95% confidence interval	
Betula, Fagus, Populus	4.45	3.34	6.66	5.90	4.76	7.76
Betula, Fagus	4.58	3.36	7.21	5.38	4.34	7.06
Quercus deciduous	19.07	14.06	29.64	18.18	13.87	26.38
Quercus ilex	23.16	17.57	33.95	27.75	16.73	81.30
Coniferous	19.17	13.97	30.57	20.86	15.96	30.07
Picea	19.85	13.53	37.29	22.93	14.99	48.72

9.4 Conclusions

- The Fuhrer Method for deriving critical levels for O$_3$ has weaknesses that could be overcome by applying more elaborate regression methods;

- In future analyses, we propose to apply an exponential growth model with random effects which is more flexible than the Fuhrer Method and allows adaptations to specific datasets;

- Estimations of dose-response curves for trees revealed a better performance of the random effects model compared to the Fuhrer approach;

- Calculations showed that the random effects model provides lower critical levels than the Fuhrer approach.

9.5 References

Büker, P., Feng, Z., Uddling, J., Briolat, A., Alonso, R., Braun, S., Elvira, S., Gerosa, G., Karlsson, P. E., LeThiec, D., Marzuoli, R., Mills, G., Wieser, G., Wilkinson, M., Emberson, L., 2015. New flux-based dose-response relationships for ozone for European forest tree species. Environmental Pollution 206**,** 163-174.

Fuhrer, J., Skärby, L., Ashmore, M. R., 1997. Critical levels for ozone effects on vegetation in Europe. Environmental Pollution 97**,** 91-106.

Pinheiro, J., Bates, D., DebRoy, S., Sarkar, D., R Core Team, 2016. nlme: Linear and Nonlinear Mixed Effects Models. R package version 3.1.-124, <URL: http://CRAN.R-project.org/package=nlme>.

10   Epidemiologal analysis of O_3 impacts on vegetation

Sabine Braun[1], Beat Achermann[2], Alessandra DeMarco[3], Håkan Pleijel[4], Per Erik Karlsson[5], Beat Rihm[6], Christian Schindler[7], Elena Paoletti[8]

[1] *Institute for Applied Plant Biology, Schönenbuch, Switzerland*
[2] Federal Office for the Environment, Berne, Switzerland
[3] *ENEA, SSPT-MET-INAT, Italy*
[4] *University of Gothenburg, Sweden*
[5] *IVL Swedish Environmental Research Institute, Gothenburg, Sweden*
[6] *Meteotest, Berne, Switzerland*
[7] *Swiss TPH, University of Basel, Switzerland*
[8] *CNR, Sesto Fiorentino, Italy*

Braun et al. (2017) describe how epidemiological methods, originally developed for the study of effects of different environmental variables on human health, can be successfully used for the study of air pollution effects on vegetation, and applied to research questions analogous to those related to human health. A more extensive use of such methods in the context of evaluating air pollution effects on vegetation is recommended. Such studies can complement and support toxicological and other experimental studies by making systematic use of information at the landscape level. In so doing, they assess the distribution of risks for adverse effects of air pollutants in ecosystems while considering important confounding factors. Statistical associations between environmental drivers and effects may thus be established. These results may further be used to identify hypotheses to be tested in experiments.

Epidemiological methods require a sufficiently large number of observations at large spatial and/or temporal scales along a distinct air pollution gradient and information on modifying factors, such as meteorological and soil characteristics. A relatively high spatial and temporal resolution is required to capture this information and thus to correctly assess the effects of air pollutants on vegetation, which may otherwise not become apparent in the analysis although relevant in reality. With an epidemiological approach the influence of several environmental drivers on effects can be considered, therefore it may be extended to scenario analyses where the combined effect of future air pollution and climate on vegetation is investigated. It will also be useful for the assessment of biological effects from different air pollution mitigation strategies at different scales. Epidemiological analysis has the potential to contribute highly significant information about air pollution effects on vegetation by combining understanding from experimental results with information from e.g. environmental monitoring, geographical information systems and remote sensing using a elaborate and well-established statistical framework.

For human health studies, epidemiology has been established as important tool to examine factors that affect the frequency and distribution of disease, injury, and other health-related events in a defined population, serving the purpose of establishing prevention and control programmes. On the other hand, gradient studies have a long tradition in the research of air pollution effects on plants. While there is no principal difference between gradient and epidemiological studies, the former address more one-dimensional transects while the latter focus more on populations and include more experience in making quantitative predictions, in dealing with confounding factors and in taking into account the complex interplay of different factors acting at different levels. Epidemiological analyses may disentangle and quantify the contributions of different predictor variables to an overall effect, e.g. plant growth, and may generate hypotheses deserving further study in experiments. Therefore, their use in ecosystem research is encouraged. Braun et al. (2017) provide a number of recommendations on: (1) spatial and temporal aspects in preparing predictor maps of O_3 exposure and meteorological covariates; (2) extent of a dataset required for an analysis; (3) choice of the appropriate regression model and conditions to be satisfied by the data; (4) selection of the relevant explanatory variables; (5) treatment of interactions and confounding factors; and (6)

assessment of model validity. For further details on the recommendations, see Braun et al. (2017).

Reference

Braun, S., Achermann, B., DeMarco, A., Pleijel, H., Karlsson, P.E., Rihm, B., Schindler, C., Paoletti, E., 2017. Epidemiological analysis of ozone and nitrogen impacts on vegetation – Critical evaluation and recommendations. Science of the Total Environment 603-604, 785-792.